PETROLEUM RESEARCH JOURNAL

TECHNICAL PAPERS

ENGINEERING

Enhanced Oil Recovery in Libya, ... *E.O. Egbogah.* 5

LPG cracking in an existing naphtha – based ethylene plant, ... *A.A. Ballut and A. Buhedma.* 12

Simple model to predict the deliverability of volumetric gas reservoirs, ... *M.A. Benrewin.* 17

EXPLORATION

On the hydrocarbon prospectivity of North Cyrenaica Region, Libya, ... *M. Sola and B. Ozcicek.* 25

Stratigraphy and lithofacies of Farwah Group and its equivalent offshore-NW Libya, ... *A.M. Sbeta.* 42

SHORT NOTES

High temperature corrosion of 316 Austenitic stainless steel in H_2S/CO_2 containing environment, ... *S.Y. Gjam and K. Abosowa.* 57

H_2S induced localized corrosion of Austenitic stainless steel bellow: A case study, ... *M.L. Mehta and A.T. Hassan.* 63

Evaluation of oil field corrosion inhibitors by NACE static test method and the wheel test method, ... *M.A. Sherif, A. Hassan and A. Abusnena.* 67

A preliminary photogeologic investigation and structures of the basement rock, Southern Part of Jabal Eighee Area, Libya, ... *M.M. Ben Isa.* 71

VOLUME 2 - 1990

Petroleum Research Centre
P.O. Box 6431 Tripoli
Great Socialist People's Libyan Arab Jamahiriya

PRJ, Vol. 2 (January 1990); P. 5–11, 1 FIG.

ENHANCED OIL RECOVERY IN LIBYA

E.O. Egbogah*, A.A. Misellati* and F.M. Krekshi*

تطبيقات وسائل الإسترداد الإضافي في الجماهيرية العظمى

د. إيجبوقا ، عزام المسلاتي وفؤاد الكريكشي

إستناداً على النتائج التي تم تحقيقها بحقل إنتصار، والذي يعد أحد أكبر الحقول الذي ينتج بوسائل الإسترداد الإضافي في العالم. بدأ خلال السنوات الأخيرة إعداد مخطط مشاريع الإسترداد الإضافي ، حيث تم إعتماده ، وبدأ العمل في إجراء الدراسات الفنية والتجارب المعملية لمجموعة من الحقول التي تم إختيارها بغرض الوصول إلى أحسن الطرق المناسبة للتطبيقات العملية وتحديد الجدوى الفنية والإقتصادية لهذه المشاريع.

تتناول هذه الدراسة إستعراض النتائج الأولية للمخطط وتناقش كميات النفط المتوقع إستخلاصها نتيجة لتطبيق وسائل الإسترداد الإضافي والمشاكل التي قد تعيق تطبيق المشاريع على جميع الحقول الليبية ، وتقترح وسائل معالجتها.

ABSTRACT

Building upon the experience of one of the world's largest hydrocarbon miscible projects at the Intisar "D" Reef, Libya is currently embarking upon what is undoubtedly the world's largest national program on enhanced oil recovery (EOR). Under the supervision of the National Oil Corporation (NOC), reservoir and process screening studies are in progress in many operating oil companies, and the results will identify appropriate EOR processes and the reservoirs to which they are amenable. These studies will also establish the technical and economic viability of the planned projects.

This paper discusses some of the preliminary results, and identifies, for the first time, the EOR target oil and the expected reserves therefrom. The technical and resource barriers to widescale application of EOR in Libya, are also dicussed and recommendations made for their remedies.

INTRODUCTION

On the average, Libyan oil reservoirs containing light oil, yield about one-third of the original oil-in-place, when produced using natural reservoir pressure (primary recovery) or by artificial injection of water or gas (secondary recovery). Currently available and emerging technologies, however, now provide the means to recover at least a further 10 to 20 per cent of the conventional oil remaining in many reservoirs. The recovery methods that are utilised to extract this oil are termed enhanced oil recovery (EOR).

There are two ways to increase crude oil reserves; discovery (exploration) and enhanced oil recovery. The preferred method of reserves additions appears to be clear. Exploration should be applied to new/young basins, such as the Murzuk and Ghadames, while EOR should be more applicable to highly explored, mature areas, such as in the Sirte basin. These seemingly clear decision path not withstanding, there are some obvious advantages of EOR over exploration. For example, exploration costs and risks which have been spiralling in the last two decades, are absent in EOR. In EOR we know where the billions of barrels of oil reserves are located. Exploration, on the other hand is highly probabilistic, and we do not know the location of the oil reserves, thus increasing the risk factor and consequent possible investment losses. Also, discoveries require sizeable new investments, while new EOR operations may utilise injection, production and transportation facilities that are for the most part, already in place. In the Jamahiriya, EOR is a proven method of oil reserves replacement; where Zueitina Oil Company operates one of the world's largest hydrocarbon miscible project at Intisar "D" Reef. Located in the Sirte basin of Libya, the Intisar EOR project produced at a

*National Oil Corporation, Tripoli, Libya, G.S.P.L.A.J.

peak rate of 155,000 STB/D in 1980 and currently produces 40,000 STB/D after 20 years of operation. The daily oil production from the Intisar 'D' Reef EOR project currently is equivalent to about 40% of all production from gas injection projects in the United States, and more than 80% of oil production from all EOR projects in Africa, Europe and Asia combined. Clearly, EOR is needed as a viable alternative to exploration.

Results of research on reserves and on exploration and production costs lead to the inescapable conclusion that petroleum will gradually be technically and economically more difficult to explore and produce. Both Simandoux [1] and Desprairies [2] conclude that for equal investments and efforts, EOR will yield significantly more conventional oil reserves than exploration in mature oil-producing basins. With these considerations in mind, the petroleum industry has focused considerable research and innovative development efforts on EOR objectives that appear to be essential in the present situation.

Enhanced oil recovery has the potential to increase the ultimate recoveries in Libya by about 20 billion barrels of conventional oil and extend the life of oil production by as long as fifty years, at current rate of production.

This paper discusses enhanced oil recovery in Libya in its multi-dimensional form, including current activities in research and development, project planning, design and implementation. The contribution of EOR in the national energy conservation, and social and economic well-being are also rationalised.

THE POTENTIAL OF EOR IN LIBYA

World-wide production statistics indicate that conventional primary and secondary recovery methods will produce only one of every three barrels of oil discovered to date. Of the remaining two-thirds, a portion is producible only through EOR technologies. Estimates indicate that the resources of oil in fields discovered to date in Libya, are about 130 billion barrels. The amount that can be recovered with current techniques is about 45.5 billion barrels (or 35%), out of which about 16 billion barrels have already been produced. Consequently, the oil that still has to be produced, (that is, the reserves of oil currently available in Libya's oilfields) is about 29.5 billion barrels (or 65% of the recoverable oil, otherwise known as reserves). At the current rate of constrained (OPEC) quota production, which is some 1.1 million barrels/day, these reserves correspond to about 73.5 years of production. For a more realistic reservoir management production rate of 1.5 million barrels per day, the life index of the remaining reserves of Libya will be 54 years.

The simple fact that emerges from the above figures is that the amount of oil left in the ground at the conclusion of current production operations is enormous. Taking only the fields discovered so far, we are talking about some 84.5 billion barrels of oil, which correspond to about 155 years of production and with a value, at current oil price of $18/bbl, of about 1520 billion dollars.

Some oil exploration experts believe that for every 5 barrels of oil already discovered to date throughout the world, some 3 more barrels are yet to be discovered in currently producing fields, as well as in such areas as the Deep Seas, the Arctic and the Amazon basin [3, 4]. This expectation can be extrapolated to the many largely unexplored basins of Libya. Thus, about 60% of the discovered 130 billion barrels of oil resources in Libya are yet to be discovered. These discoveries will lead to additional reserves of about 27 billion barrels producible by conventional techniques. This will also bring the quantity of oil in Libyan fields that represents the target for EOR technologies to about 135.5 billion barrels.

Data [5, 6, 7] indicate that in a carefully selected, well-designed, good-performing operation, an additional 30–50% of the original oil in place (OOIP, resource) can be recovered by EOR. Thus even if only 50% of the current EOR target oil in Libya were to be eventually produced, it would mean that the country has at its disposal, a further 13–21 billion barrels of oil reserves. This means that EOR clearly can constitute an important major alternative to future petroleum reserves supplies, and can serve as a solid reservoir management basis for a long-term projection of reserves availability. However, this potential is highly dependent on a broad spectrum of economic, technological and policy constraints, which require the concerted attention of both industry and national policy makers in order to realise and maximise the benefits of this resource for the people of Jamahiriya.

It is to be understood that the EOR target oil given in the foregoing sections, constitute a very gross estimate. No consideration has been given to the performance of individual major EOR technique. Considerable research and development work would be required to prove up the estimated reserves. Since many reservoirs may be suitable for the application of more than one technique, and because the economics of various techniques can change significantly with time, potential EOR reserves can readily shift from one EOR category to another. However, it is believed that such changes should not affect the total EOR potential. Thus, the total EOR potential given here are probably more meaningful than numbers on the potential of individual EOR technologies.

STAGES IN OIL RECOVERY OPERATIONS

Primary Oil Recovery:

Primary oil recovery relies on the natural reservoir energy to drive the oil through the complex pore network to producing wells. The driving energy may be derived from one or more of the following: gas that evolves from solution out of the oil; expansion of free gas; influx of natural water; or gravity force. Eventually, the natural drive energy is dissipated. When this happens, energy must be introduced into the reservoir to produce any additional oil.

Secondary Oil Recovery:

Secondary recovery involves the introduction of energy into a reservoir by injecting gas or water under pressure. Separate wells are usually used for injection and production. The added energy stimulates the movement of oil, providing additional recovery at increased rates. For clarity of reservoir engineering data and performance analysis, it is important here to outline the distinction between two secondary recovery processes involving water injection.

Water-pressure maintenance is a process whereby water is injected into the oil-water contact zone of an oil-producing reservoir to supplement the natural drive energy. A classical pressure maintenance by water injection (such as in the Parents field in France), is usually not intended to improve the recovery of oil, but rather, to increase the production rates, and thus accelerate the attainment of ultimate oil recovery. Waterflooding, on the other hand, is a secondary recovery method (such as in the BuAttifel field) in which water is injected directly into the oil leg, ostensibly to obtain additional oil recovery through an effective oil displacement and sweep of the reservoir. It is important to note that interfacial phenomena, in general, and wettability, in particular, are the controlling parameters in waterflooding.

The Remaining Oil:

Oil left at the conclusion of conventional recovery applications is retained in the pore spaces of the reservoir rock at a lower concentration than originally existed; the produced oil is replaced by gas and/or water in the pores. Rose [9] has given a detailed account of character and causes of residual oil in reservoirs, and here it suffices to say that residual oil is left macroscopically in the unswept parts of the reservoir and microscopically as droplets or ganglia in the pore network [10]. The forces which contribute to the retention of oil in the reservoir include restraining force of capillarity (blotter effect), gravity (buoyancy effect), and viscous forces (drag effect). These forces act simultaneously in the reservoir and the resultant effect depends on conditions at individual locations. The exact position of the oil depends on the nature of the reservoir topological and wettability attributes. Releasing the residual oil so that it can be produced is the sole intent of enhanced oil recovery.

WHAT IS ENHANCED OIL RECOVERY

The term "enhanced oil recovery" (EOR) refers, in the broadest sense, to any method used to recover more oil from a petroleum reservoir than would be obtained by primary recovery [5]. In primary recovery, naturally occurring forces, such as those associated with gas and liquid expansion or influx of water from aquifers, are utilised to produce oil. Conventional secondary recovery methods, such as waterfloods, are considered to be "enhanced recovery" methods under this broader definition. In this paper, we will consider EOR in a more narrow sense, and define it as the *additional oil recovery from a petroleum reservoir over that which can be economically recovered by conventional primary and secondary methods.*,

Innovative recovery technologies facilitate the extraction of oil previously inaccessible by conventional methods. These nonconventional methods, may include the introduction of extraneous energy (in the form of heat, miscible hydrocarbon fluids and carbon dioxide, or chemicals) into oil reservoirs to improve their recovery efficiency (See Fig. 1 for Oil Recovery Mechanisms). Kuuskraa [8] defines EOR as a collection of technologies, involving the use of thermal, gas, chemical means and horizontal drilling for producing more oil.

Other stand-alone methods of improving and/or sustaining oil recovery, such as infill drilling only, water injection and non–CO2 immiscible gas injection, should not be considered to be EOR per se. Nevertheless, infill drilling required for closer spaced EOR flood patterns, and water injection required to pressure up the reservoir for miscible gas injection processes, are only adjuncts to EOR. Also, immiscible gas (non–CO2) injection, if warranted for any reservoir's pressure maintenance purposes, or for gravity stable drives, should not be considered as EOR. These clear definitions are necessary for the proper credit of incremental oil recovery as well as more definitive project economics.

All enhanced oil recovery processes have several basic requirements in common:

A The process must mobilise oil which otherwise

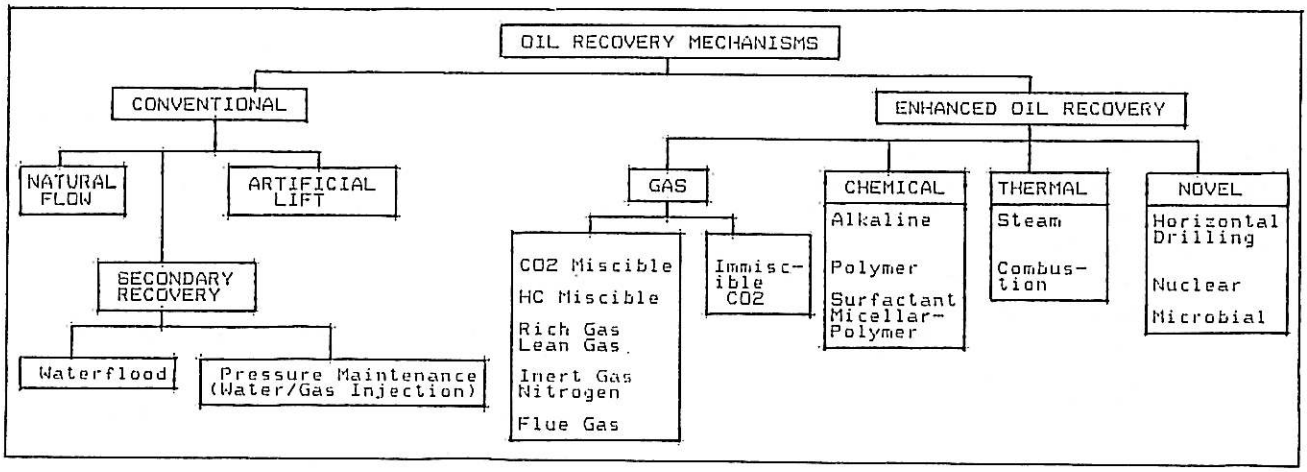


FIG. 1 Oil recovery mechanisms

would have been left unrecovered as residual oil. To mobilise such oil, the displacement efficiency must be improved.

B A substantially greater part of the reservoir must be contacted and swept by the injected fluid, that is, volumetric sweep efficiency must be improved.

C Any mobilised oil must be moved to the production wells and not retrapped in other parts of the reservoir, that is, the capture efficiency must be significant.

D Last, but not the least, the process must be economically viable.

Historically, EOR processes have been called "tertiary" processes in the sense that these were the "third" type of method to be implemented for the further development of the reservoir, and/or because it produces the "third" crop of oil. However, this has led to the severe misconception that these processes are to be applied only after the reservoir has been depleted completely by conventional "primary" and "secondary" methods. It is quite easy to see the fallacy of this conclusion. In a volumetric reservoir, no one will wait for a reservoir to produce all the oil that are producible by "primary" methods before introducing "secondary" recovery method of water injection. The terms "primary", "secondary" and "tertiary" are not to be misinterpreted to imply the time sequence in which these methods are to be implemented. They arise merely out of the chronology of their discovery by practising petroleum engineers, particularly in the United States. Unfortunate as it is, such misconceptions exist even today in the minds of some practising engineers, especially those specialising in conventional methods of petroleum development. In order to remove such misconceptions and obvious misnomer, these exotic processes were redesignated "Enhanced Oil Recovery Processes" to be consistent with our definition. We will stick to this nomenclature in this paper, and refer to all other processes such as "primary" or "secondary", as "conventional processes" to distinguish them from EOR processes.

WHEN SHOULD WE START EOR?

The timing of inauguration of enhanced oil recovery projects is critical. Experience has taught us that novel and more efficient recovery processes must be started in the reservoir as early as practically possible; not only to increase the production and ultimate recovery, but also to reduce the operating life of the field. This, no doubt, will give a more attractive rate of return on the operator's investment.

Conventional oil recovery operations in Libya fields are reaching mature status, and thus the reservoirs should be ideal candidates for EOR applications. And, most importantly, the current reserves additions through exploration do not replace production; that is, we now produce more oil than we find. In recognition of this fact, NOC is now embarking upon what may truly be described as the World's Largest EOR Program, and is working co-operatively with operating oil companies in conducting screening studies that will lead to both reservoir and process selection. Considering that at least ten years may be required to research various EOR processes, match them with reservoirs of their appropriate description, and develop the technical-economics viability criteria for the derivation of the project investment schedules, it is apparent that the time for concerted EOR action in Libya is now. The actions of NOC in this regard are therefore timely and praiseworthy.

WHAT PROCESS SHOULD WE CONSIDER?

Results of preliminary studies [11] indicate that many Libyan reservoirs lend themselves to the application of several EOR processes. No matter what process is to be applied, injectant availability, suitability and requirements must be considered early in the planning and design of an EOR project. Preliminary studies indicate that the techniques of chemical EOR are not cost-effective in Libya at the present time due to the logistics of importing disproportionately large volumes of chemicals, such as polymers, alkaline products, surfactants and co-surfactants. Microbial processes have limited database and therefore have not been considered in our screening program. Thermal processes have a possible application only in the Haram field, but has been eliminated from further consideration for other fields because the depth and pressures of these reservoirs make thermal processes economically unattractive for light oil reservoirs. Having eliminated chemical, microbial and thermal processes for now, technical and economics planning studies now focus on the assessment of gas injection processes for selected Libyan reservoirs.

The National Oil Corporation (NOC) has conducted preliminary studies on resource evaluation, allocation and utilisation of natural gases in Libya. The results reveal a critical insufficiency of suitably rich hydrocarbon resource base for EOR project implementation, thus compelling the investigation of alternative sources of other suitable gases for future planned EOR projects. This has led to the recent documentation of carbon dioxide resources and the prospects of their utilisation for EOR in Libyan oil reservoirs [12].

CONSTRAINTS ON EOR DEVELOPMENT

Constraints on EOR development include technical risks, material and human resource availability.

Technical Risks:

Complex technologies of EOR must be introduced and throughly mastered, and yet many of these are peripheral and emerging technologies which are alien to those who must practise them. This is particularly so in Libya with a limited EOR technological base.

While there is a large resource base to which certain EOR methods can be applied, enhanced oil recovery projects are difficult and costly, and the results do not become apparent until after most of the money has been invested. As a first step in examining potential development, reservoirs are screened to determine which projects might be technically feasible and what EOR processes might be appropriate. Specific candidates are then evaluated as to the amount of oil that will be left after primary and secondary recovery, and the particular charcteristics of the reservoir that will influence the amount of EOR oil. Because no two petroleum reservoirs are identical and the engineering data base is not completely until a pool is abandoned, there are many uncertainties in proceeding with reservoir development.

Technical risk arises from this complexity and uncertainty. Even though reservoir performance and recovery can now be estimated by computer modelling, the application of computer simulation and the process of scaling-up laboratory tests still result in large errors because of inadequate knowledge of the reservoir. Consequently, successful implementation of EOR schemes is by no means assured.

Technical constraints vary with each EOR process. For example, DOE/BETC [13] have indentified the major technical constraints to recovering more oil by gas injection operations. Because of our special interest in carbon dioxide flooding in Libya, we shall limit our discussions here to CO2. Carbon dioxide injection process is an example of a miscible displacement process that does not make use of the more expensive liquefied petroleum gases (LPG). However, the typical problems that need to be resolved for the successful application of this process include the following:

- The dynamic phase behaviour of CO2-oil-water systems is not sufficiently understood to be used for accurate prediction of reservoir performance.
- The type and nature of the displacement mechanisms, such as immiscible, single contact miscible, multiple contact miscible, for various reservoir conditions, are not yet fully understood.
- Mobility control is still inadequate.
- Problems of asphaltene precipitation, rock dissolution and deposition, and formation plugging, remain.

Because of the above, and other technical constraints, extensive laboratory research and field pilot testing of the desired EOR processes must necessarily be implemented. It is of course to be noted that planning, design, implementation and management of EOR pilots require considerable time and expertise which, in most cases, may not be available.

Economic Constraints:

Investment in EOR ventures depends on the investor believing that he will recover his investment in enhanced recovery within a reasonable period of time. The price of oil is only one of the factors influencing the investment decision. It is the netback, defined as the flow of revenue to the producer after deduction of all government taxes and royalties, which governs the inclination of the investor to proceed.

Royalty and tax regimes, in addition to prospective prices, can play a very important part in influencing decisions to undertake any high-risk investments. In EOR, because a return on operator's investment is realised after several years, a stable royalty, tax and pricing regime is essential. If the rules of the game are changed, a project that was economical when begun, could turn uneconomical before the incremental oil begins to flow. Thus changes in revenue sharing and in government regulations can either promote, or adversely affect EOR project starts.

Resource Constraints:

The need for research and development could be a determining factor in the rate of implementation of large-scale EOR projects in Libya. So far there is little or no evidence of R&D going on in Libya relating to EOR technology, and there is also no evidence of long-range basic research being conducted through the universities and the Petroleum Research Centre at a level commensurate with the country's EOR opportunities. Research and developoment, should therefore be launched at the said institutions. For the research to be relevant and timely, it must be carried out to take account of Libyan reservoir conditions. While certain EOR technologies are transferable, they may not always be appropriate. For example, some of the experience gained from many thin reservoirs of north America may not be transferable without adaptation to the very thick reservoirs of Libyan fields.

The most critical constraint, is skilled manpower. EOR projects require significantly more engineering expertise as well as geological reservoir description details than conventional oil recovery methods. EOR projects require multidisciplined group of experience engineers, researchers, geologists, and skilled field operators. To meet these stringent requirements, reservoir engineers and technicians require special training and experience in EOR methods. Research chemists and chemical engineers with training in petroleum processing are also required. Full-scale initiation of EOR projects in the magnitude envisaged by NOC will increase the demand for people trained in these areas, and thus will imply a need for a more substantial training effort of the local manpower.

CONCLUSIONS

Successful application of enhanced oil recovery technologies in selected producing Libyan fields can raise recoverable reserves from 35% to about 50% of the original oil in place. This is equivalent to an incremental oil recovery of about 20 billion barrels, which is nearly equal to the total remaining recoverable reserves from those fields by conventional methods.

The incremental reserves through EOR application may be considerably higher than the anticipted future exploration reserves. Efforts should therefore be devoted to the development of EOR reserves.

Enhanced oil recovery should serve as a solid basis for future reservoir management in Libya. It is a fossil energy conservation policy that will ultimately maximise the benefits of this non-renewable resource to the people. The social and economic consequences of this additional oil recovery are significant and strategic to the progressive development of the country, and could speed up the process of industrial transformation to products manufacturing technology base.

One of the most probable EOR techniques to be used in Libya is carbon dioxide injection. CO2 flooding is a proven EOR process with broad application to reservoir rock and oil type. Because of its universal applicability and demonstrated success in many fields worldwide, and its abundance in Libya (in close proximity to many EOR candidate reservoirs), widescale utilisation of the process in Libyan reservoirs should be encouraged and investigated.

Major constraints to widescale application of EOR technologies to petroleum production in Libya exist; these include, technical, economic and resource availability. These constraints could be removed (or at least substantially reduced) through training, research and development.

ACKNOWLEDGEMENT

The authors express their thanks to the Management of the National Oil Corporation for permission to publish this paper.

REFERENCES

[1] Simandoux, P. (1988) "New Technologies and Their Impact on Petroleum Exploration and Production Activities, "Proceedings, Fourth Arab Energy Conference, Baghdad, Iraq, March 14

[2] Desprairies, P. (1984) "Should Investment in Oil Exploration and Production be Slowed Down?" in: New Technologies for the Exploration and Exploitation of Oil and Gas Resources, Proceedings, 2nd European Commission Symposium, Luxemburg, Dec. 5.

[3] Balaceanu, J.C. (1988) Roundtable Discussion, Proceedings, Fourth Arab Energy Conference, Baghdad, Iraq, March 14–17.

[4] Chierici, G.L. (1989) "Enhanced Oil Recovery: A Promise and A challenge, "*Agip Review, International Edition*, n. 4, May

[5] National Petroleum Council (1984) Enhanced Oil Recovery, Washington DC, USA.

[6] Geffen, T.N. (1973) "Oil Production to Expect from Known Technology," *Oil & Gas Journal* (May 7), 66–76.

[7] Herbeck, E.F.; Heintz, P.C. and Hastings, J.P. (1976) "Fundamentals of Tertiary Recovery, "*Petroleum Engineer* (Jan) 33.

[8] Kuuskraa, V.A. (1986) "The Status and Potential of Enhanced

Oil Recovery," paper SPE/DOE 14951, presented at the Fifth Symposium on Enhanced Oil Recovery, Tulsa, OK., April 20–23

[9] Rose, Walter (1975) "Studies of Waterflood Performance 1: Causes and Character of Residual Oil," *Illinois State Geological Survey Bulletin* #80, 147–163.

[10] Dawe, R.A. and Egbogah, E.O. (1978) "Recovery of Oil from Petroleum Reservoirs, "*Jour. Contemporary Physics*, 19, 355.

[11] Technical and Economics Planning Study for EOR in the SPLJ, a study by IPEC on behalf of EOR Department, NOC.

[12] Egbogah, E.O., Krekshi, F.M. and Misellati, A.A. (1988) "Prospects for Carbon Dioxide Utilisation for Enhanced Oil Recovery Projects in Libya," Proceedings, International Conference on Gas Exploitation and Utilisation in APPA Countries, Misratha, Libya, March 24–26.

[13] DOE/BETC/RI–80/4 (1980) "Technical Constraints Limiting Application of Enhanced Oil Recovery Techniques to Petroleum Production in the United States," May.

PRJ, Vol. 2 (January 1990); P. 12–16, 4 FIGS, 4 TABLES.

LPG CRACKING IN AN EXISTING NAPHTHA-BASED ETHYLENE PLANT

A.A. Ballut* and A. Buhedma*

التكسير الحراري لغاز البترول المسال في مصنع للاثيلين قائم على النافثا

د. عبدالله بلوط وعبدالله بوهدمه

تبحث الدراسة في إمكانية التكسير الحراري لغاز البترول المسال في مصنع قائم لإنتاج الإثيلين باستخدام النافثا. وقد مكن وضع نموذج محاكاة لحركية تكسير غاز البترول المسال من حساب نواتج التكسير تحت ظروف تشغيل متعددة، وكذلك تقييم المكاسب الإقتصادية نتيجة إستبدال جزء من النافثا بغاز البترول المسال حسب مستوى الإستبدال المفترض. حيث أوضحت الدراسة بأن إستعمال غاز البترول المسال في بعض أفران التكسير يمكن أن يكون مربحاً في حالة توفر الهيكلية المناسبة لأسعار النواتج والمواد الخام.

ABSTRACT

This paper reports on an investigation of LPG cracking in existing naphtha-based ethylene plant. Rigorous simulation of LPG cracking kinetics permitted the calculation of product distribution under various operating conditions. The economic gains expected as a result of substituting parts of the naphtha by LPG were assessed under various levels of substitutions. The investigation shows that under favorable price structure of both raw materials and products switching some naphtha crackers to LPG can be a profitable proposition.

INTRODUCTION

The type of feedstock used in an ethylene plant has a major influence on steam cracker product slate and overall plant economics. Cracking of light feedstocks such as ethane produces the highest ethylene yield and the least amounts of co-products. Since such a plant is simple and straightforward it requires the lowest capital investment. On the other hand, because cracking of heavier feedstocks such as naphtha results in the production of large quantities of co-products, an elaborate separation section is required which is translated to higher capital investment.

In terms of flexibility, an ethylene plant based on heavy feedstock gives greater flexibility in terms of product slate compared with a plant feeding ethane only. Moreover, while significant changes both in equipment and operating conditions are required for an existing ethane-based plant to change to heavier feedstock such as naphtha [1], minor changes are usually anticipated when lighter feedstocks are introduced in a naphtha or gas oil-based plant.

Under certain conditions, co-cracking of light feedstock such as propane, butane, or both in naphtha based plant has merit. This is particularly true when the prices of light olefins such as ethylene and propylene enjoy greater margin compared with those of heavier products such as mixed C_4's and pyrolysis gasoline. The relative price of naphtha and LPG is another important factor.

The present paper reports on an investigation of LPG cracking in an existing naphtha-based ethylene plant. The investigation covers the rigorous simulation of LPG cracking in the existing naphtha cracking furnaces to predict the distribution of products at reactor outlet under various operating conditions. The economic gains expected as well as the extent of LPG substitution are also investigated.

KINETICS OF LPG CRACKING

In their simplest form, kinetic models of thermal cracking of hydrocarbons are empirical in nature. On the other hand, kinetic models based on free radical mechanisms for the cracking reactions: while fundamentally sound, can be quite complex for practical applications.

An intermediate approach used by many investigators is based on the so-called "molecular schemes"

*Chemical Eng. Dept., Al-Raya Al-Khadra University, Tripoli, Libya, (G.S.P.L.A.J.)

which are approximations to the true nature of the cracking reactions. This approach has been successfully utilized in the case of light feedstocks such as ethane, propane, butane and their mixtures [2, 3].

The kinetic model used in this investigation is based on molecular schemes of propane and butane cracking as developed by Sundaram and Froment [3]. The scheme, together with the kinetic parameters is given in Table 1.

STEAM CRACKER SIMULATION MODEL

The simulation of an industrial cracker which basically consists of long coils placed horizontally or vertically inside a fired furnace, requires the following set of component mass balance equations together with the energy equation and the pressure drop equation written for plug flow reactor:

A. Component mass balances

$$\frac{dF_j}{dz} = sr_j \tag{1}$$

with

$$r_j = \sum_i u_{ij} r_i \tag{2}$$

for

$i = 1 \ldots\ldots 11$

$j = 1 \ldots\ldots 16$

B. Energy equation

$$\frac{dT}{dz} = \frac{1}{F_t Cp_m}\left[Q(z)\pi D_t + s\sum_i \Delta H_i r_i\right] \tag{3}$$

The specific heat of the mixture follows from:

$$Cp_m = \sum_j \frac{F_j}{F_t} Cp_j \tag{4}$$

where

$$Cp_j = a_j + b_j T + c_j T^2 + d_j T^3 \tag{5}$$

$$F_t = \sum_j F_j + F_{steam} \tag{6}$$

and the heat of the reaction is the algebraic sum of the heats of formation of reactants and products:

$$\Delta H_i = \sum_j u_{ij} \Delta H_{fj} \tag{7}$$

C. Pressure drop equation

$$-\frac{dP}{dz} = \propto\left[\frac{2f}{D_t} + \frac{B}{R_b}\right]\frac{RT}{M_m Pg} G^2 \tag{8}$$

In equation (8), f is friction factor in straight tubes and is defined as:

$$f = 0.046 R_e^{-0.2} \tag{9}$$

Also, B accounts for the additional pressure drop in

Table 1 Molecular Reaction Scheme for LPG Cracking

Reaction	Order	A (s^{-1} or $l.mol^{-1}\cdot s^{-1}$)	E (kcal/mol)
$C_2H_6 \rightleftharpoons C_2H_4 + H_2$	1	4.652×10^{13}	65.21
$C_3H_6 \rightleftharpoons C_2H_2 + CH_4$	1	3.794×10^{11}	59.39
$C_2H_2 + C_2H_4 \rightarrow C_4H_6$	2	1.026×10^{12}	41.26
$2C_2H_6 \rightarrow C_3H_8 + CH_4$	1	3.750×10^{12}	65.25
$C_2H_4 + C_2H_6 \rightarrow C_3H_6 + CH_4$	2	7.083×10^{13}	60.43
$C_3H_8 \rightleftharpoons C_3H_6 + H_2$	1	5.880×10^{10}	51.29
$C_3H_8 \rightarrow C_2H_4 + CH_4$	1	4.692×10^{13}	50.60
$C_3H_8 + C_2H_4 \rightarrow C_2H_6 + C_3H_6$	2	2.536×10^{13}	54.06
$2C_3H_6 \rightarrow 3C_2H_4$	1	1.514×10^{11}	55.80
$2C_3H_6 \rightarrow 0.5C_6^+ + 3CH_4$	1	1.423×10^{9}	45.50
$C_3H_6 + C_2H_6 \rightarrow 1-C_4H_8 + CH_4$	2	1.000×10^{14}	60.01
$n-C_4H_{10} \rightarrow C_3H_6 + CH_4$	1	7.000×10^{13}	54.64
$n-C_4H_{10} \rightarrow 2C_2H_4 + H_2$	1	7.000×10^{14}	70.68
$n-C_4H_{10} \rightarrow C_2H_4 + C_2H_6$	1	4.009×10^{12}	61.31
$n-C_4H_{10} \rightarrow 1-C_4H_8 + H_2$	1	1.637×10^{12}	62.36
$1-C_4H_8 \rightarrow C_6^+$	1	7.685×10^{6}	29.84

coil bends and is given by:

$$B = B'\left(0.051 + 0.19\frac{D_t}{R_b}\right) \quad (10)$$

For 180 bends, $B' = 1.4$ [4]

Model Solution

The solution of the above set of conservation equations is accomplished numerically using fourth order Runge-Kutta method with Gill modification given the geometry of the coil and the following initial conditions ($Z = 0$):

$F_j = F_{j0}$
$T = T_0$
$P_t = P_{t0}$

Plant Investigated

The particular ethylene plant investigated is designed for naphtha feed only. The plant, with a capacity of 330,000 tons/year has ten cracking furnaces, seven for cracking naphtha, one for ethane-propane recycle cracking, and two for stand-by service. Each furnace consists of eight coils. Each coil is 73 m in length and has a diameter of 0.108 m.

The naphtha crackers are designed for total feed of 80.46 kg/m^{2}s, and steam to hydrocarbon ratio of 0.6 kg/kg of naphtha. The recycle cracker is designed for feed rate of 58.17 kg/m^{2}s, and steam to hydrocarbon ratio of 0.4 kg/kg of recycle mixture.

Simulation of LPG cracking

The steam cracker simulation model described by equations 1 through 10 was numerically integrated for the coil geometry previously described utilizing the LPG kinetic model given in Table 1 with the objective of determining suitable operating conditions that yield high amounts of light olefins, namely ethylene and propylene. This depends largely on the severity of cracking which in turn depends on such variables as flow rate, temperature, and steam to hydrocarbon ratio.

Several definitions of cracking severity are available depending on convenience. Percent decomposition of key reactant, methane analysis, propylene analysis, propylene to ethylene ratio, and methane to propylene ratio are just some of the many measures of cracking severity in common use. In this investigation, methane to propylene ratio is selected to measure the cracking severity of LPG since it is easily available and is often the best choice for this feedstock [5].

For the purpose of simplifying the analysis and at the same time insuring adequate cracking run, a steam to hydrocarbon ratio of 0.4 is selected. Consequently, cracking severity is determined by flow rate and temperature only. Several levels of cracking severity are simulated by varying mass velocity and average heat flux in the radiation section as follows:

Mass velocity, G: 80–90 kg/m^{2}s
Heat flux, Q: 18–22 kcal/m^{2}s

A total of 15 computer simulation runs were performed, the results of which are summarized in Fig. 1 As can be seen from this figure, higher ethylene yields are obtained at higher severities but at the same time the propylene yield is significantly reduced. The yields of both ethylene and propylene are sufficiently high only in the cracking severity range of 1.5–2.5. Thus, only this range is considered for further study concerning the economic merit of LPG utilization as an alternative feedstock. Six case studies are identified for the purpose as detailed in Table 2.

Economic Analysis

The economic viability of LPG cracking under the operating conditions cited in Table 2 is analysed on the following bases:

- Product distribution of the whole plant
- Price levels of both products and raw materials.

Since product distribution of the whole plant depends on the level of substitution of naphtha by LPG, three levels of substitution are considered:

	LPG	*Naphtha*
Level 1	1 cracker	6 crackers
Level 2	2 crackers	5 crackers
Level 3	3 crackers	4 crackers

The final product distribution is calculated on the

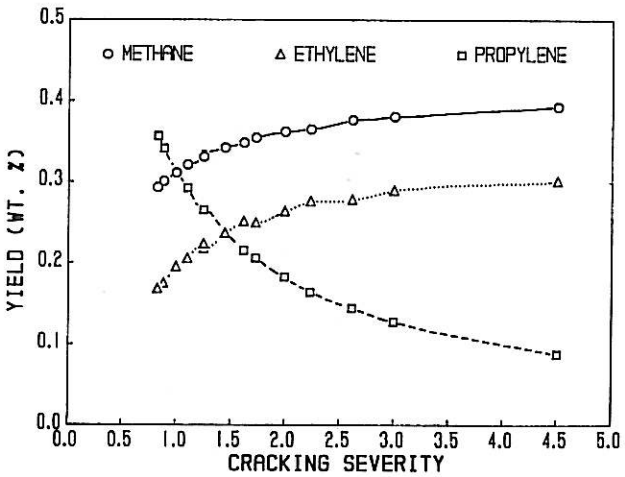


FIG. 1. Effect of cracking severity for LPG feed

Table 2 Case studies for LPG Cracking

Case No.	Flow velocity kg/m²s	Heat flux kcal/m²s
1	80	18
2	80	19
3	85	19
4	85	20
5	90	21
6	90	22

basis of the total effluent from all crackers including the ethane-propane recycle cracker.

Also, since wide variations in prices are usually observed for raw materials and products during the past few years, two sets of prices are assumed as shown in Table 3. The first price set is average prices quoted during the first quarter of 1989. This set may represent a price level that is considered favorable economically. The second price set may be taken to represent somewhat unfavorable price level.

The results of the economic analysis are summarized in Figs. 2, 3 and 4. Fig. 2 illustrates the effect of operating variables on overall plant revenue when only one naphtha cracker is switched to LPG under the first price level. It is quite evident from this figure that positive economic returns are possible in all cases. However the highest incremental profit case (case 5) is also high heat flux case. Thus, final selection among the various cases must also consider any additional operating costs involved.

The effect of varying the level of substitution of naphtha by LPG is illustrated in Fig. 3 for the first price level. The sensitivity of the substitution to the assumed price level is shown in Fig. 4 when the second price set is used in the economic analysis. As expected, this figure shows the great sensitivity of feedstock substitution schemes to prevailing market prices of both feedstocks and products.

Implications for Separation Section

Whenever a change of feedstock is considered, the effect under the new operating conditions upon the

Table 3 Price levels assumed for raw materials and products (cents/lb)

	Level I	Level II
Feedstocks		
Naphtha	7.86	5.95
LPG	5.36	5.59
Products		
Ethylene	31.0	21.6
Propylene	25.5	15.14
Mixed C4's	4.0	4.0
Pyro. Gas.	10.2	7.77

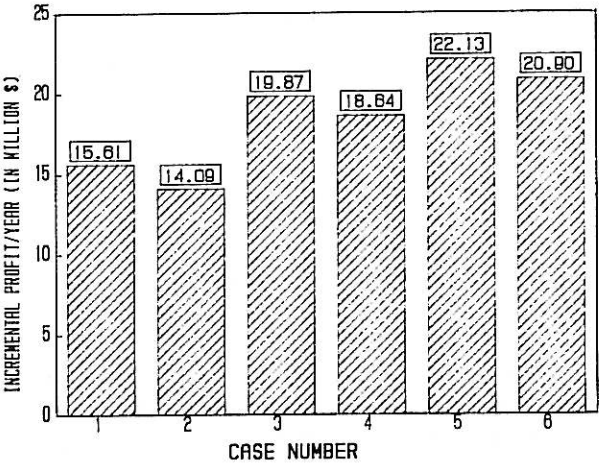


FIG. 2. Effect of operating conditions on ethylene plant revenue

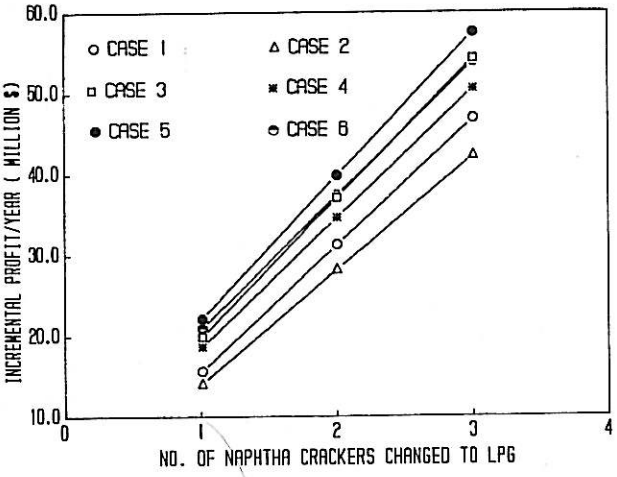


FIG. 3. Substitution level Vs. plant revenue (Price level I)

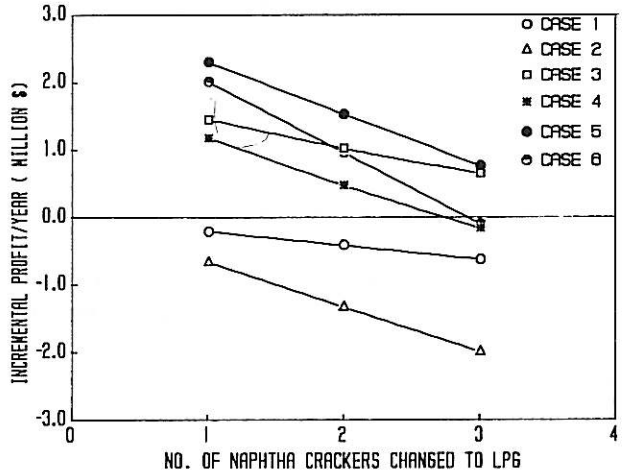


FIG. 4. Substitution level Vs. plant revenue (Price level II)

Table 4 Percent Change in Flow rate Relative to Design Case

Case No.	No. of LPG Furnaces	Quench Section	Light ends Sep. Section
5	1	2.55	5.51
	2	4.08	10.54
	3	5.62	15.57
6	1	2.55	5.01
	2	4.08	9.53
	3	5.62	14.06

separation section must be carefully assessed. Table 4 shows the results of the change in flow rates to the various parts of the separation section computed for the high mass velocity case. As can be seen from this table, flow rate increase to the quench tower is no more than 6% when three naphtha crackers are changed to LPG so that the thermodynamic and hydraulic behavior are not dramatically changed. In the case of the light ends separation section the increase in flow rate is in the range of 5–15%. This also can be considered tolerable but warrants a check on the performance of this section by means of thermal and hydraulic analysis particularly for the cases with greatest increase in flow rate.

CONCLUSIONS

An investigation of switching some naphtha cracking furnaces to LPG in an existing naphtha-based ethylene plant is performed. Rigorous simulation of LPG cracking permitted the calculation of product distribution in the reactor effluent. It was also used to determine the most suitable operating conditions for LPG cracking under existing plant conditions. In addition, the investigation shows that under favorable price structure of raw materials (naphtha and LPG) and products (ethylene, propylene, mixed C_4's, and pyrolysis gasoline), switching some of the naphtha cracking furnaces to LPG can enhance the economic returns of the existing plant. This is particularly true when the market price for naphtha enjoys a commanding lead over LPG.

ACKNOWLEDGEMENT

The authors are grateful to RASCO for providing the necessary data and to N.O.C. planning department for assistance rendered during this research. The computing time provided by N.O.C. computer department is also gratefully acknowledged.

NOTATION

A	frequency factor
B	factor for pressure drop in bends
C_p	specific heat
D	internal coil diameter
E	activation energy
F_j	molar flow rate of component j
F_t	total molar flow rate
f	friction factor
G	mass flow velocity
g	acceleration of gravity
ΔH	heat of reaction
i	reaction index
j	component index
M_m	molecular weight of mixture
P	pressure
Q	heat flux
R	gas constant
R_b	radius of bend
R_e	Reynolds number
r_i	reaction rate
r_j	component reaction rate
s	coil cross sectional area
T	temperature
u_{ij}	stoichiometric coefficient of component j in reaction i
Z	distance along coil
α	conversion factor from Kgf/m^2 to atm

REFERENCES

[1] Aguilar, E., et al., 1988, Analysis Shows Revamp Route to Naphtha Feed, *Oil & Gas Journal*, p. 48.

[2] Sundarm, K.M. and Froment, G.F., 1977, Modeling of Thermal Cracking Kinetics-I: Thermal cracking of ethane, propane, and their mixtures, *Chem. Eng. Sci.*, V. 32, p. 601.

[3] Sundarm, K.M. and Froment, G.F., 1977, Modelling of Thermal Cracking Kinetics-II: Thermal cracking of i-butane, n-butane and mixtures of ethane, propane and butane, *Chem. Eng. Sci.*, V. 32, p. 609.

[4] Froment, G.F. and Bischoff, 1979, Chemical Reactor Analysis and Design, John Wiley & Sons, New York.

[5] Davis, H.G. and Farrel, T.J., 1973, Relative and Absolute Rates of Decomposition of Light Paraffins Under Practical Operating Conditions, *Ind. Eng. Chem. Pro. Des. & Dev.*, 12, p. 171.

PRJ, Vol. 2 (January 1990); P. 17–24, 7 FIGS, 3 TABLES.

SIMPLE MODEL TO PREDICT THE DELIVERABILITY OF VOLUMETRIC GAS RESERVOIRS

M.A Benrewin*

نموذج رياضي بسيط لحساب توقعات الإنتاج من المكامن الغازية الحجمية

المبروك أحمد بن روين

تم تطوير نموذج رياضي بسيط يمكن إستخدامه في حساب توقعات الإنتاج من المكامن الغازية الحجمية تحت ظروف مختلفة للإنتاج. كما تم أيضاً إختبار هذا النموذج الرياضي على مكمن غازي، وكانت النتائج إيجابية ومعقولة وفي مستوى ما هو متعارف عليه في صناعة الغاز. وبالإمكان إستخدام هذه الطريقة الرياضية في الدراسات المبدئية لتطوير حقول الغاز على أن يؤخذ في الإعتبار بعض القيود المفروضة عند إستخدام النموذج.

ABSTRACT

There are many ways to predict the deliverability of gas reservoirs ranging from a simple material balance equation to very complicated gas models.

A simple mathematical model was developed in this study which can be used to predict the deliverability of volumetric gas reservoirs under different production scenarios. The model was tested with real data and proved to be reasonable for initiating any development plan for volumetric gas reservoirs. Some limiting assumptions were imposed on the model and must be considered when using it.

INTRODUCTION

Predicting deliverability from a gas reservoir is an essential element in deciding whether or not it can be developed economically. An optimum development plan depends on the specific characteristics of the reservoir and the market conditions.

If a gas reservoir is to be produced against a constant back pressure of a pipeline, it is important to know if contract rates can be met, and for what time period. When contract rates are predicted to be in deficit, remedial alternatives must be investigated to sustain the required rate.

There are many ways to predict the deliverability of gas reservoirs ranging from a simple material balance equation to very complicated compositional model. In this paper a mathematical model was developed to predict the deliverability of a volumetric gas reservoir, for different producing scenarios, to meet and maintain desired contract demand rates.

MODEL FORMULATION

Consider the situation when a pipeline company prepares a contract for purchase of gas from a gas reservoir. The contract may include a variable demand rate schedule and may also require that the gas be delivered at a specific delivery pressure.

If that gas reservoir is to be produced against a constant back pressure of a pipeline, the production performance will consist of an initial period of a constant rate followed by a decline. To control the decline and maintain the deliverability, it will be necessary to:

1. reduce the delivery pressure,
2. reduce the tubing head pressure and install gas compressor, or
3. drill more wells.

The reservoir development problem becomes one of providing sufficient well deliverability capacity to meet the target rates. Then, facilities need to be constructed to transport gas from the well head to the pipeline, at the specified delivery pressure. The production must pass through separators, dehydrators, meter runs and flow lines to the pipeline. Some pressure drop is associated with each of these equipment parts.

*Petroleum Engineering Department, Al-Raya Al-Khadra University Tripoli, Libya, (G.S.P.L.A.J.)

There should be a relationship between the delivery conditions (rates and delivery pressure) and the ability of the reservoir to meet those conditions. The relation can be formulated by integrating the reservoir, wellbore and flow facilities by specifying the delivery conditions (rates and delivery pressures) at the pipeline; pressure losses in the surface facilities and wellbore can be calculated to provide the correct pressure drop between the reservoir and the wellbore. From this pressure drop the deliverability of the wells and the reservoir can be determined.

This study was concerned with the development of volumetric gas reservoir near a large pipeline. Some assumptions are to be considered to simplify the formulation of the model.

1. A volumetric dry gas reservoir under natural depletion, no water influx, and no water or hydrocarbon liquid production. There is no need for gas separators, dehydrators.
2. All producing wells are a short distance from the transmission line so the pressure drop in the gathering line is negligible.
3. The largest pressure drop was assumed to occur between the gathering stations and the farthest well. Accordingly, any well can be assumed to behave as the farthest well.

Fig. 1 shows a schematic drawing of the proposed network to be modelled. The surface facilities in the field consist of a transmission line between the well and the delivery point at the pipeline.

By specifying the delivery pressure and the daily required rate, the well head pressure can be computed by calculating the pressure drop along the transmission line using Weymouth's equation for horizontal flowlines [1]:

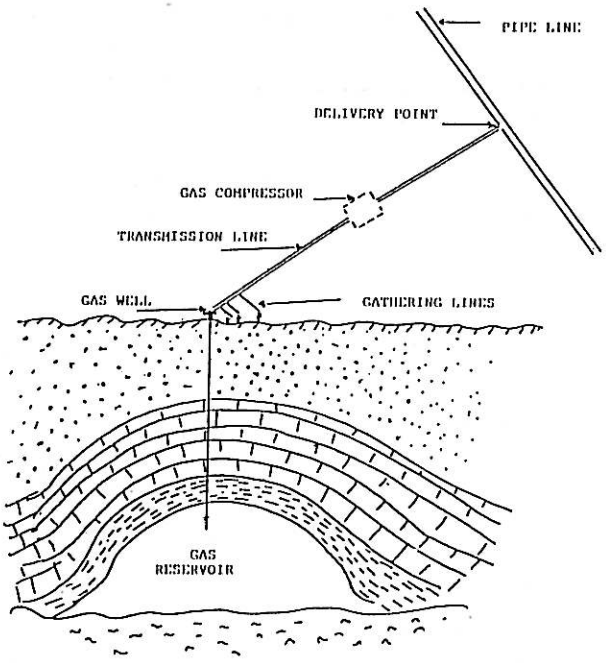


FIG. 1. Model Layout.

$$Q = 5615.5 \frac{T_{sc}}{P_{sc}} \left(\frac{(P_{in}^2 - P_{out}^2) \cdot d^5}{\gamma_g \cdot T \cdot L \cdot f \cdot Z} \right)^{0.5} \quad (1)$$

The same equation can be used in a situation where a gas compressor is installed on the transmission line. The output pressure of the compressor can be calculated by computing the pressure drop between the delivery point and the gas compressor station. The brake horse-power of the compressor can be calculated by assuming different suction pressures and using the following equation:

$$-W = \frac{K}{K-1} \cdot T \cdot C \left(\left(\frac{P_{out}}{P_{in}} \right)^{Z\left(\frac{K-1}{K}\right)} - 1 \right) \cdot E \quad (2)$$

Where E is the efficiency of the compression.

Also, the well head pressure can be calculated by computing the pressure drop between the suction pressure of the gas compressor and the well head.

The well head pressure influences the bottom hole flowing pressure of a well. Low well head pressure increases the rate of flow due to the low back pressure on the reservoir. The bottom hole flowing pressure can be computed using the Cullender and Smith equation [2]:

$$\frac{\gamma_g \cdot L}{53.34} = \int_{P_{tf}}^{P_{wf}} I \cdot dP \quad (3)$$

$$I = \frac{X}{(x^2 + 666.6 \cdot f \cdot Q^2/d^5)} \quad (4)$$

$$X = \frac{P}{T \cdot Z} \quad (5)$$

The Cullender and Smith equation can be evaluated numerically in a two-step calculation. Simpson's rule may be used to perform the integration:

$$\frac{\gamma_g \cdot L}{53.34} = \frac{2}{3} (ITf + 4IMf + IWf)(P_{wf} - P_{tf}) \quad (6)$$

The back pressure behaviour of a gas well is usually related to the daily rate of delivery of the gas and the pressure drop within the reservoir. Rawlins and Schelhardt [3] presented an empirical equation which relates the flow rate and the pressure difference between the bottom hole pressure and the reservoir pressure as follows:

$$Q = c(P_{ws}^2 - P_{wf}^2)^n \quad (7)$$

The factors "c" and "n" are considered to be constant

throughout the life of the well. By knowing the average values of c, n, from testing number of wells, and bottom hole flowing pressure, the static reservoir pressure can be calculated.

For natural gas reservoirs, under volumetric control the cumulative gas produced at any reservoir pressure is the difference between the volumetric estimates of gas-in-place at the initial and subsequent pressure conditions. This relation is known as the Material Balance equation, which can be expressed as:

$$G_P = c \cdot GI\left(\frac{P_i}{Z_i} - \frac{P}{Z}\right) \quad (8)$$

Accordingly, knowing the initial gas in place (GI) and the subsequent reservoir condition, the cumulative gas production can be determined.

Also, the production time can be easily calculated as a result of dividing GP by total daily contract rate.

Calculation Procedures and Model Description

Based on the above discussion, the calculation procedures can be summarized as follows:

1. Knowing the delivery conditions (contract rate and delivery pressure), the pressure drop along the transmission line and the well head flowing pressure can be computed using Weymouth equation.
2. Knowing the well head flowing pressure, the bottom hole flowing pressure can be computed using Cullender and Smith method.
3. The calculated bottom hole flowing pressure is then used with the back pressure equation to calculate the static reservoir pressure.
4. Knowing the initial reservoir pressure and the current static reservoir pressure the deliverability of the reservoir can be computed from the material balance equation.

The above procedures require trial and error calculations which are best carried out on a computer.

A computer program was developed to carry out the calculations.

It is composed of a main program and nine subroutines. The subroutines are listed below, along with their main functions.

GASMODE: Carries all the calculations for the model.
GASPRO: Calculates the gas properties such as gravity, molecular weight, etc.
ZSTAR: Calculates the gas compressibility factor [4].
VISC: Calculates gas viscosity.
FRICT: Calculates friction factor.
FBHP: Calculates bottom hole flowing pressure using Cullender and Smith equation.
PREDR: Calculates pressure drop along any horizontal flow line using Weymouth's equation.
GPP. Calculates gas production and static reservoir pressure using the back pressure and material balance equation.
COMPHP: Calculates the brake horsepower for the gas compressors.

MODEL STUDIES

The developed computer model was used to predict the performance of the carbon gas field [5]. The data used to run the model are listed in Table 1 and 2. The following four production scenarios were studied:

1. Base Case: Natural depletion until the contract rate can no longer be met.

Table 1. Carbon reservoir – Well effluent

Well: **CWNG Carbon** 10–19–29–22
Date of Sampling: **January** 26, 1968
Date of Report: **January** 29, 1968

Component	*Well Effluent*
O_2	0.003
H_2	1.912
CO_2	0.219
C_1	85.518
C_2	6.462
C_3	3.311
iC_4	0.797
nC_4	0.451
iC_5	0.302
nC_5	0.225
C_6	0.685
C_7^+	0.115
	100.000

All measurements at 14.65 psia and 60°F

Pressure of the sample: 1002 psig

Temperature o the sample: 68°F

Properties of C_7^+
Density = 0.7471 gms/cc
API Gravity = 57.9
Molecular Weight = 119.0

2. Scheme I: Same as the base case except the delivery pressure was continually reduced to maintain the contract rate, after the point in the base case where deliverability declined.
3. Scheme II: Same as the base except the compressor was installed to maintain the rate.
4. Scheme III: Same as the base case except infill drilling was initiated to maintain the rate.

Table 2. Carbon reservoir – Average reservoir properties

Initial Reservoir Pressure, psia	1462
Reservoir Temperature, °F	115
Porosity, percent	19.4
Permeability, millidarcies	196.3
Water Saturation, percent	29.5
Bulk Volume, acre-feet	325,873
Initial Gas-In-Place, billion scf	219.7
Reserves per Acre-Foot, million scf/acre-ft.	674.2
Average Absolute Open Flow, million scf/d	26.03
Average Exponent, "n"	0.887
Average Performance Coefficient, "C"	256.81

The above schemes were studied under different flow rates ranging from 20.3 to 29.3 MMSCFD. Some of the results obtained by the model are shown in Table 3 and Figs. 2, 3 and 4. Base Case-natural depletion against a delivery pressure of 950 psia until the demand rate of 29.3 MMSCFD could no longer be met, recovered 58 billion SCF of gas in 5.4 years. This is 26 percent of the initial gas in place.

Scheme I: Implementing a strategy of lowering the delivery pressure to maintain the demand rate after 5.4 years, recovered an incremental 37 percent of the initial gas in place, for a total recovery of 63% at a delivery pressure of 250 psia.

Scheme II: Utilizing gas compression to maintain the demand rate after 5.4 years, recovered an incremental 43 percent of the initial gas in place, for a total recovery of 69 percent at a suction pressure of 100 psia.

Scheme III: Adapting a strategy of infill drilling after 5.4 years, had minimal incremental recovery about 1% and was not considered a feasible development alternative.

The model can also be used to study the effect of tubing size on the gas recovery as shown in Figs. 5, 6, 7. The results show that using large tubing size yields more recovery due to low pressure losses in this tubing.

The results obtained by the model for the carbon gas field were consistent with the common figures for the kind of gas reservoir.

As a general result, the model can be used to predict the deliverability of any volumetric gas reservoir under different production scenarios. The assumptions which imposed on the model should be considered.

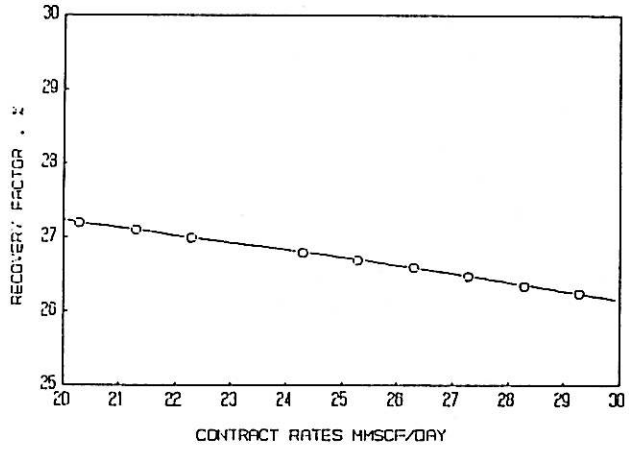


FIG. 2. Recovery factor Vs rates-Base case.

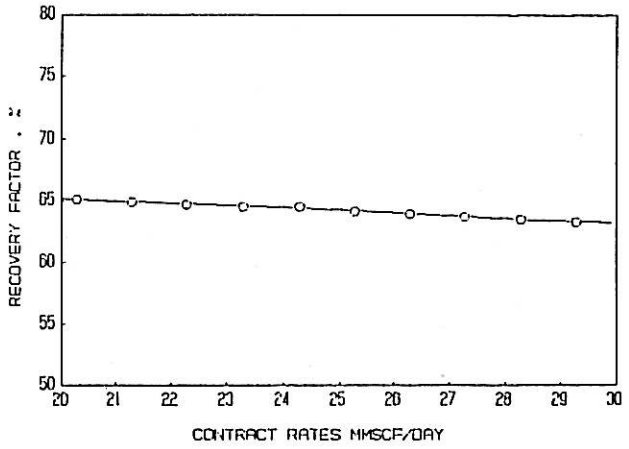


FIG. 3. Recovery factor Vs rates-Scheme I.

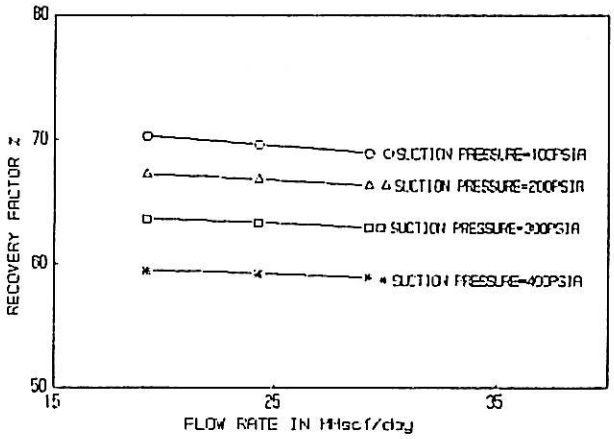


FIG. 4. Recovery factor Vs rates-Scheme II.

Table 3. Sample of model results

BASE CASE: CONTRACT RATE = .29300E+02

DELT. TIME YEARS	CUM. TIME YEARS	FLOW RATE SCF/DAY	DELT. GAS. PR SCF	CUM. GAS. PR SCF	REC. FACTOR FRACTION	RES. PRESS PSIA	DELIV. PRESS PSIA
0.53924E+01	0.53924E+01	0.29300E+02	0.57669E+11	0.57669E+11	0.26243E+00	0.11551E+04	0.95000E+03

SCHEME I = CONTRACT RATE = 0.29300E+02

DELT. TIME	CUM. TIME	FLOW RATE	DELT. GAS. PR	CUM. GAS.PR	REC. FACTOR	RES. PRESS	DELIV. PRESS
0.70341E+00	0.609300E+01	0.29300E+02	0.75226E+10	0.65191E+11	0.29666E+00	0.11092E+04	0.90000E+03
0.68484E+00	0.67806E+01	0.29300E+02	0.73241E+10	0.72515E+11	0.32999E+00	0.10641E+04	0.85000E+03
0.66509E+00	0.74457E+01	0.29300E+02	0.71127E+10	0.79628E+11	0.36235E+00	0.10198E+04	0.80000E+03
0.64404E+00	0.80897E+01	0.29300E+02	0.68877E+10	0.86516E+11	0.39370E+00	0.97660E+03	0.75000E+03
0.52146E+00	0.87112E+01	0.29300E+02	0.66461E+10	0.93162E+11	0.42394E+00	0.93443E+03	0.70000E+03
0.39697E+00	0.93082E+01	0.29300E+02	0.63843E+10	0.99546E+11	0.45299E+00	0.89348E+03	0.65000E+03
0.37178E+00	0.98799E+01	0.29300E+02	0.61148E+10	0.10566E+12	0.48082E+00	0.85387E+03	0.60000E+03
0.34455E+00	0.10424E+02	0.29300E+02	0.58237E+10	0.11148E+12	0.50732E+00	0.81577E+03	0.55000E+03
0.51558E+00	0.10940E+02	0.29300E+02	0.55138E+10	0.11700E+12	0.53241E+00	0.77932E+03	0.50000E+03
0.48447E+00	0.11425E+02	0.29300E+02	0.51812E+10	0.12218E+12	0.55599E+00	0.74475E+03	0.45000E+03
0.45188E+00	0.11876E+02	0.29300E+02	0.48327E+10	0.12701E+12	0.57798E+00	0.71219E+03	0.40000E+03
0.41728E+00	0.12294E+02	0.29300E+02	0.44626E+10	0.13147E+12	0.59829E+00	0.68187E+03	0.35000E+03
0.38099E+00	0.12675E+02	0.29300E+02	0.40745E+10	0.13555E+12	0.61683E+00	0.65394E+03	0.30000E+03
0.34214E+00	0.13017E+02	0.29300E+02	0.36590E+10	0.13921E+12	0.63348E+00	0.62868E+03	0.25000E+03
0.29955E+00	0.13316E+02	0.29300E+02	0.32036E+10	0.14241E+12	0.64806E+00	0.60641E+03	0.20000E+03
0.25186E+00	0.13568E+02	0.29300E+02	0.26935E+10	0.14511E+12	0.66031E+00	0.58757E+03	0.15000E+03
0.19526E+00	0.13764E+02	0.29300E+02	0.20882E+10	0.14719E+12	0.66982E+00	0.57289E+03	0.10000E+03

Table 3 (*cont*)

SCHEME II: INSTALL GAS COMPRESSOR

DELT. TIME YEARS	CUM. TIME YEARS	FLOW RATE SCF/DAY	DELT. GAS. PR SCF	CUM. GAS. PR SCF	REC. FACTOR FRACTION	RES. PRESS PSIA	DELIV. PRESS PSIA
0.87794E+01	0.14172E+02	0.29300E+02	0.93891E+11	0.15156E+12	0.68969E+00	0.54200E+03	0.95000E+03

SUCTION PRESSURE=100.0 DISCHARGE PRESSURE=959.847 BRAKE HORSE POWER=2652.76831 CONTRACT RATE=29300E+02

DELT. TIME YEARS	CUM. TIME YEARS	FLOW RATE SCF/DAY	DELT. GAS. PR SCF	CUM. GAS. PR SCF	REC. FACTOR FRACTION	RES. PRESS PSIA	DELIV. PRESS PSIA
0.82442E+01	0.13637E+02	0.29300E+02	0.88167E+11	0.14584E+12	0.66364E+00	0.58244E+03	0.95000E+03

SUCTION PRESSURE=200.0 DISCHARGE PRESSURE=959.847 BRAKE HORSE POWER=2007.79883 CONTRACT RATE=29300E+02

DELT. TIME YEARS	CUM. TIME YEARS	FLOW RATE SCF/DAY	DELT. GAS. PR SCF	CUM. GAS. PR SCF	REC. FACTOR FRACTION	RES. PRESS PSIA	DELIV. PRESS PSIA
0.75478E+01	0.12940E+02	0.29300E+02	0.80719E+11	0.13839E+12	0.62975E+00	0.63436E+03	0.95000E+03

SUCTION PRESSURE=300.0 DISCHARGE PRESSURE=959.847 BRAKE HORSE POWER=1411.89893 CONTRACT RATE=29300E+02

DELT. TIME YEARS	CUM. TIME YEARS	FLOW RATE SCF/DAY	DELT. GAS. PR SCF	CUM. GAS. PR SCF	REC. FACTOR FRACTION	RES. PRESS PSIA	DELIV. PRESS PSIA
0.67158+01	0.12108E+02	0.29300E+02	0.71823E+11	0.12949E+12	0.58926E+00	0.69538E+03	0.95000E+03

SUCTION PRESSURE=400.0 DISCHARGE PRESSURE=959.847 BRAKE HORSE POWER=981.69214 CONTRACT RATE=29300E+02

SCHEME III INFILL DRILLING: NO OF WELLS=25.00

DELT. TIME YEARS	CUM. TIME YEARS	FLOW RATE SCF/DAY	DELT. GAS. PR SCF	CUM. GAS. PR SCF	REC. FACTOR FRACTION	RES. PRESS PSIA	DELIV. PRESS PSIA
0.37031E-01	0.55710E+01	0.29300E+02	0.39603E+09	0.59580E+11	0.27112E+00	0.11434E+04	0.95000E+03

INFILL DRILLING: NO OF WELLS=30.00

DELT. TIME YEARS	CUM. TIME YEARS	FLOW RATE SCF/DAY	DELT. GAS. PR SCF	CUM. GAS. PR SCF	REC. FACTOR FRACTION	RES. PRESS PSIA	DELIV. PRESS PSIA
0.26207E-01	0.55972E+01	0.29300E+02	0.28027E+09	0.59860E+11	0.27240E+00	0.11417E+04	0.95000E+03

INFILL DRILLING: NO OF WELLS=35.00

DELT. TIME YEARS	CUM. TIME YEARS	FLOW RATE SCF/DAY	DELT. GAS. PR SCF	CUM. GAS. PR SCF	REC. FACTOR FRACTION	RES. PRESS PSIA	DELIV. PRESS PSIA
0.19914E-01	0.56172E+01	0.29300E+02	0.21297E+09	0.60073E+11	0.27337E+00	0.11404E+04	0.95000E+03

INFILL DRILLING: NO OF WELLS=40.00

DELT. TIME YEARS	CUM. TIME YEARS	FLOW RATE SCF/DAY	DELT. GAS. PR SCF	CUM. GAS. PR SCF	REC. FACTOR FRACTION	RES. PRESS PSIA	DELIV. PRESS PSIA
0.15924E-01	0.56331E+01	0.29300E+02	0.17029E+09	0.60243E+11	0.27414E+00	0.11394E+04	0.95000E+03

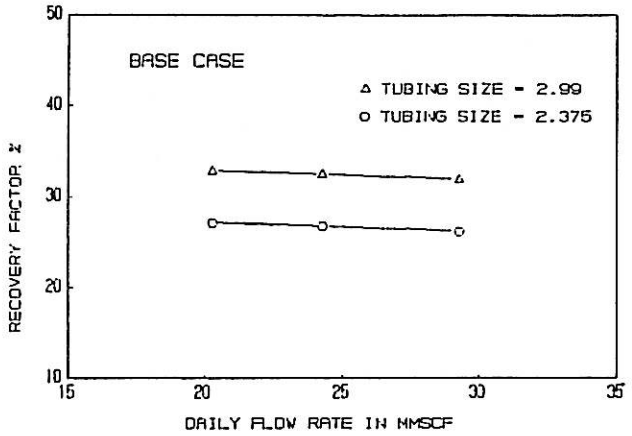


FIG. 5. Effect of tubing size on gas recovery-Base case.

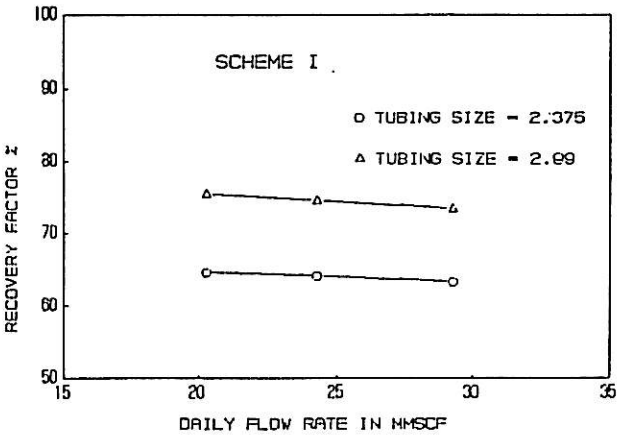


FIG. 6. Effect of tubing size on gas recovery-Scheme I.

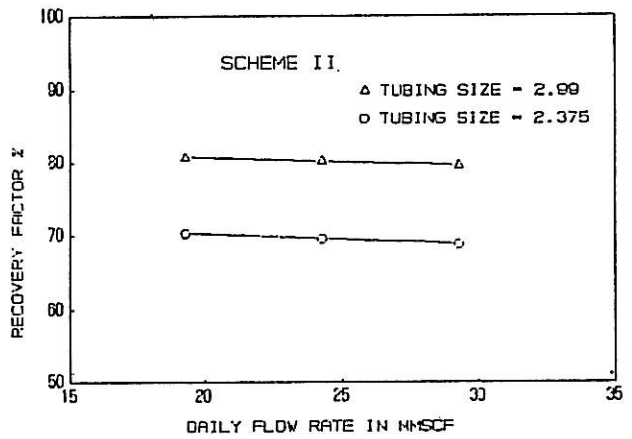


FIG. 7. Effect of tubing size on gas recovery-Scheme II.

CONCLUSIONS AND RECOMMENDATIONS

Based on the work carried out in this study, the following conclusions were made.

1. A simple mathematical model has been developed which predicts the deliverability of any volumetric gas reservoir.
2. The model can be used to predict the deliverability of volumetric gas reservoirs under different production scenarios.
3. The model results are very reasonable to be used for initiating development plans.
4. The assumptions imposed on the model should be considered when using the model.
5. The model can be used to investigate many variables such as flow rates, tubing sizes, pipe line sizes, etc.
6. This model can serve as an important planning tool for proper development and management of a volumetric gas reservoir.

ACKNOWLEDGEMENT

The author would like to express his sincere appreciation to Dr. D.L. Flock and to Professor P.M. Dranchuk of University of Alberta for the supervision of the work.

Also Eng. Bashir Khalil of N.O.C. for his Technical Assistance and continuous support throughout the course of this work.

NOMENCLATURE

Q	Flow rate or production rate (MMSCF/d)
Z	Gas compressibility factor
d	diameter (inch)
L	length (miles)
f	friction factor
K	specific heat capacity ratio
T	Temperature (°F)
E	Efficiency of the compression
G_p	Gas produced (BSCF)
$-W$	Theoretical Horse power per MMSCF
γ_g	Gas gravity
P	Pressure (psia)
P_{sc}	Pressure standard condition (psia)
P_{ws}	Pressure, reservoir at static condition (psia)
P_{wf}	Pressure, bottom hole flowing (psia)
P_{tf}	Pressure, Tubing flowing (psia)
P_i	Initial Pressure (psia)
P_{in}	Inlet Pressure (psia)
P_{out}	Outlet Pressure (psia)

REFERENCES

[1] Ikoku, ChI. U., 1984, Natural Gas Engineering, John Wiley, p. 284.

[2] Cullender, M.H. and Smith, R.V., 1956, Practical Solution of Gas Flow Equation for Well and Pipelines with Large Temperature Gradients: *Trans. AIME*, Vol. 207, 281–287.

[3] Rawlins, E.L. and Schellhardt, M.A., 1936, Back Pressure Data on Natural Gas Wells and their Application to Production Practice: U.S. Bureau of Mines, Monograph 7.

[4] Dranchuk, P.M. and Abou-Kassem, J.H., 1975, Calculation of Z-Factor for Natural Gases Using Equation of State, *JCPT*.

[5] Johnson, J., Carbon Gas Field, Reservoir and Economic Study: University of Alberta.

PRJ, Vol. 2. (January 1990); P. 25–41, 19 FIGS.

ON THE HYDROCARBON PROSPECTIVITY OF NORTH CYRENAICA REGION, LIBYA.

M. Sola* and B. Ozcicek**

الإحتمالات البترولية لمنطقة برقة — ليبيا

د. مصطفى صوله وبرهان اوزشيشك

تشكل منطقة برقة الجزء الشمالي الشرقي من ليبيا ، بينما تتركب المعالم التكتونية للمنطقة من مسطح برقة والأحواض والمرتفعات المحيطة به ، حيث يحتوي هذا المسطح على صخور رسوبية سميكة ترجع إلى الحين القديم ، والتي ربما لم تتأثر بعوامل التعرية حتى الحركة الهيرسينية .

خريطة الخاصية البوجيرية للمنطقة يتركز بوسطها مجال سالب يصل إلى – 20 ميلليجال ويعزى هذا إلى تواجد قطاع سميك من الصخور الرسوبية مقارنة بالمناطق المحيطة بها كما أكدته معلومات الآبار العميقة بالمنطقة . وتوجد تدرجات بمجال الخاصية البوجيرية وهي تطابق الفوالق الرئيسية التي تحدد معالم المسطح ، ويعكس المجال الموجب في إتجاه الشمال وجود صخور القاع على أعماق ضحلة بمرتفع الجبل الأخضر.

التباين في مجال الخاصية المغناطيسية المسجل بالمنطقة قد يكون ناتجاً عن صخور القاع نفسها ، أو عن مصادر بصخور القاع على أعماق تتراوح ما بين 1–8 كلم ، بينما التدرج في التباين الضعيف نسبياً قد يكون ناتجاً عن مصادر بالصخور الرسوبية .

وتغطي المسوحات السيزمية الإنعكاسية حوالي 30,000 كلم طولي بالمنطقة ، وقد ساعدت نتائج هذه المسوحات ، خاصة بعد ظهور وسائل التقنية الحديثة ، على تحديد أدق للمعالم التركيبية والتطابقية المعقدة في المنطقة .

وتؤكد المعلومات الجيولوجية والجيوفيزيائية ، ومعلومات تسجيلات الآبار بالمنطقة على وجود صخور رسوبية سميكة تحوي صخور المصدر وصخور المكمن . وعليه فإن الإمكانيات البترولية للمنطقة تبدو مشجعة .

ABSTRACT

The north Cyrenaica region forms part of the north-eastern area of Libya. The Cyrenaica Platform and the uplifts, basins and sub-basins surrounding it constitute the main tectonic elements of the region. The Cyrenaica Platform accomodates considerably thick paleozoic sediments which appear to have escaped erosion until the Hercynian Orogeny.

A negative Bouguer anomaly (closure) of the order of twenty milligals is recorded over the Cyrenaica Platform. This anomaly is attributed to the thick sedimentary cover in this Platform compared to the parts around it. The deep well drilling data also support this view. Relatively high gravity gradients are present in the Bouguer gravity map bordering the Platform. These gradients are interpreted in terms of the major fault patterns. A large positive Bouguer gravity anomaly is located in the northern most extension of the region, outside the Cyrenaica Platform. It is apparently associated with the basement high in Al Jabal Al Akhdar Uplift.

The magnetic anomalies recorded in the region are believed to have been caused by basement or intrabasement sources at depth varying from 1 to 8 kilometers. The narrow and relatively weak magnetic trends are attributed to sources within the sediments.

The seismic reflection data in the region totals about 30,000 line-kilometres. The data of early seismic surveys (1960's) are invariably of poor quality compared to the recent improved coverages.

The results of seismic coverages, by modern techniques, have helped to sharpen the insights into the complicated structural and stratigraphic features occuring in the region. The available geological, geophysical and drilling data indicate the presence of thick sedimentary sequence containing source and reservoir rocks. The potential of the region for hydrocarbon accumulations, therefore, appear encouraging.

*Petroleum Research Centre, Tripoli, G.S.P.L.A.J.
**National Oil Corporation, Exploration Dept., Tripoli, G.S.P.L.A.J.

INTRODUCTION

The north Cyrenaica region occupies the northeastern corner of Libya. The region covers an area of around 200,000 square kilometers. It is bounded by the longitudes 20° E and 25° E and the latitudes from 29° N to 32° N. The surface elevations range from the sea level in most parts to a maximum of 250 m in Al Jabal Al Akhdar Uplift in the north. The region is surrounded by the Mediterranean sea to the north, the Egyptian Plains to the east, the Kufra Basin to the south and the Gulf of Sirte to the west (Fig. 1). Barr (1968) and Rahlich (1978) worked extensively on the geology of the Cyrenaica region. These and other studies reveal that the subsurface geology in this region is extremely complicated. Since the present work seeks to assess the hydrocarbon prospectiviy of the region, only an overview of the complicated structural environment is presented without detailed accounts of these studies.

Geophysical surveys commenced in the Cyrenaica region from the early 1950's. A large amount of gravity, magnetic and seismic data have so far been obtained. Also, over a hundred wells have been drilled. The results of these concerted efforts provide the basis for interpreting the geologic framework of the region. Vis-a-vis the old reflection seismic data, the recent results from modern seismic practice show that most of the wells in the Cyrenaica Platform and Al Jabal Al Akhdar Uplift happen to be off-located. The poor quality data of the earlier years thus appear to have caused the drilling of unproductive wells. Seismic sections from improved data acquisition and processing techniques compared with those of the same lines shot earlier clearly demonstrate the point. The situation therefore calls for a reassessment of the hydrocarbon prospectivity of the region. The new data in integration with the earlier ones is useful in two ways. First, it helps to find the causes for the failed wells.

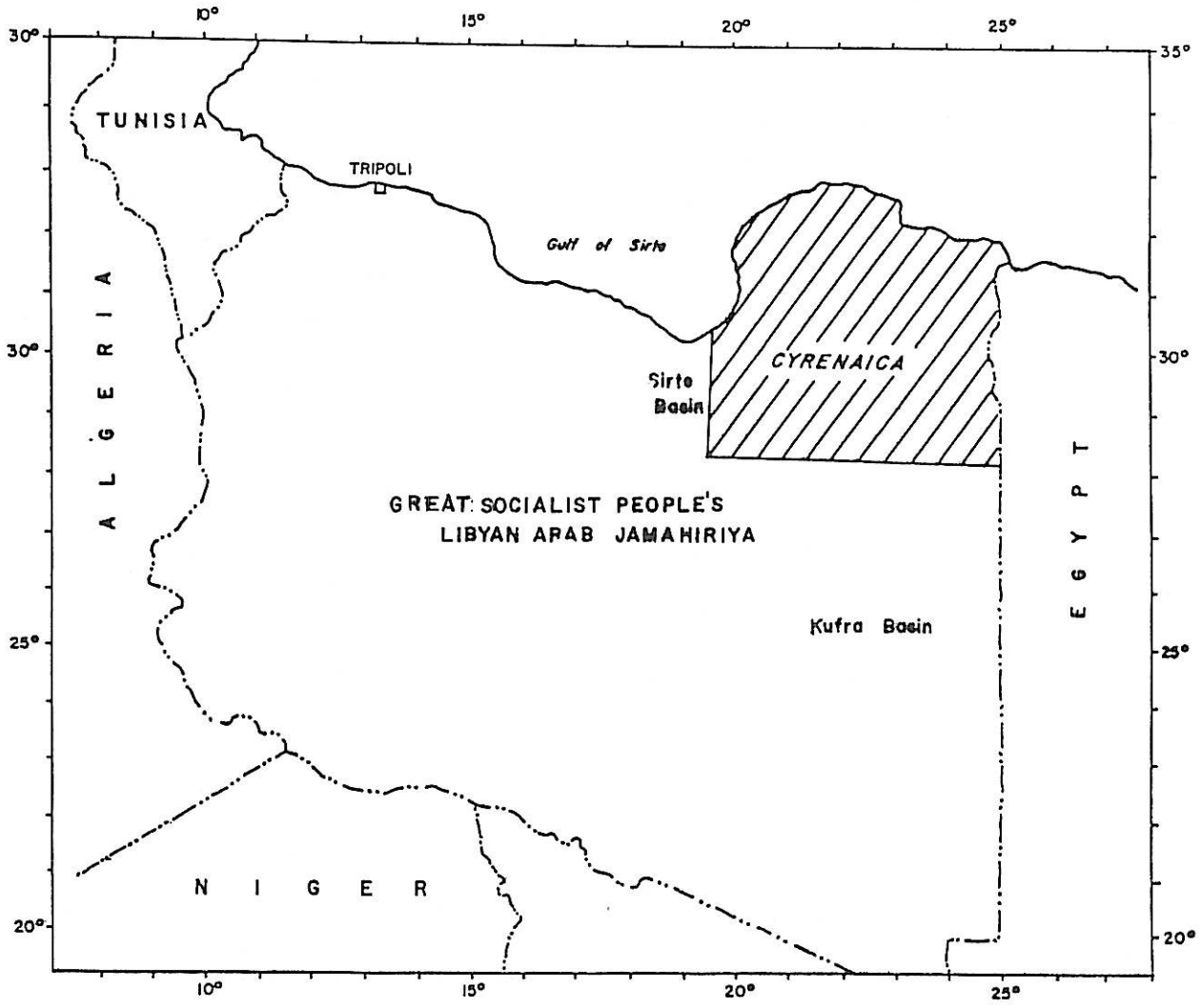


FIG. 1. Geographic location of Cyrenaica region

Second, it facilitates to improve the understanding of the complicated structural setting through more precise subsurface information than was available. An appraisal of the hydrocarbon prospectivity of the north Cyrenaica region is attempted here against this background. The work emphasises the promising prospectivity as indicated from the available subsurface data particularly from seismics.

GEOLOGY AND STRUCTURE

The north Cyrenaica region is covered by upper Cretaceous Tertiary and Recent sedimentary formations. The last includes marine sediments as well. Outcrops of all formations are rich in fossils Francis *et. al.* (1977), Zert (1974), Swedan *et al.* (1977), Klen (1974) and Rohlich (1974). Al Jabal Al Akhdar Uplift and the Great Sand Sea are the major geologic features of the region (Fig. 2).

The former occuring at the northern fringes of the Cyrenaica region contains sedimentary sequences dipping steeply towards the north. Elongated cliffs is therefore the prominent features of the terrain here. They are cut across by deep and broad wadis originating at the highs. Consequently, these parts contain thick and broad valley fills. Upper cretaceous rocks are exposed at the western margin of the Uplift. The Great Sand Sea located at the south of the platform passes eastwards into the Egyptian plains.

The rest of the Cyrenaica region has Tertiary and Quarternary deposits at the surface. Large escarpments and undulating gravel plains are present in the central and eastern parts of the region. Patches of Sabkha and sand dunes occur in the west and northwestern parts. These varied surface lithologies and topographic peculiarities affect the quality of the geophysical data, particularly, the gravity and seismic surveys in the region.

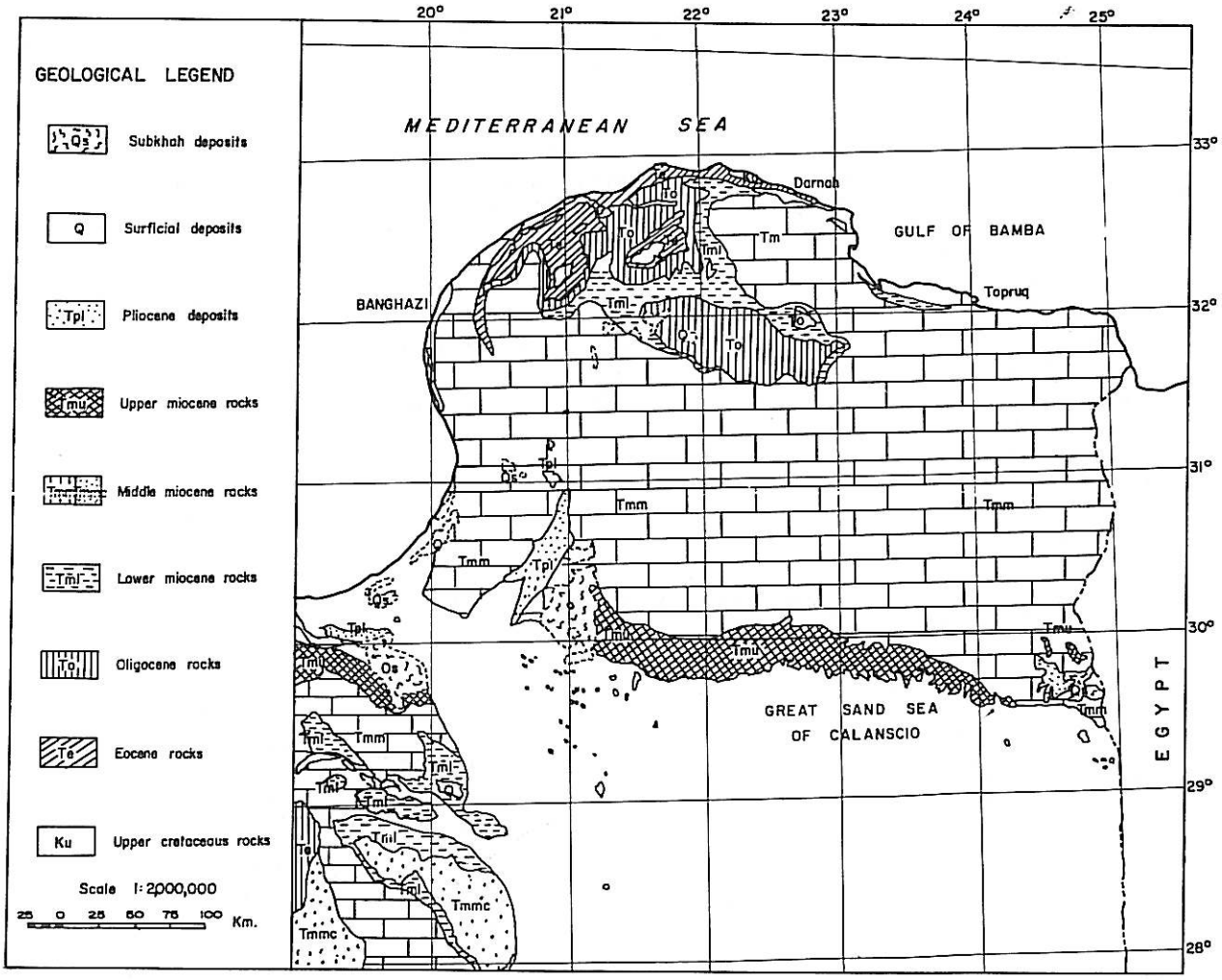


FIG. 2. Geological map of North Cyrenaica

The tectonic activity in the north Cyrenaica region, Rohlich, (1980), dates from the Caledonian to Middle Tertiary times. The repeated tectonic disturbances of this period have subjected the region to uplift, subsidence, tilting, faulting, folding and erosion. The major structural elements infered from geological, geophysical and drilling data are synthetised in Fig. 3.

They include the stable Cyrenaica platform in the centre. It abutts against the relatively unstable Al Jabal Al Akhdar Uplift in the north. The nearly east-west oriented Marmarica Hinge separates these two. In the northwest, however, the platform is limited by the Hamama graben and Antelat trough. The platform is bounded in the east by the Marmarica basin. These two are isolated by a Mesozoic (Marmarica) fault. The stable platform is limited in the south by the Jaghbub uplift. In the southwest, it is margined by the Sirte embayment. Goudarzi (1980) proposed a Tertiary fault line between the two at the southwestern limits of the platform. The Antelat trough occurs immediately east of this fault. It forms the unstable element at the northwestern part of the stable platform region. The geologic features of these major elements are reviewed below:

Cyrenaica Platform

The Cyrenaica (stable) platform is expected to have a total sedimentary thickness of about 5000 meters. The major part (4000 meters) of this sedimentary sequence is believed to be Paleozoics, ranging in age from Cambro-Ordovician to late Carboniferous, (Fig. 4). The rest is the combined Mesozoic and Tertiary thickness.

These sequences are unconfortably overlain by members of the Upper Cretaceous, (Fig. 5). The

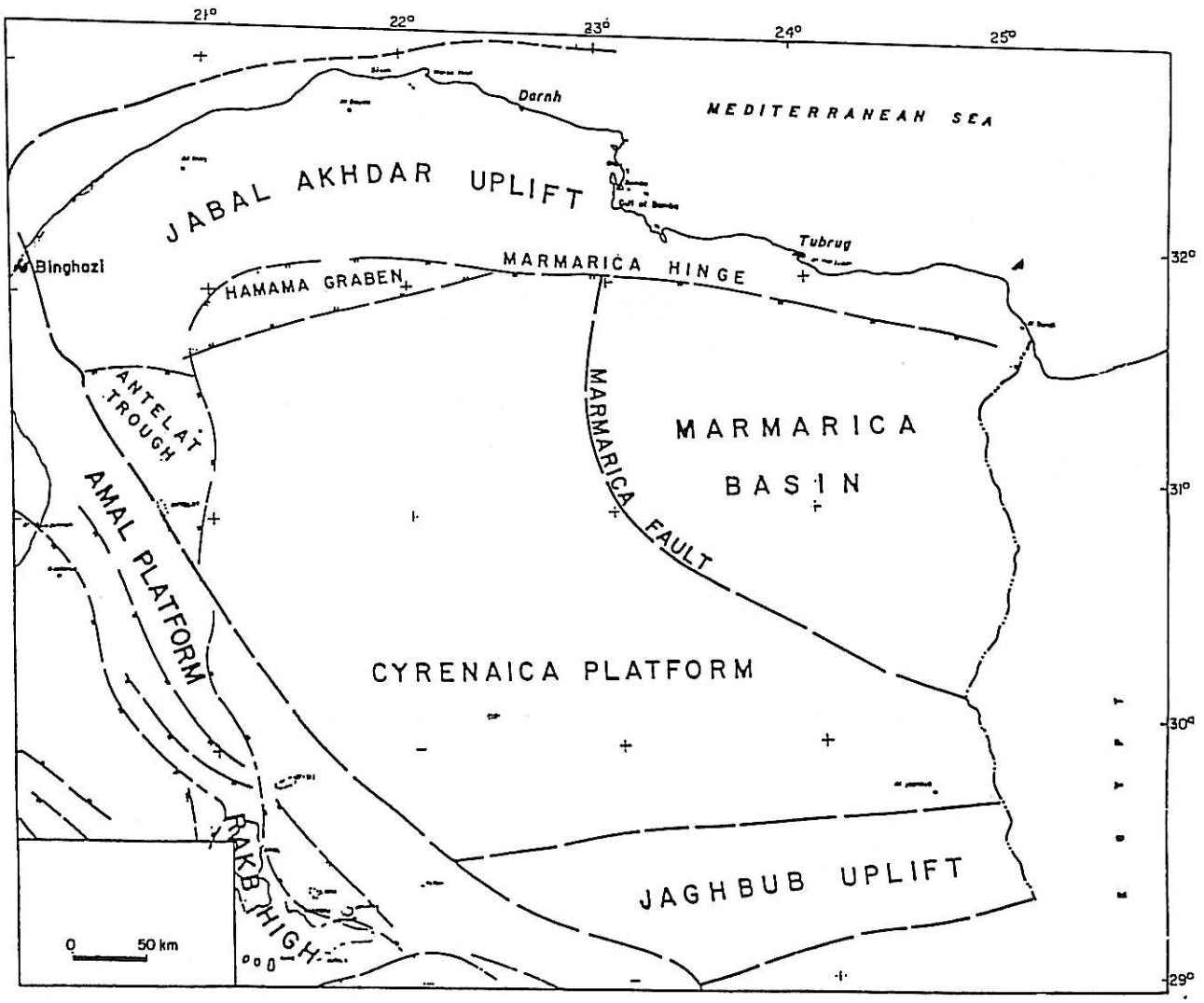


FIG. 3. Tectonic elements of North Cyrenaica

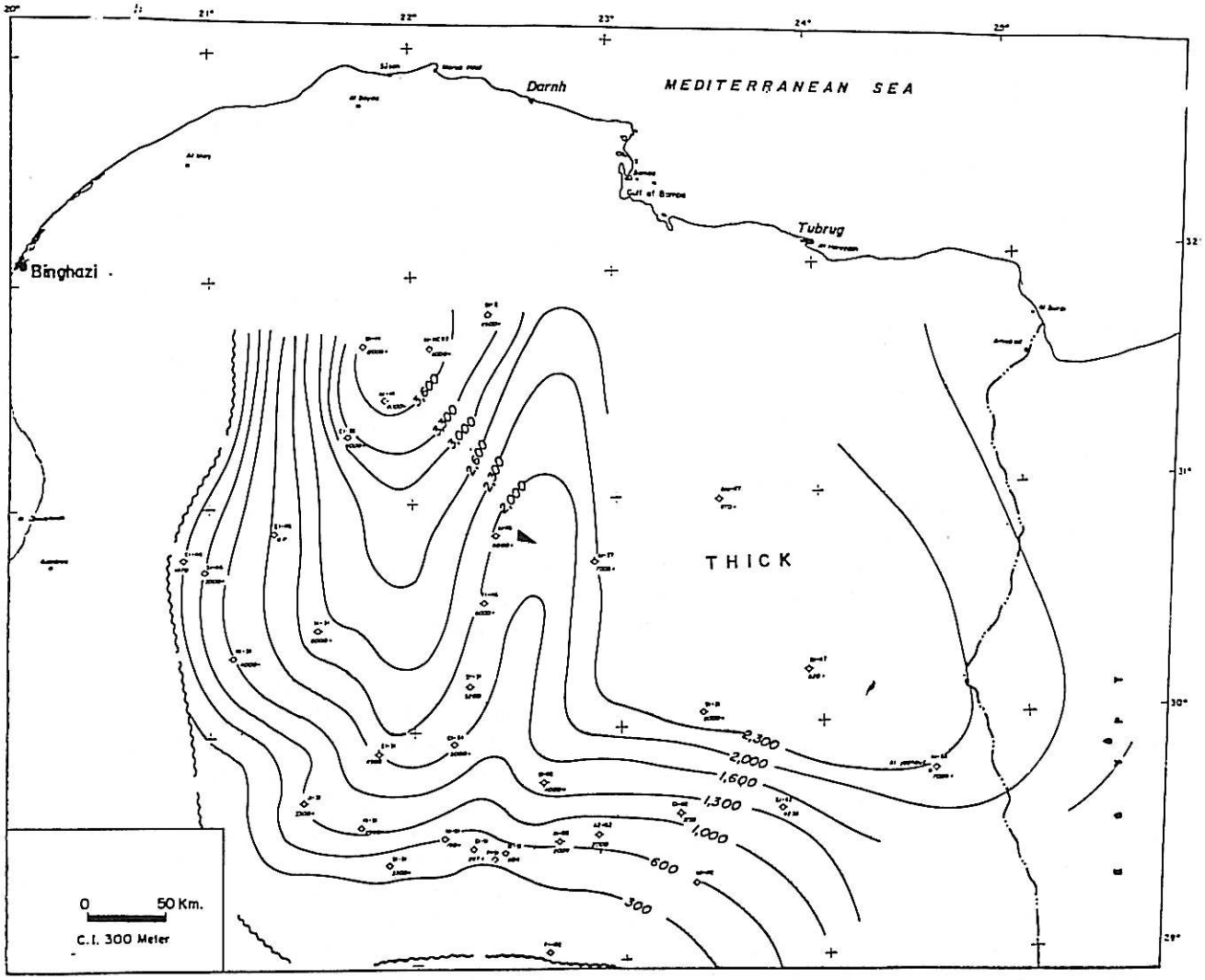


FIG. 4. Isopach map of total Paleozoic North Cyrenaica

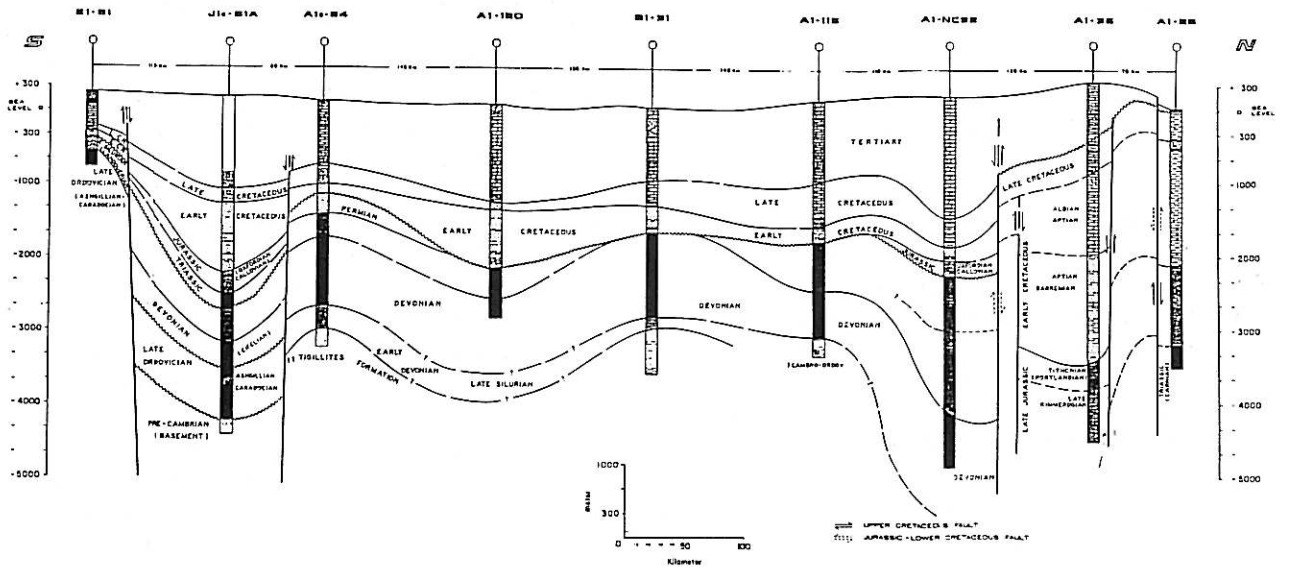


FIG. 5. Subsurface distribution of the Paleozoic to Tertiary Group of formations along N–S Line through the Cyrenaica region

maximum thickness of the Paleozoics in the stable platform part of the Cyrenaica region is brought out by this cross section. The thick Paleozoic sequence thins down to 300–400 meters towards the south and southeast extremities of the platform. Note the section also brings out the faulted contacts limiting the Cyrenaica platform in the northern as well as in the southern extremities.

Unstable platform constituents

The geoelements constituting the unstable platform portions are characterized by rapid subsidence throughout the Mesozoic era compared to that in the stable platform. The geoelements include Al Jabal Al Akhdar Uplift, the Antelat Trough, Hamama Graben and the offshore Basement Ridge.

The Cyrenaica platform abutts against the uplifted and exposed block of Al Jabal Al Akhdar. It comprises of a gentle domal complex exhibiting a rough northeast-southwest trend. The oldest formation reached by drilling in these parts lies within the Jurassic. The late Jurassic-early cretaceous thickness in the uplifted block is of the order of 4000 meters. This contrasts with their thickness of about 1000 meters in the Cyrenaica platform. The abrupt thickening of the formations of particularly the early cretaceous times is indicative of their deposition in a rapidly sinking trough during this period.

The Hamama Graben and Antelat Trough at the north and northwest margins of the platform are down-faulted blocks. They contain large thicknesses of the Jurassic/Cretaceous formations. These fault blocks are terminated in the north by a nearly northeast-southwest running late Cretaceous fault.

The offshore Basement Ridge is the one inferred from the magnetic data by Shell (1974). The Marmarica Basin at the eastern fringes of the platform is a fault basin. An arcuate Mesozoic fault separates this basin from the platform. The northern limit of the Basin is formed by the east-west oriented upper Cretaceous fault. Al Jabal al Akhdar was uplifted to the north of this fault. Thick marine sediments of Jurassic age are present in this Basin (El-Arnauti 1985).

The Jaghbub uplift bordering the southern limit of the Cyrenaica Platform appears to be a basement high as based on the available drilling data. Marine upper Cretaceous formations are present here on an undifferentiated basement. The uplift is believed to have taken place during the Caledonian orogeny with possible rejuvination in the Hercynian cycle. The Sirte Embayment is the last geoelement bordering the platform at the southwest margin. The two are inferred to be separated by an arcuate fault of probable Tertiary age. The major structural features of the Embayment trend nearly in the northwest-southwest direction.

GEOPHYSICAL STUDIES

Numerous geophysical surveys have been carried out in connection with oil exploration in the north Cyrenaica region. The early geophysical surveys date back to 1950's where a considerable amount of gravity and magnetics along with seismic reflection survey data have been acquired.

The geophysical activity slowed down during the seventies owing to poor siting of wells. It is now found to be the result of poor quality data of the early surveys used in siting them. However, geophysical operations at increased pace commenced by the early eighties. It is now continuing with data of greatly increased quality due to the improved data acquisition and processing technology employed in the recent years.

Data quality

The reflection seismic data so far acquired in the region totals to about 30,000 line-kilometers. They consist of the early single fold, and the later, multifold coverages. The sources employed include the conventional dynamite to modern vibroseis with Geoflex, Thumper and Dynoseis operational phases used at different time intervals. The basic data and that of the test lines run are maintained in the Data Center of the National Oil Corporation (NOC).

The quality of the seismic data acquired until the late sixties is generally poor. With the introduction of sophisticated instruments and advanced field techniques, the later seismic coverages yielded comparatively better quality data. The surface conditions in the different parts of the north Cyrenaica region vary considerably. Consequently, special needed to select the optimum data acquisiton parameters. Also the source comparison test is required in each part of the region to select the most effective one. Presently the choice is between the dynamite and vibroseis sources. The best of the two must be used as per the results of test runs in each area of different surface geology. A case in point is presented in Fig. 6.

The reflection seismic section obtained with the dynamite source is presented in Fig. 6a. The same line covered by vibroseis survey yielded the section in Fig. 6b. Note the significant energy level and horizontal resolution achieved with the dynamite source. The poor ground coupling in the area apparently resulted in the relatively poor tracing of the same reflectors in the section with the vibroseis source. Better quality seismic sections facilitated by vibroseis source compared to that from dynamite have also been reported. The example above emphasises the extent to

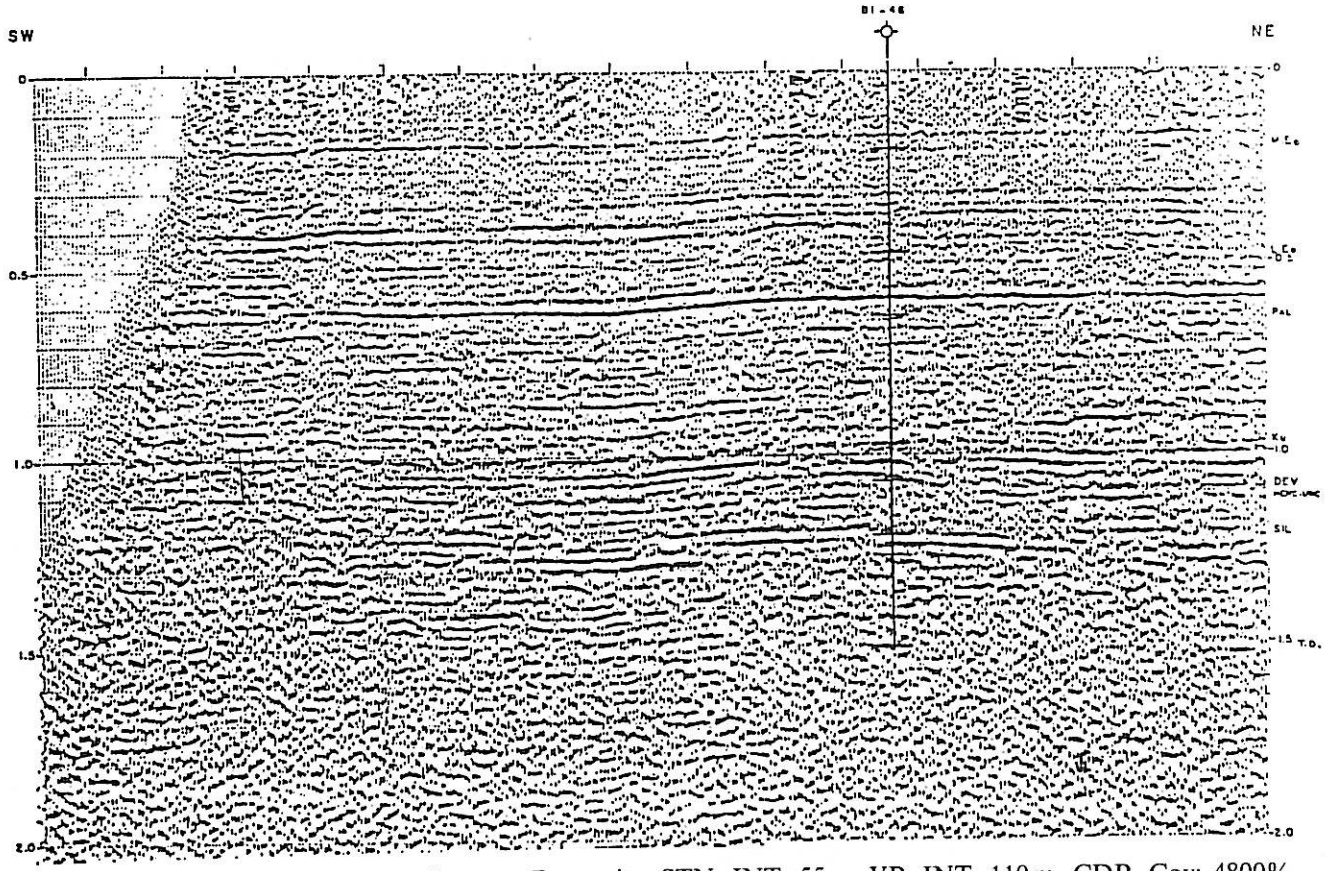


FIG. 6a. Source Comparison test [source: Dynamite, STN. INT: 55 m, VP. INT: 110 m, CDP. Cov: 4800%, DATUM: MSL.]

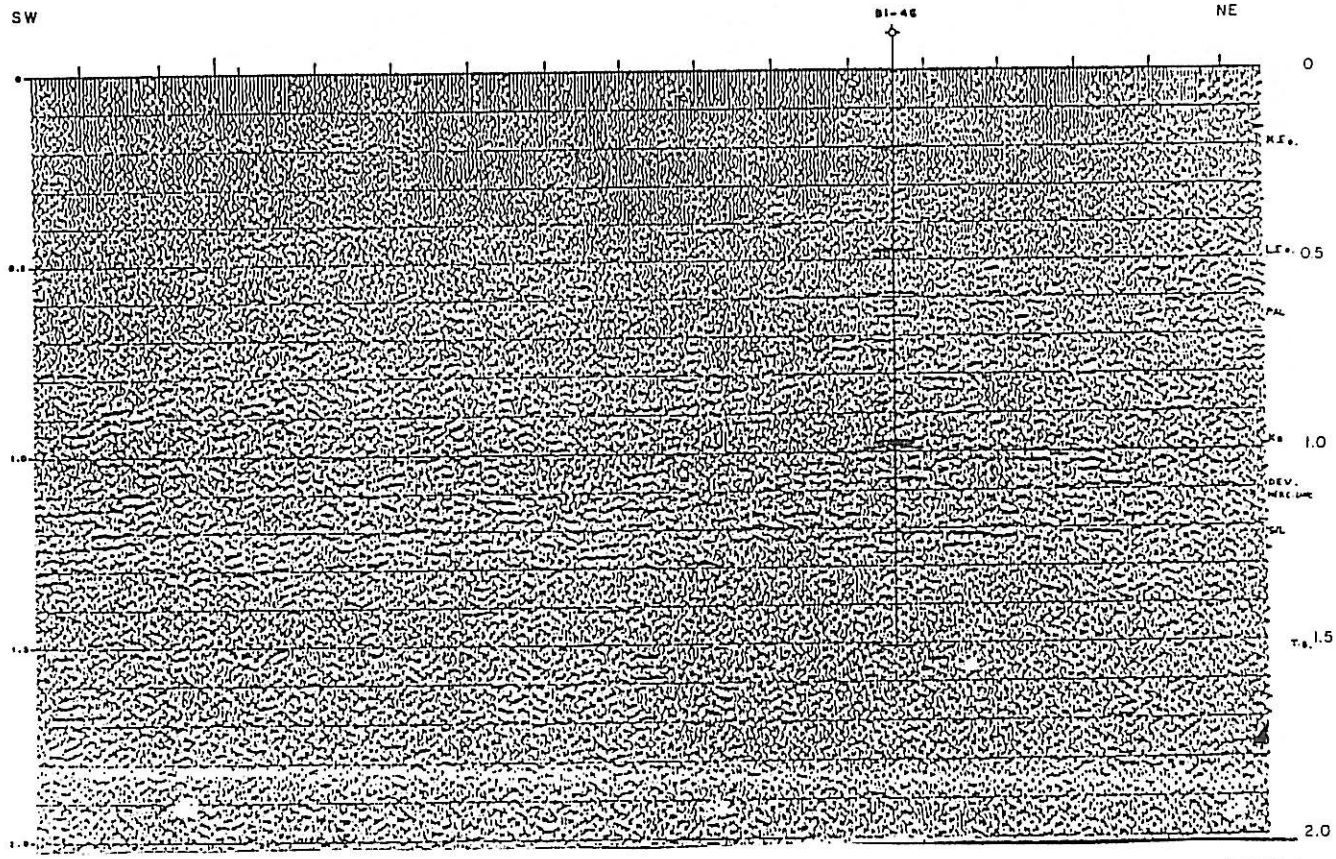


FIG. 6b. Source Comparison Test [Source: Vibroseis, STN. INT: 55 m, VP. Int.: 55 m, CDP. cov: 4800% DATUM: M.S.L.]

which the surface conditions control the eventual seismic results and the need for test surveys to improve the data quality in the different parts of this region.

The rugged topography and lateral density changes near the surface are considered to have caused correction errors in the gravity data of the region. It is therefore desirable to closely study the surface rock densities and evolve appropriate terrain correction strategy for improving the reliability and geologic effectiveness of the Bouguer gravity data in the Cyrenaica region.

INTERPRETATION

Gravity and magnetic studies have greatly helped to infer the structural framework and estimate the basement depth in the region. The Bouguer gravity map of the north Cyrenaica region is shown in Fig. 7. A large negative closure of about twenty milligals is present with northeast-southwest orientation over the platform part of the region. This anomaly occurs over the same part with the expected maximum thickness of the sediments as based on the drilling results. This closure is surrounded by a radial zone of relatively large gravity gradients. These zones correspond with the major fault occurences at the margins around the Cyrenaica Platform. In Al Jabal Al Akhdar Uplift, the Bouguer gravity map shows the presence of strong positive gravity anomaly which is presumably due to shallow basement.

A test study was made with the Bouguer gravity data of the region to map the Mesozoic-Tertiary unconformity. Fig. 8 consolidates the data and the results of the modeling along a north-south line. The gravity residual was computed assuming a linear regional gravity gradient. A density contrast of 0.25 gm/cc was assumed to determine the depth to the Mesozoic-Tertiary (density) surface. Note this depth to be about 500 m in the central portion of the gravity profile

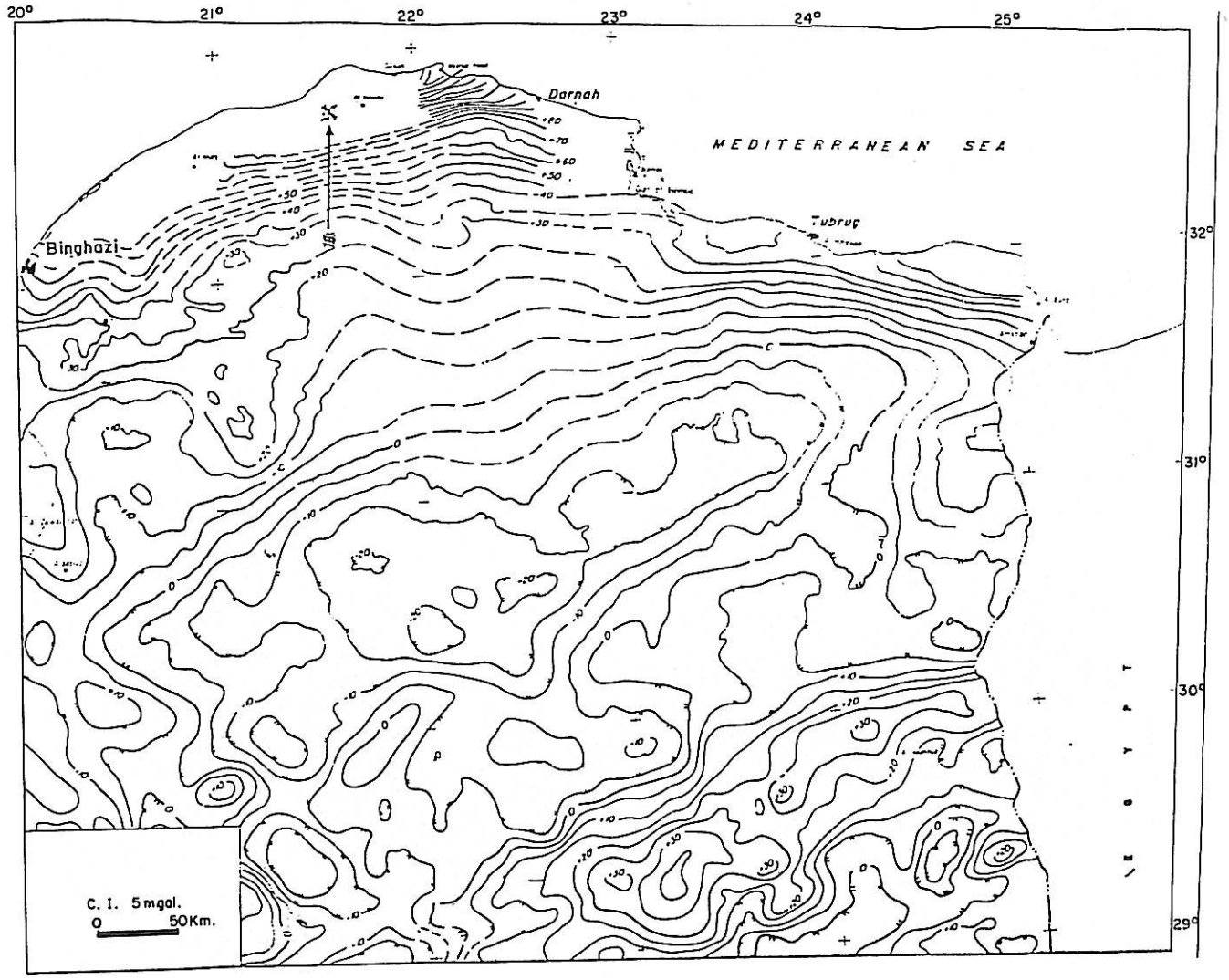


FIG. 7. Bouguer Gravity map of North Cyrenaica

(Fig. 8). The attempt opens up possibilities for the extention of the approach to map the Mesozoic-Tertiary interface in such areas as the Antelat Trough.

The magnetic field map of the north Cyrenaica region is shown in Fig. 9. The presence of relatively high frequency anomaly components in the south-eastern half, vis-a-vis the low frequency ones in the northwestern half of the region, apparently evidence the relatively shallow nature of the basement in the former compared to the depth in the northwestern parts. Inversion of the magnetic data in terms of the depth to the basement shows its variation from 1 to 8 km. The distribution of depths to the magnetic basement is roughly in agreement with the structural categorisation of the region, (Fig. 10). The stable deep basement beneath the central platform is seen to rise towards the northern offshore as well as in the southern inland parts of the region.

The seismic reflection survey has enormously contributed to the examination of the hydrocarbon potential of the region. The seismic results have enabled the marking of about forty favourable structural and stratigraphic features in the region. Some of the earlier seismic lines were subsequently re-shot by modern means to reckon the discrepancies, if any. The appraisal below highlights the outcome from the seismic surveys over the region.

REFLECTION SEISMIC SIGNATURES OF STRUCTURAL AND STRATIGRAPHIC TRAPS

Seismic signatures of some stratigraphic and structural traps are described here presenting some typical examples. Fig. 11 shows a distinct stratigraphic trap signature between 1.4 and 1.5 seconds on the line shot in the Amal Platform. The build up is possibly of Paleocene age. A prominent structural rise is indicated in the parallel seismic section (Fig. 12) between the two-way times 1.3 and 1.5 sec. The structural feature is reported to be of upper Cretaceous to Paleocene age.

The seismic signature of a deposit of lower Eocene age can be noted below the markedup segment in Fig. 13, at the two-way time of 1.55 seconds. The example is from the Antelat Trough. It is known to be located on a Paleocene platform of this region. A strati-structural feature is indicated in the seismic section of Fig. 14. It also pertains to the Antelat Trough. The feature at about 1.08 seconds right below the arrowed segment, is located in Lower Eocene dolomite. The well B1-41 is to the left of this feature and penetrates the horizon by over 40 milliseconds at its apex. It is classified as a marginally economic resource. The amplitude anomaly found on the feature is indicative of possible enhanced fracture porosity in the structure.

An example of a typical stratigraphic trap in the seismic sections of the Cyrenaica Platform part of the region is shown in Fig. 15. The feature below the arrowed segment at two-way time 1.1 to 1.2 seconds, is located in a Paleozoic horizon. The amplitude anomaly over the top of the structure and the observed polarity reversal there implies a probable reef development in a carbonate environment. Fig. 16 shows an example of a paleogeomorophological feature subcrop high. It is reported to be of carboniferous age on an Hercynian unconformity. As earlier, this feature lies below the segment of the line marked at 1.06 seconds. The truncated beds of the Devonian sequence can also

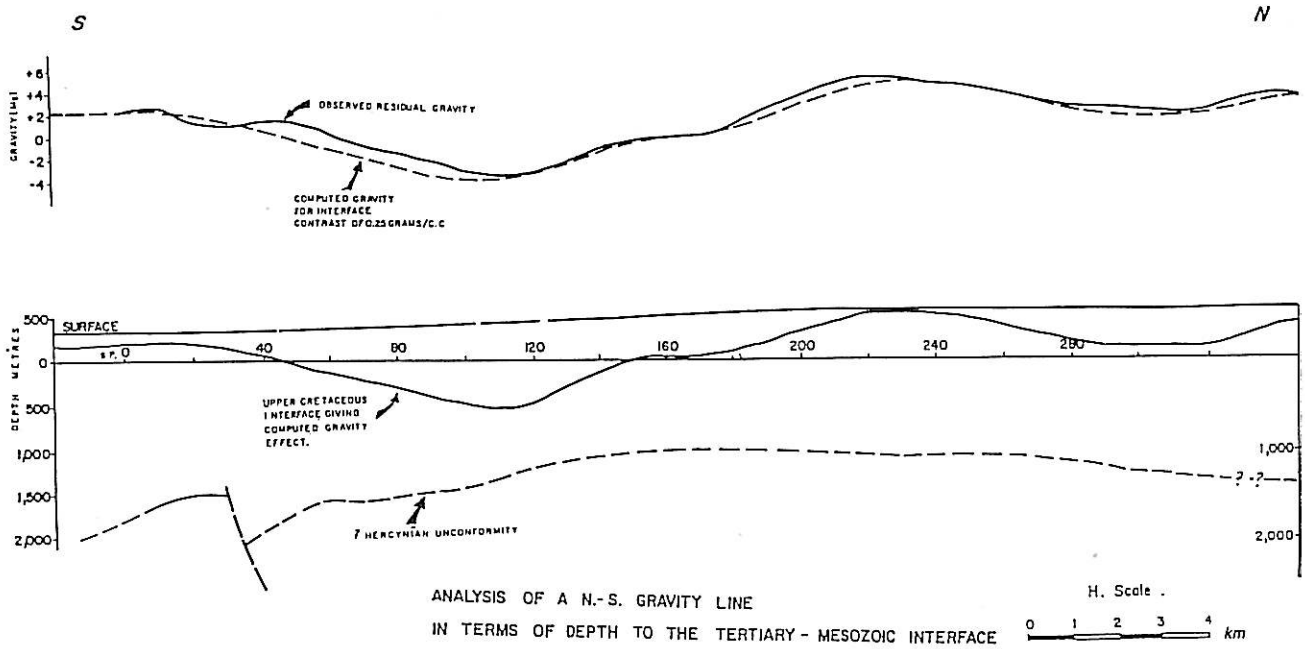


FIG. 8. Interpretation of Gravity profile.

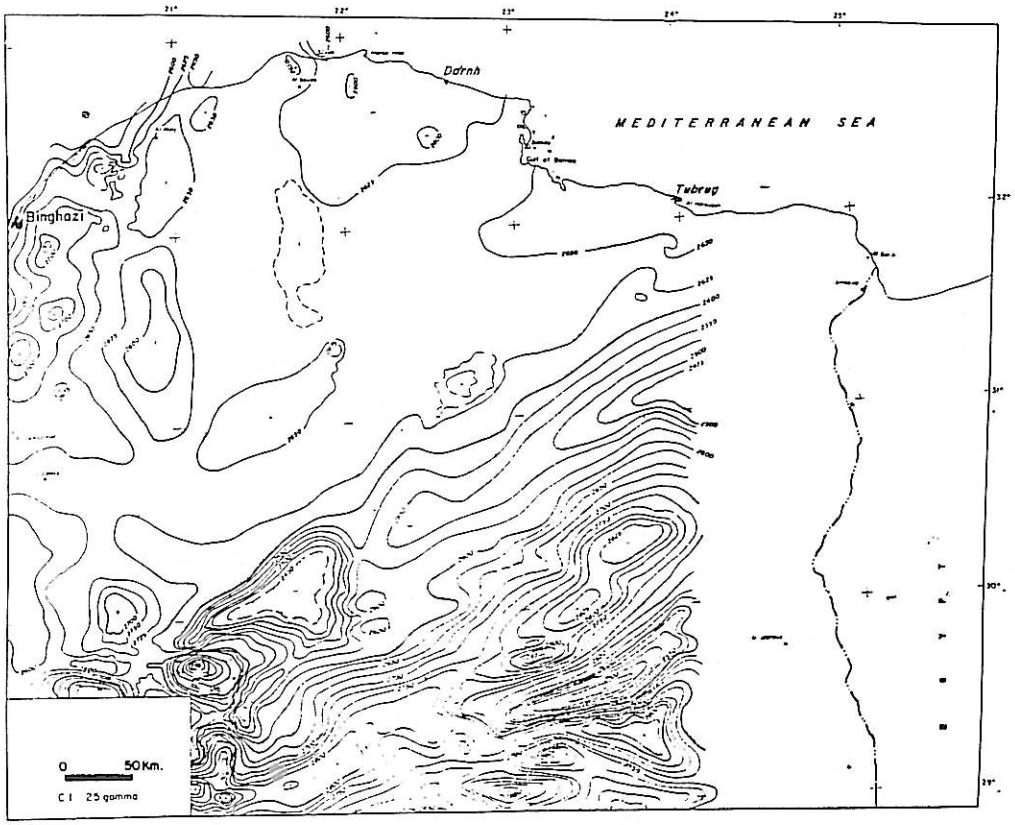


FIG. 9. Regional Magnetic Map of North Cyrenaica

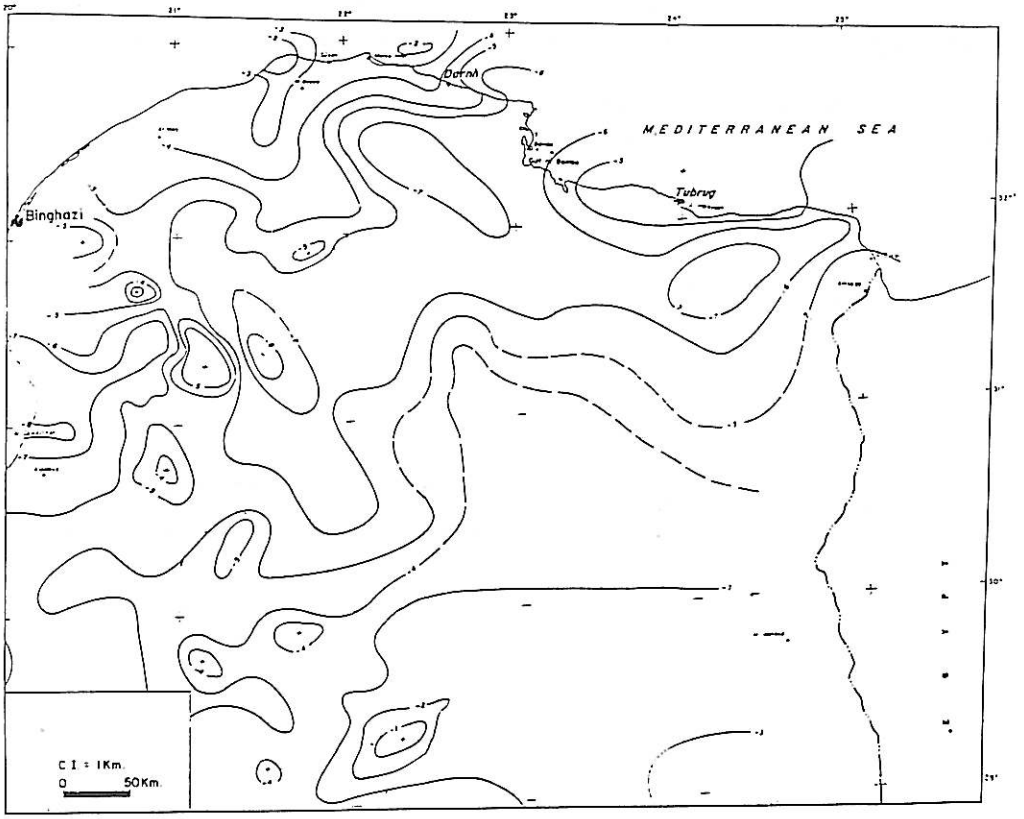


FIG. 10. Magnetic Basement Map of North Cyrenaica

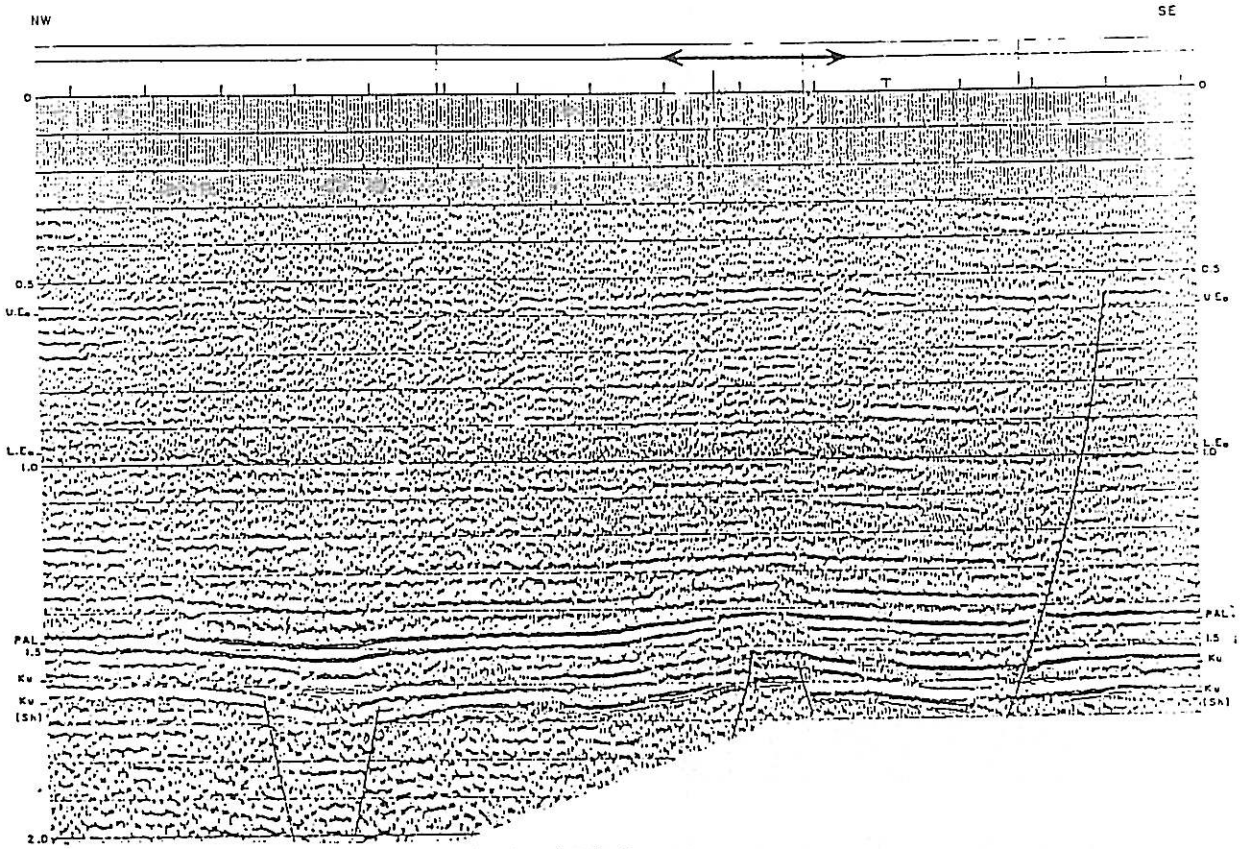


FIG. 11. Paleocene Build-up Features in Amal Platform

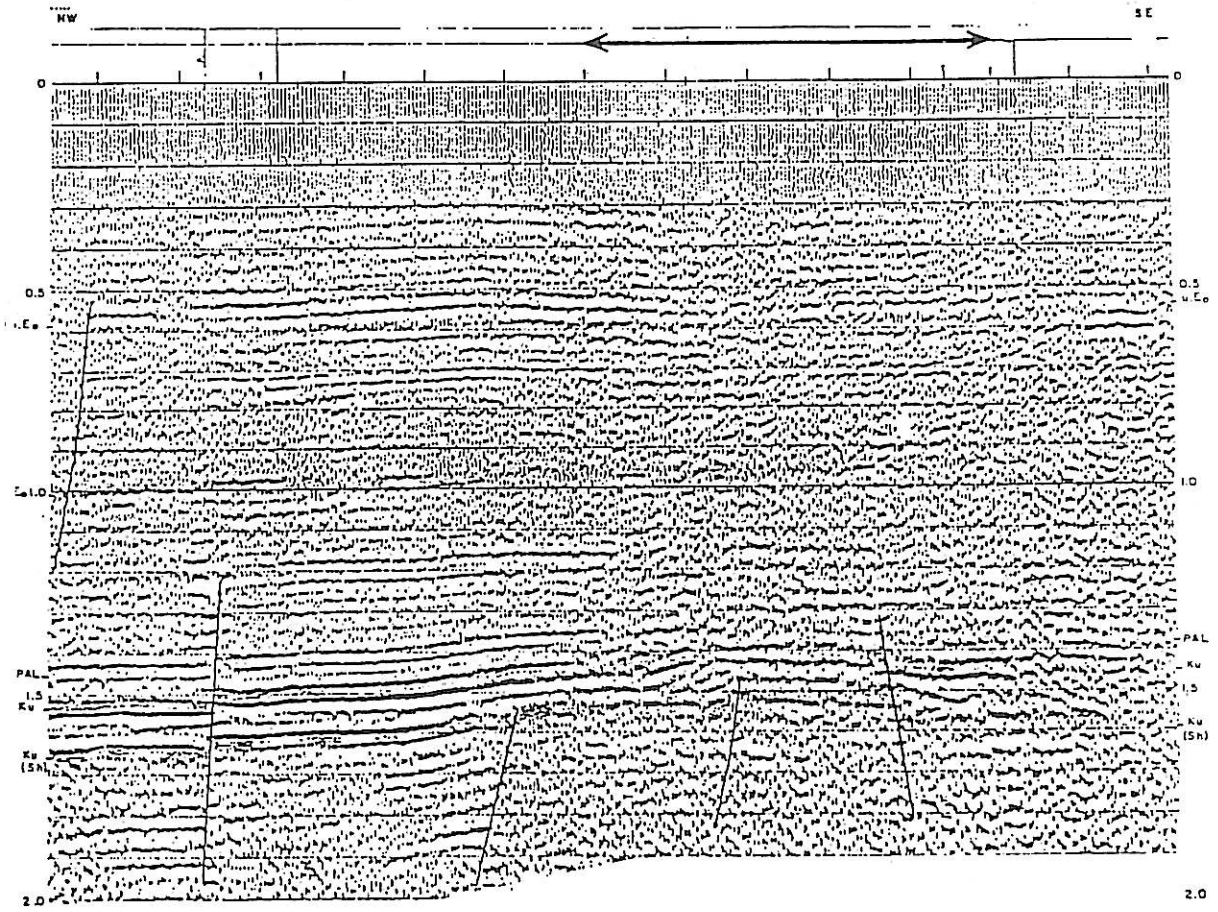


FIG. 12. Paleocene Structure in Amal Platform

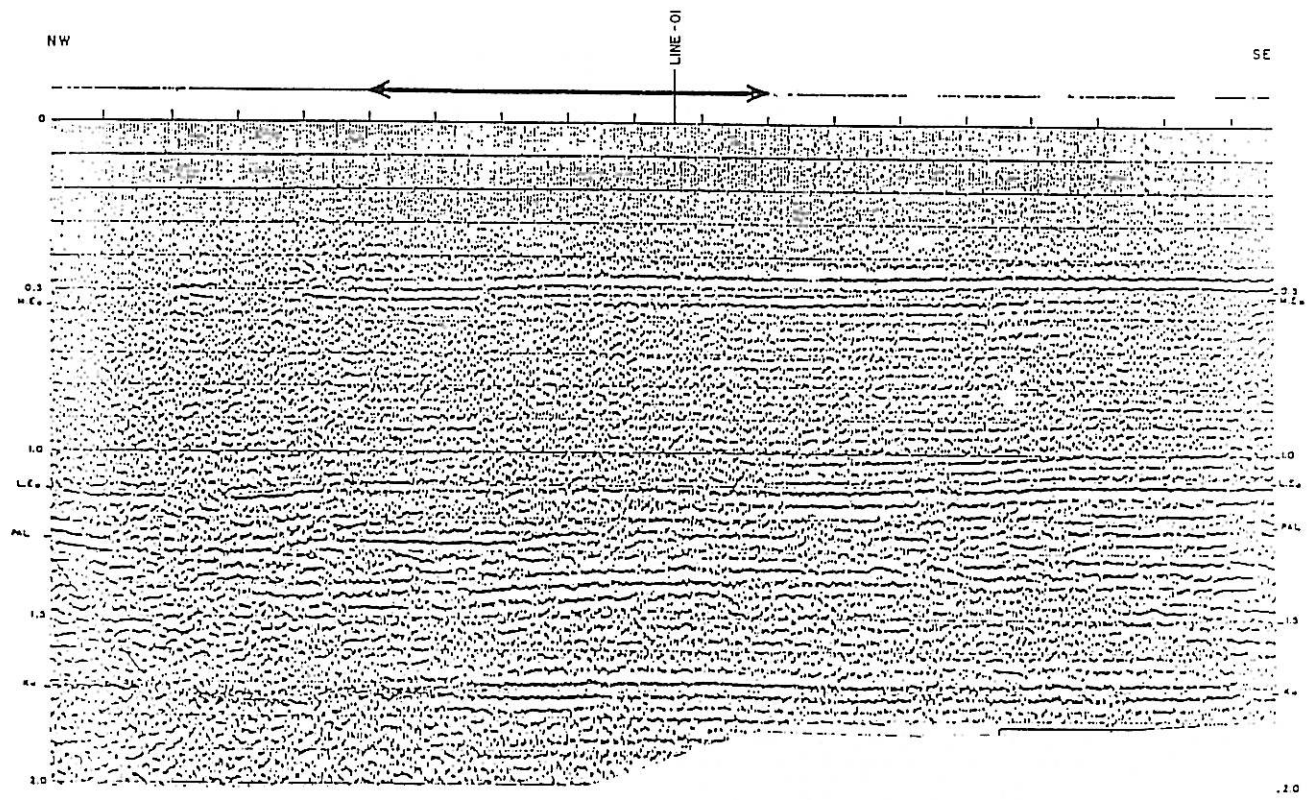


FIG. 13. A Lower Eocene Shoal Deposits in Antelat Trough

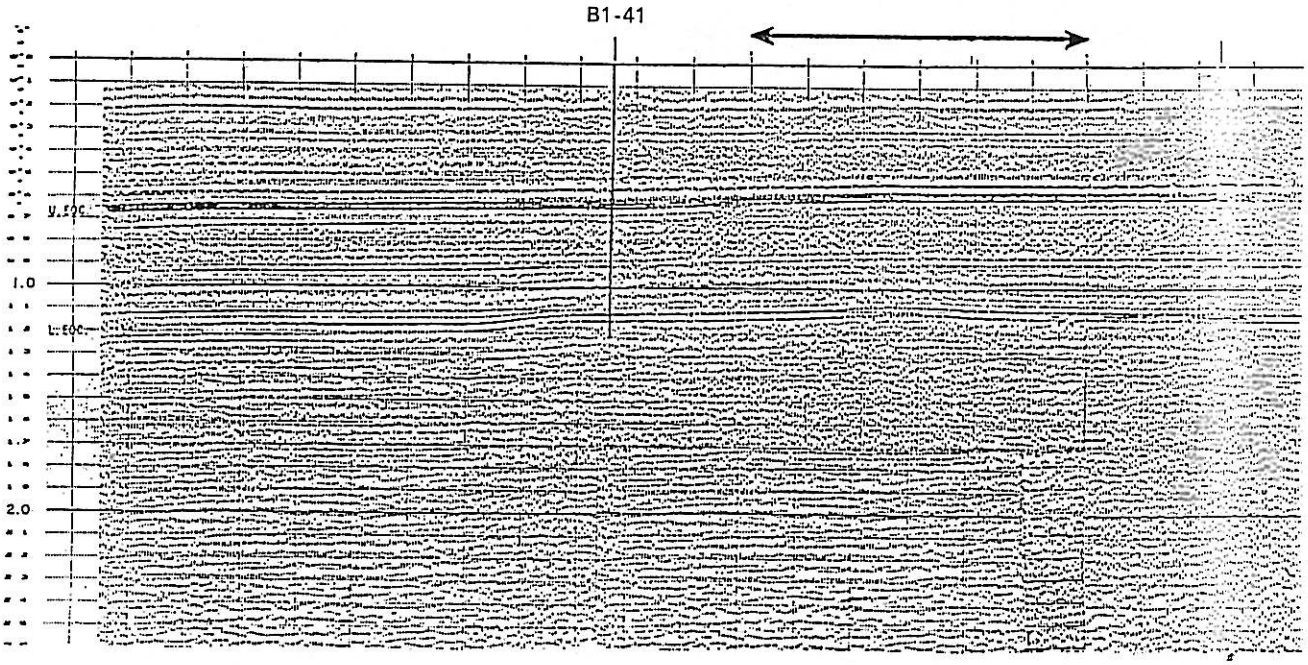


FIG. 14. Strati-Structural features in Antelat Trough

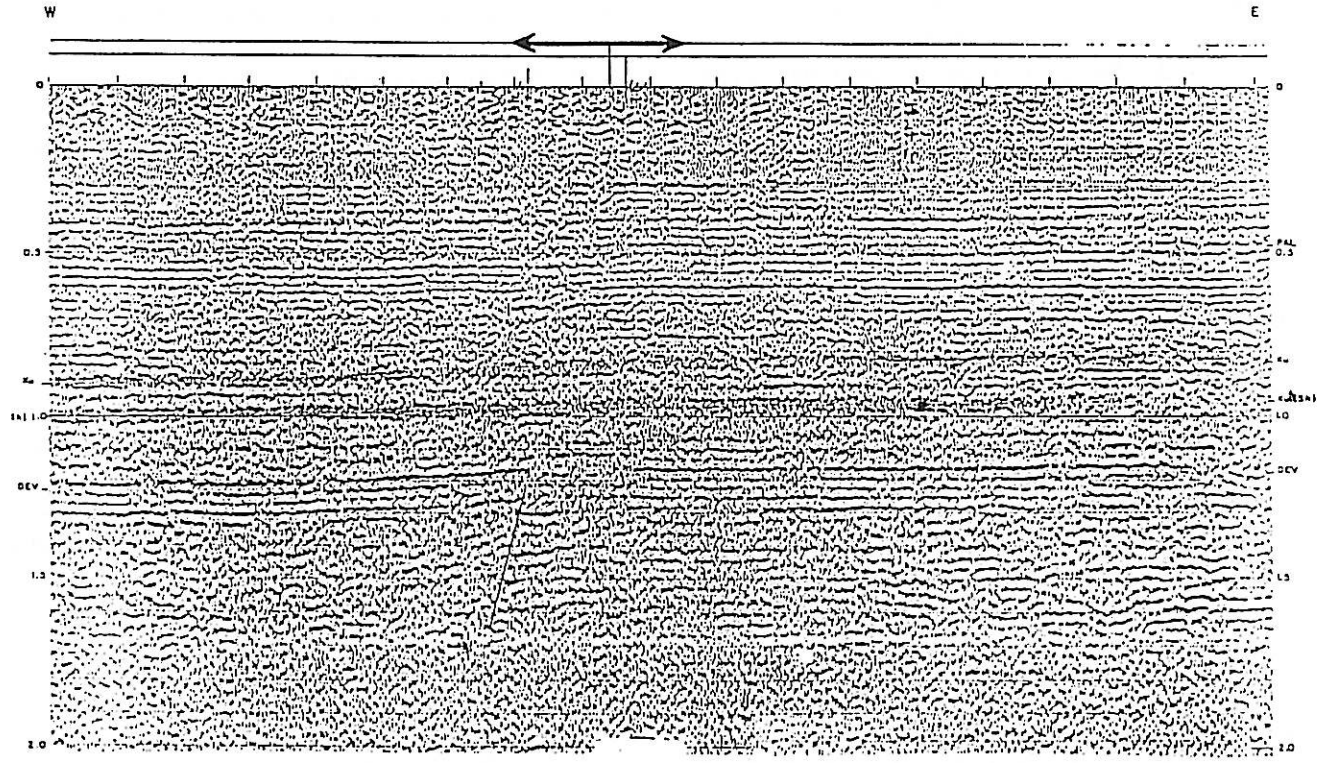


FIG. 15. A Stratigraphic feature on A Devonian Structure in Cyrenaica Platform

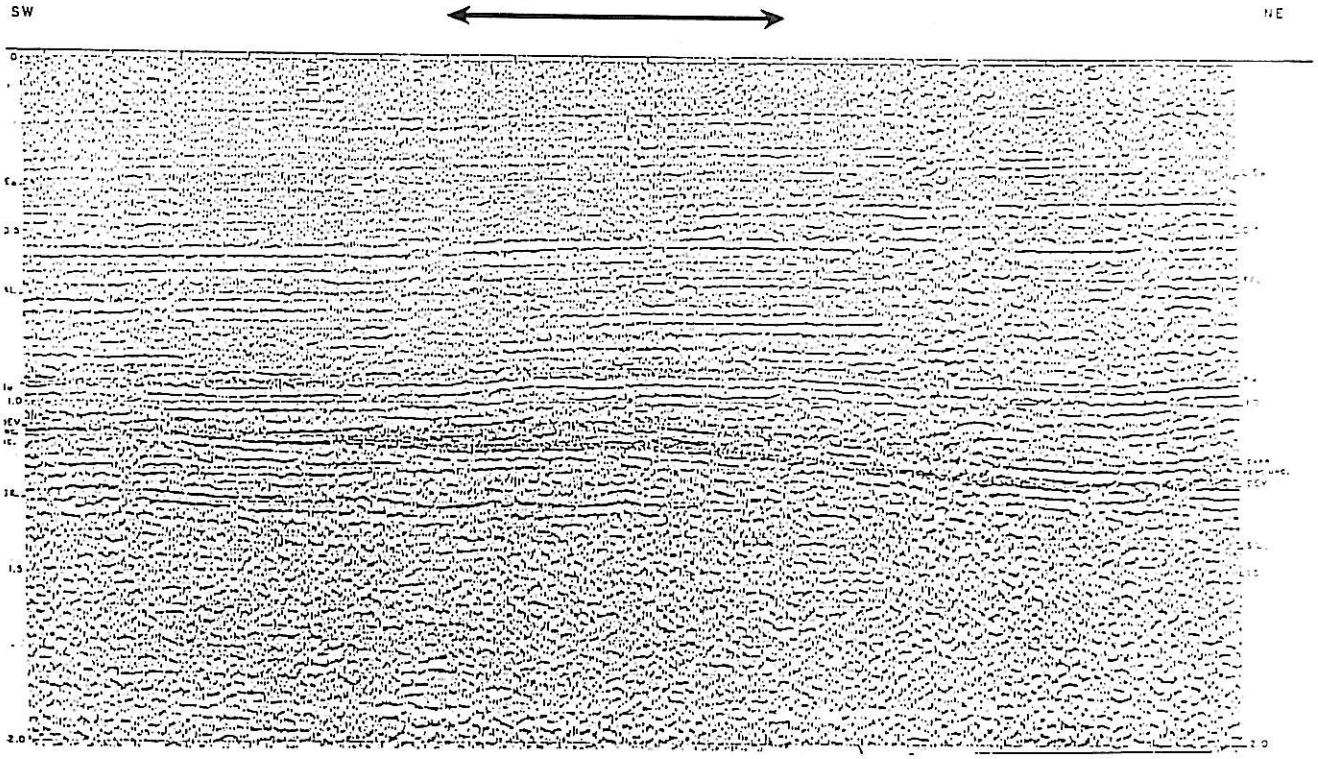


FIG. 16. A Carboniferous structure in Cyrenaica platform

be recognised a little left of the segment towards the southwest end. Such erosional hills and truncated beds are believed to be very prospective within the subcrop area of the Paleozoic formations of the region.

LOCATION OF OLD WELLS

The new seismic data was interpreted and the results were considered together with those of the old seismic data. The attempt shows that a number of wells drilled in the Cyrenaica region happen to be off-located, or were sited on the eroded crests of anticlines. Further, it is found that some wells did not go deep enough due to technical constraints. The examples here illustrate the inadequacy of the early seismic data. The failure of a majority of the wells drilled over the region is now found to be due to their improper locations based on the poor quality seismic sections of those times.

The seismic reflection section of an old line containing the well C1-46 later covered by modern means is presented in Fig. 17. It closely evidences the improper locaton of this well. The more encouraging structure is away from it towards the northeast part of the section. The well reportedly has strong oil-shows from the Tertiary, Mesozoic and Paleozoic formations. Another equally interesting case is presented in Fig. 18. The seismic section here pertains to a line reshot using modern techniques along an old line. The well B1-14 was located on the basis of the earlier seismic data. Note that the well penetrates actually the flank of the structure.

The location was deemed optimal based on seismic data. The re-assessment of seismic data thus consistently evidence the manner in which the wells have been off-located. The example also illustrate the greater efficiency that can be achieved with the modern seismic data acquisition and processing techniques.

HYDROCARBON PROSPECTIVITY

The hydrocarbon prospectivity of the north Cyrenaica region can be assessed based on the geological and drilling data integrated into the reflection seismic signatures of the subsurface structural setting. The results of the assessment so made are consolidated in Fig. 19.

Cyrenaica Platform

Mainly folded and faulted structural traps of Paleozoic age appear to be the promising hydrocarbon prospects of the province. Stratigraphic traps of the same age may exist along the Plaform margin including the Amal Platform. The Silurian and Devonian

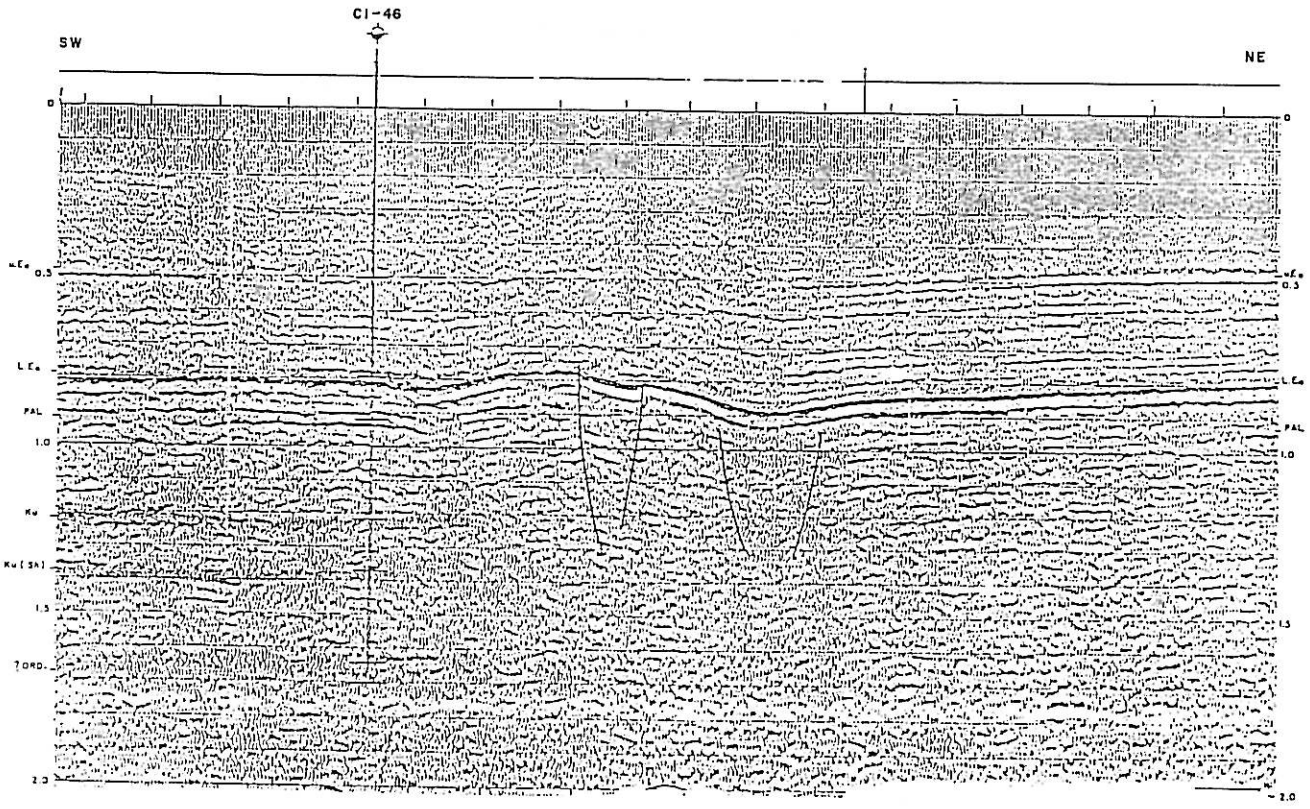


FIG. 17. A Lower Eocene structure in western margin of Cyrenaica Platform.

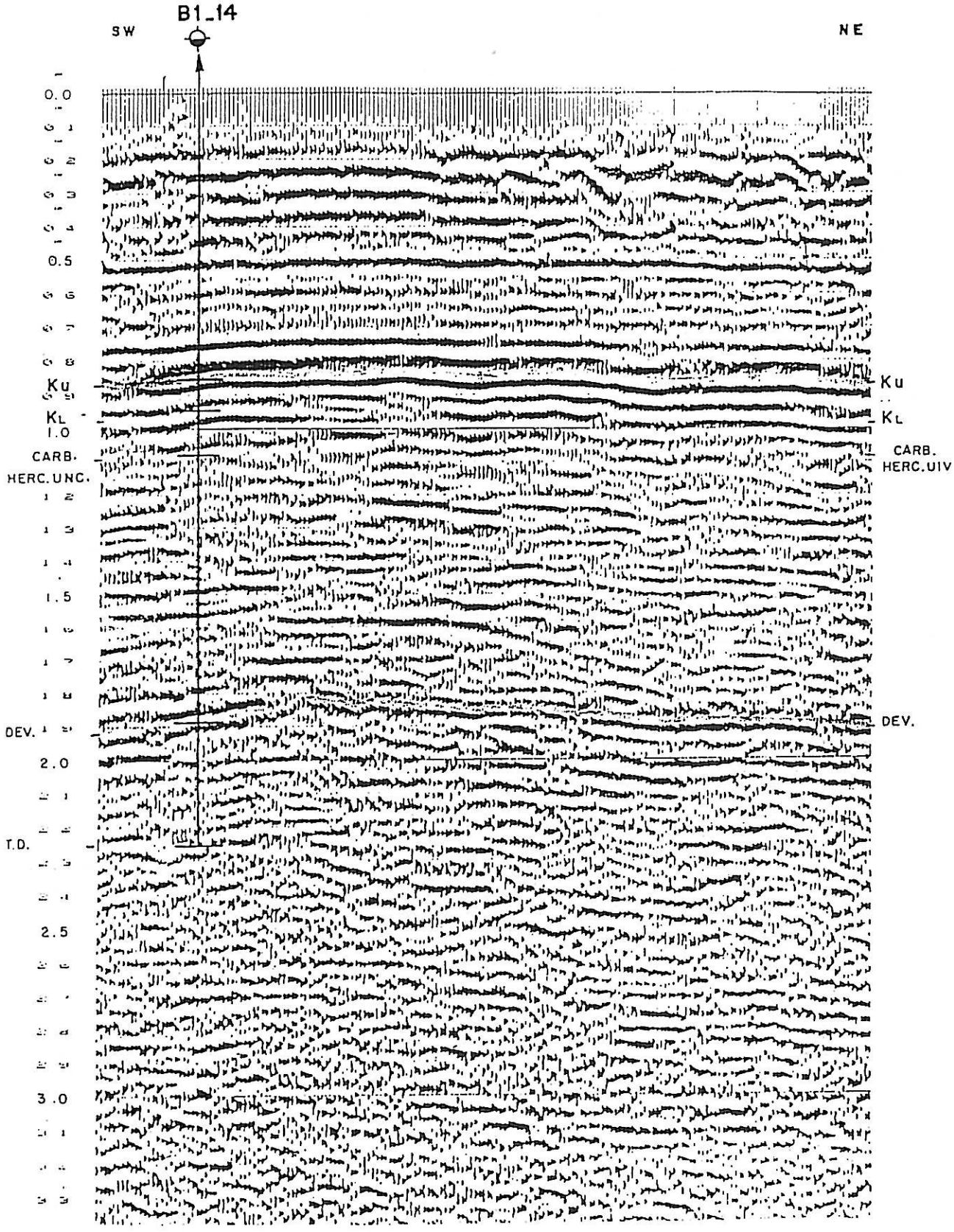


FIG. 18. Location of Well B1-14 on the Recently shot line Cyrenaica Platform.

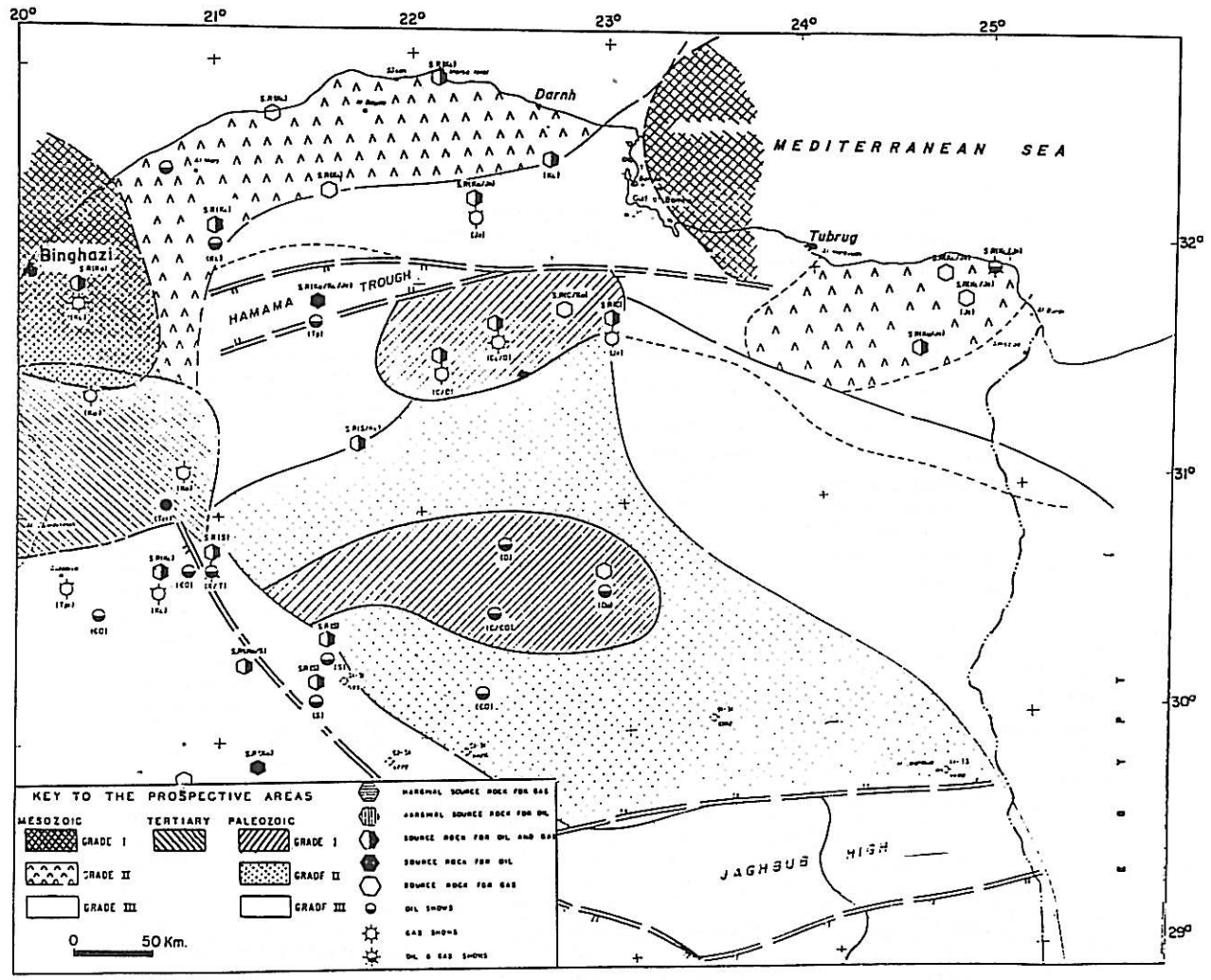


FIG. 19. Summary prospect map North Cyrenaica.

carboniferous shales are the source rocks of this tract. The sandstones ranging in age from Cambro-Ordovician to late Carboniferous have the potential to be the reservoir rocks. Some Mesozoic prospects are likely to be encountered along the eastern margin of the platform.

Al Jabal Al Akhdar Uplift and Marmarica Basin

The preserved, deep-seated, faulted and folded structures of Mesozoic age are the most promising traps of this geoelement. Less prospective are apparently the relatively highly uplifted structures since they are likely to be subjected to long periods of erosion, flushing or destruction of the hydrocarbon accumulations in such traps. Also the structures of Paleozoic age, not penetrated by drilling up to now, can be considered to be prospective. Jurassic, lower and upper Cretaceous shales constitute the main source rocks of this area. The Triassic shales reached in two wells have favourable source rock characteristics, Omer *et al.*, (1982). The thick shales of the Lower Cretaceous and compact evaporites as well as carbonates of the Upper Cretaceous are likely to be the main cap and seal rocks of the area.

Antelat and Hamama Trough

Structural and stratigraphic traps of Cretaceous and Tertiary age appear to be the main targets of this area. The Jurassic and Tertiary shales are the likely source rocks here Geochem (1982). The lower Cretaceous and Tertiary carbonates have the potential to be good reservoir rocks in this area.

Offshore

The upper Cretaceous structures situated to the north of Benghazi and Gulf of Bomba are very promising features in the offshore areas.

CONCLUSIONS

The above overview of the geologic and structural setting from the surface geologic and geophysical studies indicate that the hydrocarbon prospectivity of the north Cyrenaica region is quite promising. Significant level of oil and gas shows have been recorded in several wells of the region. The prospects include:

(a) the Paleozoic structural and stratigraphic features in the Cyrenaica Platform.
(b) the deep-seated faulted and folded structures of Mesozoic age in Al Jabal Al Akhdar Uplift and Marmarica Basin, and
(c) the Mesozoic and Tertiary traps in the Antelat and Hamama troughs.

Gravity and magnetic data have greatly helped in defining the major tectonic elements of the North Cyrenaica region. The former can be of additional use in inferring the Mesozoic structures.

ACKNOWLEDGEMENT

We would like to thank Dr. A. Mouzoghi J.V.D. General Manager and Mr. I. Baggar, the Exploration Manager of the National Oil Corporation for their encouragement and permission to present this paper at the Ninth Geophysical Convention, Turkey.

We also thank Mr. J. Molanazadeh, Dr. M. Salem, Dr. Bakbak and Dr. Busrewil for reading the manuscript and helpful comments on many aspects.

REFERENCES

BARR, F.T., 1968, Upper Cretaceous Stratigraphy of the Jabal Al Akhdar, Northern Cyrenaica. In; *Geology and Archaeology of Northern Cyrenaica, Libya.* F.T. Barr, ed., Petrol. Explor. Soc. Libya, p. 131–147, pls. 1–3, Tripoli.

CAVAGGION, M. and EL-ASHURI, O., 1986, *Revision of the Geology of Northern Cyrenaica,* (NOC. unpublished report)

CONANT, L.C. and GOUDARZI, G.H., 1967, Stratigraphic and tectonic framework of Libya. *Bull. Amer. Assoc. Petrol Geol.*, v. 51, no. 5, p. 719–730. Tulsa.

EL-ARNAUTI, A. and SHELMANI, M., 1985, Stratigraphic and Structural setting, N. Cyrenaica region (*Jour. Micropal. vol. 4, part 1, p. 1–10. eds.*) Thusu, B and Owens, B.

FRANCIS, M. and ISSAWI, B., 1977, Geological map of Libya 1:250.000, Sheet NH 34–2, SoluQ, Explanatory Booklet, Tripoli, I.R.C.

GOUDARZI, G.H., 1980, Structural Geology of Libya. In; *Third symposium on the Geology of Libya*, eds. M.J. Salem and M.T. Busrewil, vol. 3, p. 879–89.

KLEN, L., 1974, Geological map of Libya, 1:250.000, sheet: NI 34–14, Benghazi, Explanatory Booklet, Tripoli, I.R.C

OMAR, K.Z., FERJANI, K., KARKI, M.T., 1982, Geology and Hydrocarbon prospects of Cyrenaica, Jabal Al-Akhdar and related areas. (NOC unpublished report).

OZCICEK, B., 1986, A review of the seismic data quality in North Cyrenaica region, N.E. Libya (NOC unpublished report).

ROHLICH, P., 1974, Geological map of Libya, 1:250.000, sheet NI 34–15, Al Bayda. Explanatory Booklet Tripoli, I.R.C.

ROHLICH, P., 1978, Geological development of Jabal Al Akhdar, *Libya, Geol. Rundsch.* 67, 401–412.

ROHLICH, P., 1980, Tectonic development of Al Jabal Al Akhdar In; *Third Symposium on the Geology of Libya*, eds. M.J. Salem and M.T. Busrewil vol. 3, p. 923–931.

SWEDAN, A. and ISSAWI, B., 1977, Geological map of Libya, 1:250.000. sheet NH 34–4, Birhacheim. Explanatory Booklet, Tripoli, I.R.C.

ZERT, B., 1974, Geological map of Libya, 1:250.000, sheet NI 34–16, Darnah. Explanatory Booklet, Tripoli, I.R.C.

PRJ, Vol. 2 (January 1990); P. 42–56, 9 FIGS, 1 TABLE.

STRATIGRAPHY AND LITHOFACIES OF FARWAH GROUP AND ITS EQUIVALENT: OFFSHORE – NW LIBYA

A.M. Sbeta*

طبقيات وسحنات مجموعة فروة وما يعادلها بالمنطقة البحرية شمال غرب ليبيا

د. علي محمد سبيطة

مجموعة فروه والتكوينات الأخرى الموازية : تاجوراء وحلاب (عصر الأيوسين) المبكر ترسبت على الرف الأرضي المستقر شمال اللوحة الأفريقية.

بدأت عملية الترسب لمجموعة فروة بالسحنات (1، 2) من تكوين بلال في رفوف الهور المتوسط الداخلي حيث تقع هذه السحنات في المنطقة الجنوبية والجنوبية الغربية من منطقة الدراسة.

وعند منتصف منطقة الدراسة كان رف الهور المتوسط مناسباً لترسب السحنة رقم (3) لتكوين بلال. وفي إتجاه الشمال توجد سحنات تكوين حلاب في رف بحري عميق.

بعد تكوين بلال نجد تكويني تالجة وجيراني الذين ترسبا في ظروف بيئة ضحلة ومحجوزة في الجزء الجنوبي من الرف البحري، ولكن في وسط الرف كانت الظروف البيئية أحسن وملائمة لترسب صخور غنية بالحفريات (المنخربات الكبيرة)، وهذا يدل على بداية تعميق هذا الرف البحري.

إن زيادة عمق مياه هذا الرف البحري أدت إلى تكوين وتجميع ترسبات من الصخرية الغنية بالنيومولیت (تكوين جدير)، مغطية أولاً حافة الرف ثم إنتشرت إلى باقي أجزاء الرف، هذه الرسوبيات كان يحدها جنوبا سبخات بها صخور تكوين حلاب، ولكن نتيجة الظروف الملائمة المحلية حول البئر ف 1 – ن س 41 تكونت عند عقد مرجانية خلال عصر الأيوسين الأول.

بنهاية ترسيب صخور تكوين جدير حدث توقف في العملية الترسيبية، وهو حدث جيولوجي معروف ومؤكد، بعدها بدأت صخور تليل في الترسيب وإبتداء دورة إنحسار ترسيبية مع بداية عصر الأيوسين المتوسط والأعلى.

ABSTRACT

The Farwah Group of Early Eocene age and its equivalents Tajoura, Hallab Formations were deposited on the continental stable shelf along the northern margin of the cratonic African plate.

The deposition started with shallow water facies that range in depositional environment from inner to middle shelf lagoon, where the inner shelf lagoon setting is represented by facies belts 1 and 2 of Bilal Formation and occupy the southern and the southwest part of the shelf. In the centre the less restricted middle shelf lagoon prevailed where facies belt 3 of Bilal Formation was deposited. These facies grade into a deeper shelf environment in the north direction, as indicated by the deposition of the basinal facies of Hallab Formation.

This is followed by the sedimentation of Taljah and Jirani dolomite type facies, which indicate rather shallow and a more restricted condition and dominate the southern edge of the shelf; on the other hand, the centre and the north part of the shelf is characterized by a less restricted condition where sediments rich in large foraminiferas were very common, thus indicating the start of the transgression which began in the Lower Ypresian in the north and reached the south during the Upper Ypresian to Lutetian.

During that time, the increase of water depth initited a favourable condition for nummulite accumulation (Jdeir Formation) along the shelf margin, and later spreading over the rest of the shelf, forming a large, broad nummulitic bank with a bank-back condition, bordered by Sabkhah setting in the southern part of the shelf. These

*Geology Dept., Al-Fateh University, Tripoli, Libya, G.S.P.L.A.J.

nummulitic facies grade northward into basinal facies of Hallab Formation which dominate the deep basin off the shelf. Locally, within the back-bank, a bryozoan build-up and high energy facies developed, suggesting a local condition to such deposition existed near the F1-NC41 well during the Early Eocene time.

The termination of Late Palaeocene-Early Eocene cycle is marked by a widespread break in sedimentation that is widely recognised. This break between the Ypresian and Lutetian, signalled the beginning of the Middle and Upper Eocene regressive cycle. This cycle is represented by the shales and limestones of Tellil Group.

INTRODUCTION

The Farwah Group of late Paleocene to Early-Middle Eocene age is encountered in many wells drilled in the offshore Tarabulus basin. The nummulitic and dolomitic units of this group are the main target for oil exploration in the basin and they are the producing pay zone in the offshore Bouri Field.

This paper covers only part of the study conducted on the Eocene of the continental shelf offshore Tripoli and deals mainly with the Farwah Group and its lateral equivalent in the offshore.

The objective of this work is to define the different lithofacies, map their distribution in space and time and construct a model for the depositional environment of Early Eocene. This was achieved by detailed log analysis and correlation with synthesis of the available data of over 30 wells drilled in the offshore concessions, NW Libya (Fig. 1). Wilson (1975) Models for carbonate facies is used for interpreting the different carbonate setting.

GENERAL STRATIGRAPHY

The oldest rocks encountered in the offshore Tarabulus is Bir Al Ghanam Formation of Late Triassic to Middle Jurassic age and was reached at L1-137 well one of the southern most of the offshore wells just north of Sabratah. On the other hand, wells drilled in the onshore close to the coast, in the Jifarah, for example A1-38 well have penetrated over 8000 feet thick pre-Jurassic rocks that range in age from Late Permian to Middle Jurassic. The formations from base to top are Bir Al Jaja (Late Permian), Al Guidr (Early to Middle Triassic), Kurrush (Middle Triassic), Al Aziziyah (Middle to Late Triassic), Abu Shaybah (Late Triassic to Early Jurassic), Abu-Ghaylan (Late Triassic to Early Jurassic) and Bir Al Ghanam (Late Triassic to Middle Jurassic). These Formations probably extended northward into the pelagian block as suggested by Pitman et al (1981), and in general they exhibit lithologies and stratigraphic relationship similar to the well described units in the surface outcrop in Jabal Nefusah. However Bir Al Jaja and Al Guidr Formations are only known from the subsurface

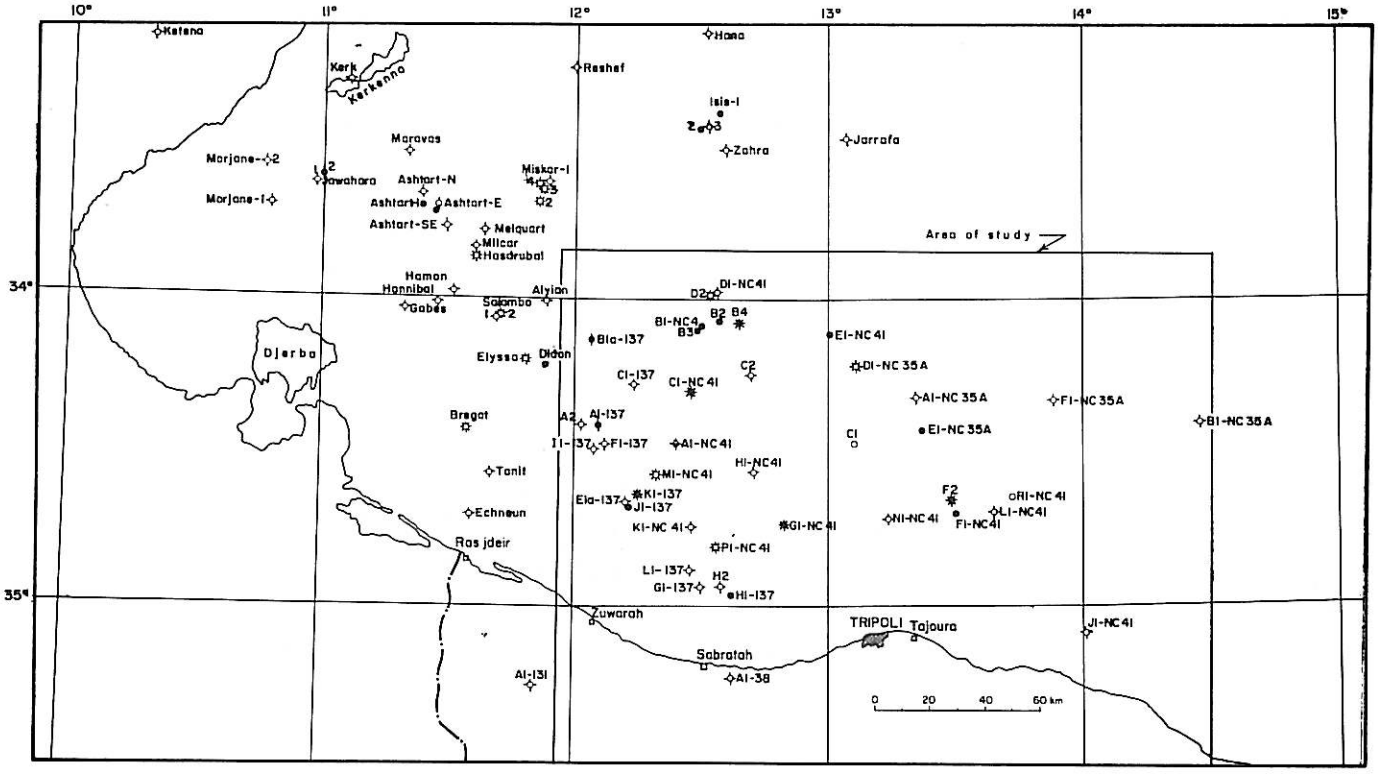


FIG. 1. Location Map and area of study.

of the onshore wells. Mesozoic rocks of Jabal Nafusah are well discussed and described in many recent publications that include: Hinnawy and Chesthiteve (1975); Fatmi et al (1978); Bannerjee (1980); Fatmi, *et al* (1980).

Busson 1967, Fourni 1978 publications cover the Cretaceous, Paleogene and Neogene of the Tunisian onshore and offshore stratigraphy. Hammuda et al 1985 dealt mainly with the stratigraphic nomenclature of the NW. offshore basin of Libya with correlation of the Tunisian sequence.

The Stratigraphy of the Early Eocene

No record of Eocene rocks are known from the northwestern onshore Libya (The Jifarah plain). On the other hand Eocene sequence corps out further inland in the Hamadah al Hamra and Hun Graben region. The only reported Eocene rocks are in the offshore Tarabulus basin. However Eocene rocks are reported from the onshore and offshore Tunisia by many authors (Bishop 1975, Founrie 1975.)

The general Eocene stratigraphy of the offshore Tarabulus basin and its correlation with the Tunisian section is summarized in Table 1.

During Late Cretaceous a major tectonic movement started and continued till Late Paleocene where most of the southern flank of the Tarabulus basin was uplifted and eroded; resulting in the erosion of some Upper Cretaceous and most of the Paleocene rocks in the south. This movement is less apparent in the north where Paleocene rocks are overlain by Lower Eocene sediments. Locally, Lower Eocene overlie volcanic rocks (Fig. 2).

The Early Eocene Transgression started from the north and advanced southward overstepping (onlapping) the Paleocene, Maastrichtian, Campanian and Santonian units (Fig. 2). According to work done by Aquitain using the nummulities the transgression started in the Upper Paleocene to Lower Ypresian in the north and reached the south during Upper Ypresian to Luthetian.

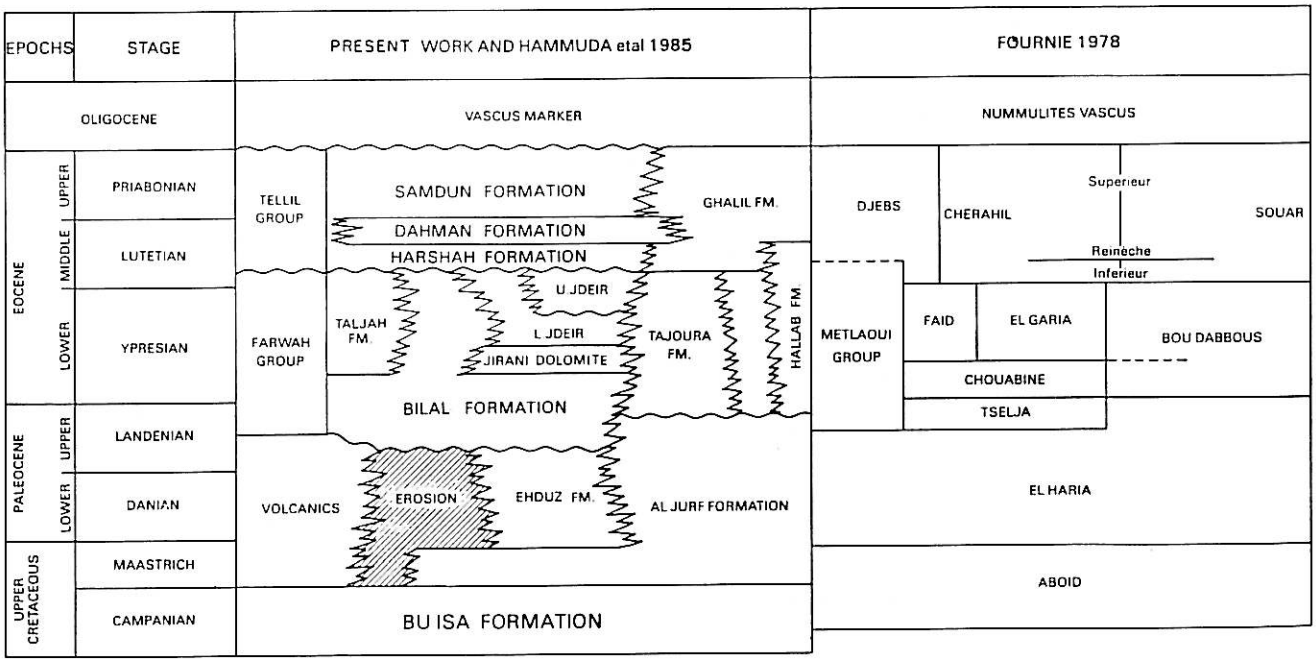
This followed by Middle and Late Eocene regression where restrictive shallow water shales, limestone and evaporite dominated most of the shelf. Northward, the shallow water facies grades into basinal facies of shale, marl and mudstone.

The Eocene as recognised in Tarabulus basin consist mainly of two major lithologic sequences. Farwah Group and Tellil Group which mainly cover the centre and west of the Basin. Ghalil and Hallab Formations are laterally equivalent to Farwah and Tellil, and occur mainly in the north and northeast. However towards the east, shallow water facies of Tajoura Formation are encountered in few wells. Here in this paper Farwah Group and its equivalent are dealt with.

Farwah Group

The Farwah Group, first introduced by Sbeta (1981) in a report presented to N.O.C. Stratigraphic committee which later incorporated with the other committee member work in their publication (1985) entitled "The Stratigraphic Nomenclature of the Northwestern Off-

Table 1 Correlation chart of the Eocene in the offshore N.W. Libya and Tunisia.



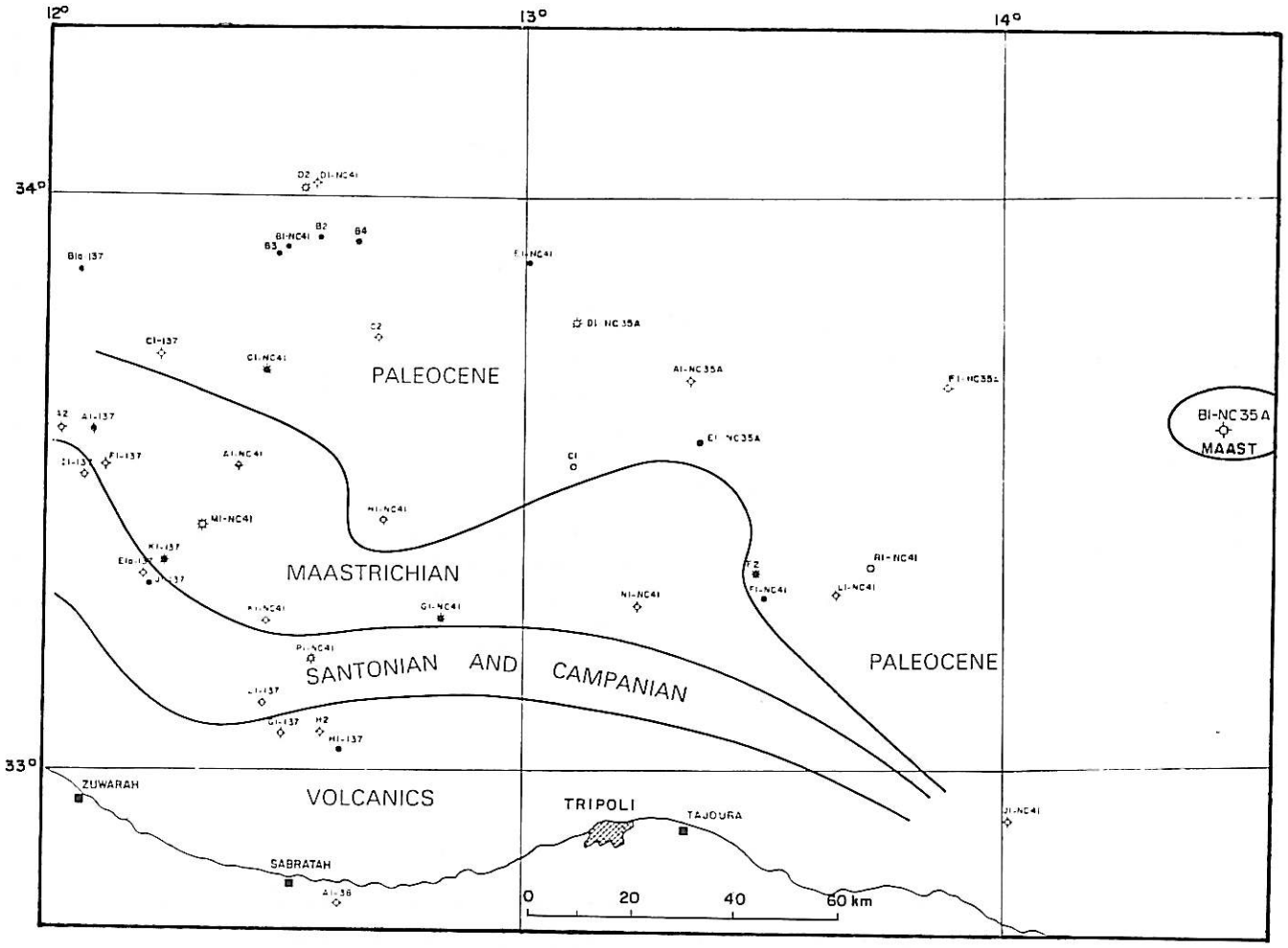


FIG. 2. Pre-Eocene Paleogeographic map.

shore Libya", edited by Hammuda O.S. *et al.* and published by ESSL. The new name introduced after it was apparent that correlation with the Tunisian section is not always possible or correct. Names used by oil company operators are not clearly defined and in many cases, arbitrary names were used from the Tunisian onshore section. On the other hand, the operators are emphasising the biostratigraphic aspect of the units rather than their lithostratigraphic character. For these reasons new formational names were introduced to cover the Libyan section of the Palagian block.

The Farawah Group that range in age from Landenian to Early Lutetian is composed of thick sequence of carbonate locally shalley, dolomitic and evaporitic. It is underlain by the Paleocene shale of Al-Jurf Formation in the northern sector. In the centre of the basin, limestone and shales of Bu Isa and Jamil Formations of Late Cretaceous unconfortably underlie the Farwah Group. In the far south, Farwah overlie volcanics. This unconformity is widely recognised, but it is less apparent in the north and east where the contact between Farwah Group and the underlying rocks of Paleocene is graditional.

The Farwah Group is conformably overlain by the regressive sequence of Tellil Group of shales and limestones and locally the pelagic facies of Ghalil Formation. Laterally towards the north and east Farwah Group passes into single Formation Tajoura or Hallab.

The thickness of Farwah Group range from over 1400 feet at H1-NC41 in the centre of the basin and thins towards the north and south, where it reaches only 7 feet at L1-137 and locally at M1-NC41 the Farwah Group is absent.

The Farwah Group consists of maximum three formations that are present in the northern section of concession NC41 (Fig. 3). They are in descending order: Jdeir Formation, Jirani Dolomite and Bilal Formation. In the southern edge of the basin Taljah Formation replaces Jdeir and Jirani Dolomite and grades into Bilal Formation, so that the Farwah sequence is Taljah Formation at the top and Bilal at the base. After detailed work two members recognised

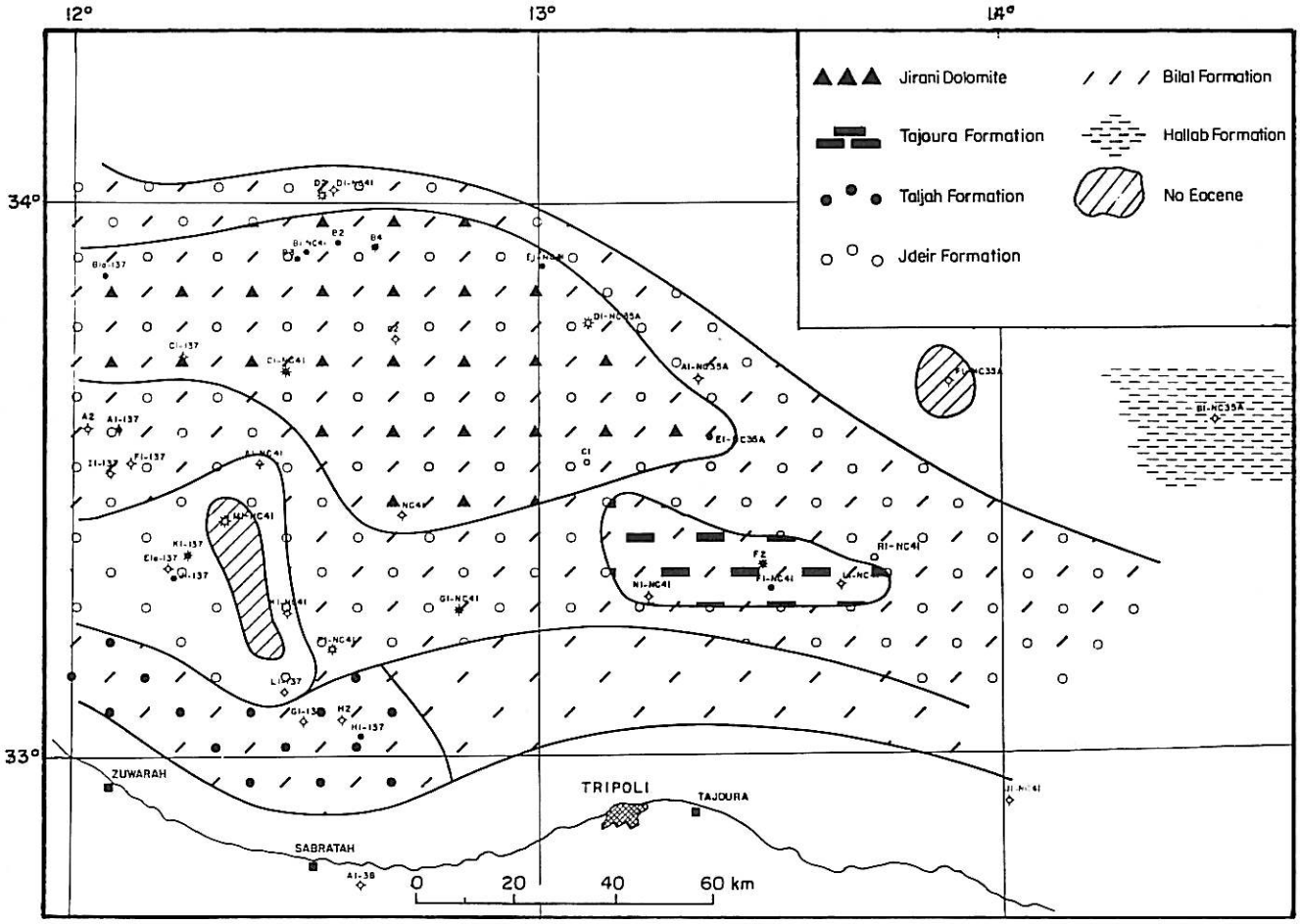


FIG. 3. Distribution of the different formation of Farwah Group; Tajoura and Hallab Formations.

within the Jdeir Formation, namely, Upper Member rich in Nummulite and Lower Member rich in Orbitolities and Alveolina.

These formations, within Farwah Group, are easily recognisable by their lithological and log character. They are mapable and widely distributed (Fig. 3).

Hallab Formation

The Hallab Formation is encountered in well B1-NC35A and interpreted to be widely spread in the eastern and northern sector of Tarabulus Basin. The Formation is mainly shale, marl, limestone and chalky limestone with abundant planktonic Forams and has a thickness of 160 feet.

The Hallab Formation at B1-NC35A unconfortably overlie Masstrichtian shallow water limestone and is overlain by deep platform shales of Ghalil. The faunal assemblage in Hallab indicate Early to Middle Eocene age and is considered to be lateral equivalent to Tajoura Formation and Farwah Group and perhaps equivalent to Bou Dabbous Formation in the Tunisian section.

Tajoura Formation

Introduction by Sbeta (1981) for the shallow water facies of bryozoan and oolitic limestone that was encountered at F1-NC41. It is over 570 feet thick and is overlain by the shales and carbonates of Tellil Group and underlain by the Paleocene carbonate of Al-Jurf Formation. The Tajoura Formation is also encountered at L1, F2 and N1-NC41. The stratigraphyic position of Tajoura suggests Early Eocene age and could be correlated with Hallab Formation in the east and probably with Jdeir and Jirani Formations in the centre.

LITHOFACIES ANALYSIS OF FARWAH GROUP (LATE PALEOCENE TO EARLY EOCENE)

Eleven wells from concessions NC41 and 137 have been examined in detail, using all available information. Data from other drilled wells are also consulted and analysed. Consequently several lithofacies belts are recognised within each formtion and their thick-

ness and lateral distribution are recorded in isopack and lithofacies map.

Lithofacies and Environment of Bilal Formation

Bilal Formation is widely distributed and present in most of the studied area except in the area between L1-137 and K1-137 and in the vicinity of J1-NC41 area and F1-NC35A (Fig. 4). It lies at the base of Farwah Group and normally is overlain either by Taljah Formation in the south or Jirani dolomite or Jdeir Formation in the centre and north of the area. Generally it is unconfortably underlain either by Paleocene or older rocks.

The formation shows great variation in thickness, the thickest section is at H1 and C2 NC41 which is over 500 feet, however, the formation thins to about 33 feet at II-137 and 50 feet at G1-137 in the southern and western parts respectively (Fig. 4). It also thins towards the east and the north. The depositional axes run along NW-SE direction from C1-NC41 to C1-NC35A. Bilal Formation is missing in the southwestern part along a line from G1-NC41 and is replaced either by Jdeir Formation or Tajoura Formation. In the southwestern part Bilal is missing due mainly to erosion and/or lithofacies change.

Bilal Formation shows appreciable variation in sedimentary lithofacies and generally comprise a mixture of lithologies that include mudstone, wackestone, packstone, shale, marl, dolomite, anhydrite, sandstone, conglomerate and phosphatic horizons.

By closer examination of these lithologies and their distribution, the following major lithofacies belts are recognised (Fig. 4).

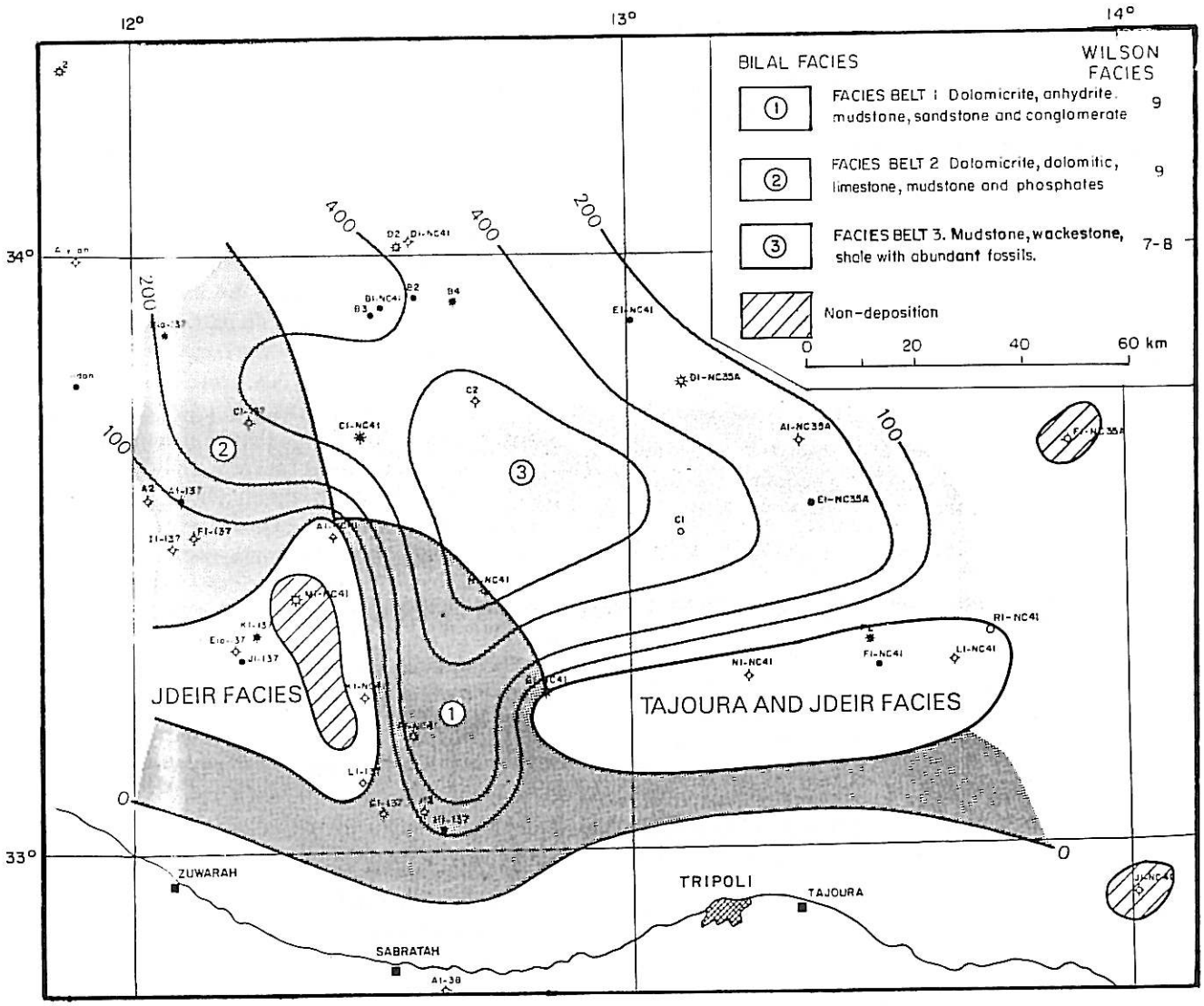


FIG. 4. Farwah Group. facies and thickness of Bilal Formation.

Lithofacies Belt 1

The lithofacies belt 1 composed of, in order of importance, dolomicrite, anhydrite, mudstone, sandstone and conglomerate at H1 and NC41 levels of phosphatic rocks occur and shale locally dominate at P1-NC41.

This lithofacies becomes very sandy and conglomeratic at H2-137 with levels of grey sandy dolomicrite and streaks of bitumonous shale; thin beds of anhydrite also common. At the base polygenic conglomerate becomes the dominant lithology. At H1-137 and G1-137, this lithofacies is represented by sandy dolomicrite, dolomicrosparite whitish light tan locally silty. In places coarse sandstone level occur and few beds of shale and anhydrite are observed. Northward, this lithofacies becomes more shaley with thin beds of wackestone-packstone and locally dolomitic and slightly sandy. In the transition area between lithofacies belt 1 and 3, few phosphatic beds occur at G1 and H1-NC41.

Lithofacies 1 is encountered in the wells drilled in southern part of concession 137 and is located between two area of non-deposition of Bilal Formation and perhaps extends eastward and westward along the present shoreline. This lithofacies is interpreted to represent shoreline lithofacies of sabkha and alluvial fan setting.

Lithofacies Belt 2

This lithofacies consists predominantly of dolomicrite, dolomitic limestone and mudstone with levels of phosphatic rocks. Shales, marls, and sandy horizons are subordinate, locally thin beds of anhydrite occur. Lithofacies 2 become more dolomitic at A2 and I1-137 wells with grey green silty argillaceous mudstone, at A1-137 well thin beds of sandy packstone are observed. However, at Bla-137 and C1-137 this lithofacies is found to contain wackestone, abundant grey brownish shale and marl interbedded with anhydrite. At C1-137 well sand, grey brownish shale and red silty marl with trace of lignite dominate this lithofacies.

Lithofacies 2 is reported from the wells drilled in the NW part of concession 137. It is interpreted to be deposited in shallow water shoreline between supratidal to intertidal with less restriction than facies 1. In lithofacies 1 anhydrite is dominant whereas facies 2 the phosphatic level is common. At lithofacies 2 the coarse clastic is less important than in the case of facies 1, though sandy and silty levels do occur. Lithofacies 2 is only 23 feet thick at I1-137 well and thickness northward in the direction of Bla-137 and C1-137 wells. South of I1-137 well no Bilal lithofacies is present, but grades into the Jdeir type lithofacies as shown in Fig. (4).

Lithofacies Belt 3

It consisted mostly of brown to dark brown mudstone, wackestone interbedded with shale and locally becomes chalky, pyritic and gluaconitic. At D2 and B2-NC41 wells marl with planktonic foraminifera appear. This lithofacies dominate the rest of NC41 concession (Fig. 4). It is interpreted to be probably deposited at shelf lagoon that is slightly restricted southward and becomes more open northward with the influence of deep shelf and perhaps deep marine conditions as indicated by the presence of planktonic marly facies at D2 and B2-NC41 wells.

This lithofacies is the most dominant and covers the centre and the northern sector of the shelf. It reaches a thickness of over 500 feet at C2-NC41 and thins towards the east and south.

Depositional Environments of Bilal Formation

In general, Bilal lithofacies are deposited in arid shallow water shelf lagoon which is very restricted in the south, with the deposition of dolomicrite, anhydrite, sandstone and conglomerate. The source of such coarse clastic perhaps is an alluvial fan or fluvial deposits from the close by land where a large channel is located just east of the positive area that border lithofacies 1. The restricted lithofacies 1 is suggested also to occur parallel to the Eocene shoreline.

The Bilal lithofacies becomes slightly less restricted in the northwest part, where dolomicrite and phosphorite rocks are common, and only locally anhydrite beds are observed. On the other hand, Bilal lithofacies becomes less restricted with marine condition in the centre and north where wackestone and packstone lithofacies with abundant skeletal fragments and small formas are common. A deeper shalf environment perhaps border the shelf lagoon north of D2-NC41.

Two large areas of Bilal non-deposition is interpreted to occur in the east and west of the southern edge of the basin leaving a corridor where lithofacies 1 occur. In the eastern section Bilal is perhaps partially replaced by either Jdeir or Tajoura formations. Bilal is missing in the western section due to the erosion of most of the Farwah Group.

Lithofacies and Environment of Jirani Dolomite

Two main facies are recognised:

1. Dolomatized wackestone/mudstone with beds of wackestone and dolomicrite.
2. Dolomatized wackestone and dolomicrite with anhydrite nodules.

The thickest section of this formation is along a line extending from C1-NC35A to Bla-137 wells and rea-

ches a maximum thickness of over 500 feet near C2-NC41 (Fig. 5).

Lithofacies Belt 1

It is the most widely recognised lithofacies and it is of interbedded mudstone dolomitic mudstone, dolomicrosparite and dolosparite with levels of wackestone and mudstone that become common at the base. The limestone is light grey to brown slightly argillaceous, the dolomite is light grey to light brown micro-crystalline, vuggy with good intercrystalline porposity. Locally at E1-NC25A dolomitic limestone beds have nummulite and other fossil fragments. This lithofacies show some variation where phosphatic and pelycepods beds are present at Bla-137 and peloidal lithofacies at E1-NC35A and C1-137.

At B2-NC41 the dolomite is very finely crystalline with some kaolinitic clays and black laminea. Sometimes abundant burrows and birdseye structures are observed and fossils are absent. The dolomite is interbedded with peloidal and skeletal wackestone with few miliolid, ostracods and algae. Similar facies are encountered at B1 and B3-NC41, but the dolomite become coarse, friable and argillaceous at C1-NC41.

Lithofacies Belt 2

This lithofacies is described from three wells only C1-137, C1 and H1-NC41. Lithofacies 2 are not much different from lithofacies 1, but it is characterized by the occurrence of anhydrites, silty and sandy horizons and varicoloured silty marls with poorly fossilliferous wackestone.

At H1-NC41 this lithofacies is light brown to grey dolomicrosparite to dolosparite with beds of poorly fossilliferous mudstones and wackestones and few horizons of anhydrites, at C1-NC41 the sandy, silty varicoloured marly levels appear with trace of anhydrite. The upper beds of C1-137 have mainly mudstones and wakestones which is locally peloidal, whereas the lower and thicker section is mainly dolomicrosparite interbedded with anhydrites, mudstones, dolomicrites with few beds of wackestones.

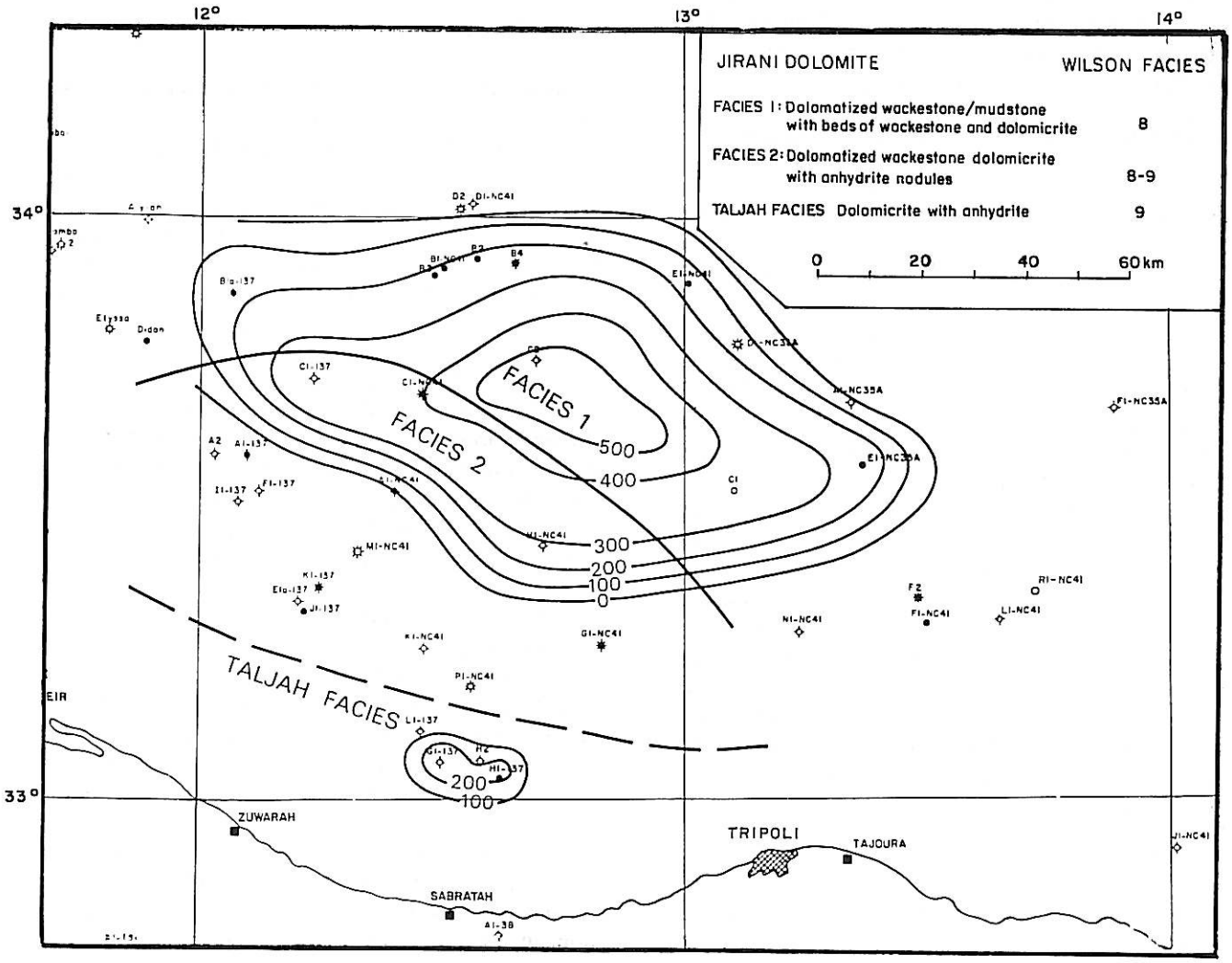


FIG. 5. Farwah Group. facies and thickness of Jirani and Taljah.

Depositional Environment of Jirani Dolomite

From Fig. 5 one can see that facies 1 of Jirani Dolomite are present in wells drilled in the northern and northwestern section of Tarabulus basin, where the middle shelf lagoon condition prevailed which is probably slightly restricted with intermittent inner shelf condition affecting the area that dominates the southern part of the basin.

The wackestone lithofacies with skeletal fragments of pelycepods, nummulite and locally milioloid and ostracods would suggest that lithofacies 1 is deposited in the slightly sometimes restricted middle shelf lagoon that later uplifted and dolomitized as the presence of kolinitic clays, phosphates and dolomite would suggest. The occurence within this lithofacies of supratidal dolomite, birdseye and perhaps stromatolite indicate the fluctuation of sea level and the proximity of inner shelf condition which actually border this middle shelf condition in the landward direction.

As for the lithofacies 2 which dominate the basin, it is interpreted to be deposited in the inner shelf condition in semi-arid to arid climate where anhydrite, dolomite and mudstone lithofacies would predominate. This lithofacies are located not far from land as the presence of sandy and silty level would suggest.

Lithofacies and Enviromnent of Taljah Formation

These lithofacies are present only at 3 wells in the southern edge of the shelf (Fig. 5). The wells are H1, H2 and G1-137 and the section is mostly composed of grey to beige dolomicrite with thin beds of white crystalline anhydrite. At H2 and H1 thin streaks of bitumenous shale occur within the dolomite beds and the anhydrite is nodular at H1-137. The lithofacies becomes argillaceous with whitish, light beige, light brown mudstone, locally sandy at G2-137. They range in thickness from 165 feet at G1-137 to 125 feet at H1-137 and only 84 feet at H2-137.

Taljah lithofacies are interpreted as shoreline sediments of the inner shelf environment that border the Lower Eocene rocks of Jirani, lower and upper Jdeir lithofacies. The Taljah Formation lithofacies are deposited in sabkha and supratidal conditions where stromatolite horizons with birdseye structures and mudstone were laid down and then penecontamporanously dolomatized. The hypersaline condition initiate the deposition of evaporites which made it intolerable from marine life. In addition, the presence of silty and sandy facies suggest proximity to land.

Lithofacies of Jdeir Formation

The shallow water carbonates of Jdeir is characterized by two major lithofacies suites which correspond to the two members of the Jdeir Formation; Lower Jdeir and Upper Jdeir. The Lower Jdeir lithofacies consists mainly of large foraminifers and skeletal wackestone and packstone and the Upper Jdeir is mainly nummulitic packstone to grainstone. These two major lithofacies suites show some variation in thickness and sedimentary lithofacies (Fig. 6).

The Jdeir Formation is encountered in most of the wells drilled in Tarabulus basin and the Isopach Map (Fig. 6) shows an over 600 feet thick lithofacies of Jdeir deposited along a line extending from D2-NC41 to A1-NC35A with a gentle gradual thinning in the west and southwest direction, suggesting the existence of the gentle sloping shelf during the deposition of Jdeir Formation. However, Jdeir lithofacies thins towards the north, northeast an locally south of A1-NC35A in a rather abrupt way. The local thick sequence of Jdeir represent the margin of the bank that extended along the shelf margin at the early Eocene time, where it is suggested a higher rate of sedimentation dominated the shelf bank. The possible sudden thinning, in the north direction, perhaps indicate a lower rate of sedimentation for the basinal mudstone, shale and marls that dominate the shelf margin.

Lower Jdeir Lithofacies (Fig. 7)

These lithofacies are mainly wackestone and wackestone packstone grading to mudstone and in places argillaceous, chalky an dolomitic and range in colour from light brown to dark brown. The Lower Jdeir lithofacies is characterized by the abunant occurrence of large foraminifers that include Alveolina, Orbitolite, Discocyclina and locally small forminifers, Miliolid and Ostracods. Fragments of pelecepods, gastropods echinoids and in places traces of nummulite debris are present.

These lithofacies show some sedimentological variation as it becomes chalky mudstone argillaceous and slightly dolomitic at C1-137 well. It grades to foraminifers packstone where large foraminifers are abundant including some nummulites at A1-NC35A. In many wells wackestone/packstone lithofacies is the dominant one with variable percentage of large foraminifers and skeletal debris of different fossils. At C1-NC35A, 154 feet of foraminifers packstone and wackestone is encountered and at D1-NC35A over 250 feet of skeletal packstone wackestone lithofacies occur interbedded with thin beds of chalky mudstone. This mudstone facies is more common at the northern edge replacing the packstone at E1 and B2-NC41 wells and the lower Jdeir lithofacies becomes dolomitic at C1-NC41 and peloidal at B2-NC41 well.

The Lower Jdeir lithofacies occur in most wells in the central part of the basin and generally passes into restricted near shore facies of Bilal and Taljah Formations in the southwest and south direction or into the high energy and reefoidal lithofacies of Tajoura Formation in the southeast direction (Fig. 7). Towards the

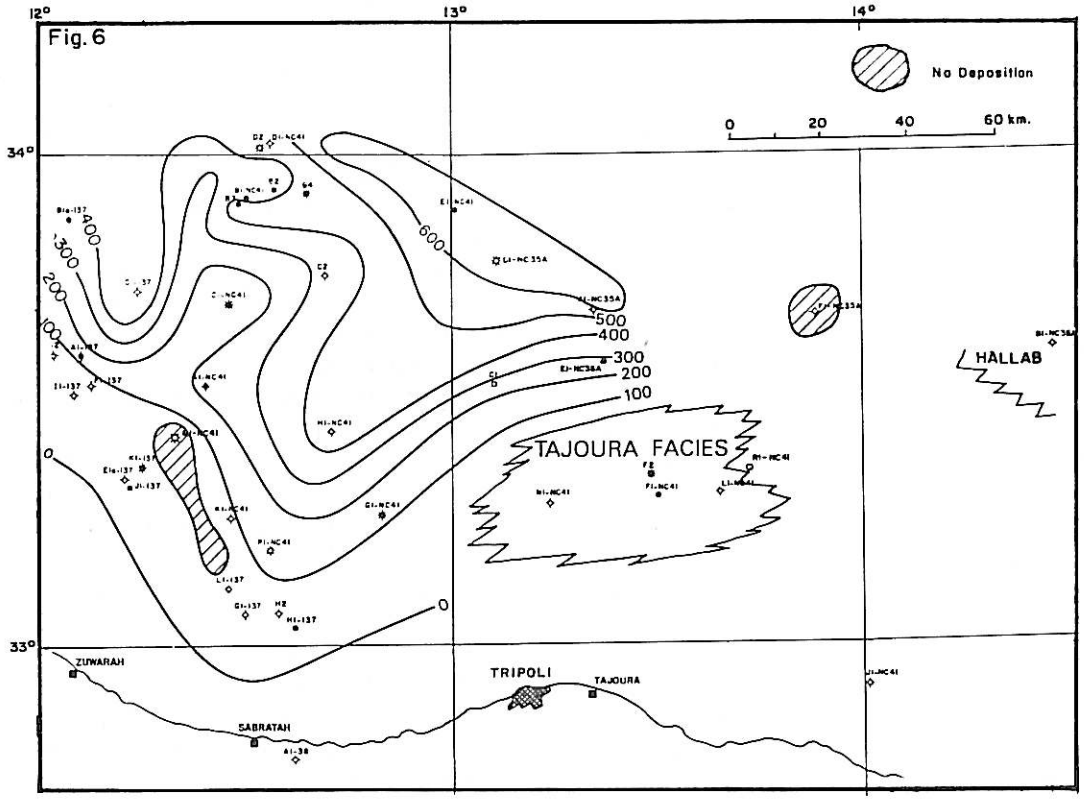


FIG. 6. Isopach map of Jdeir Formation.

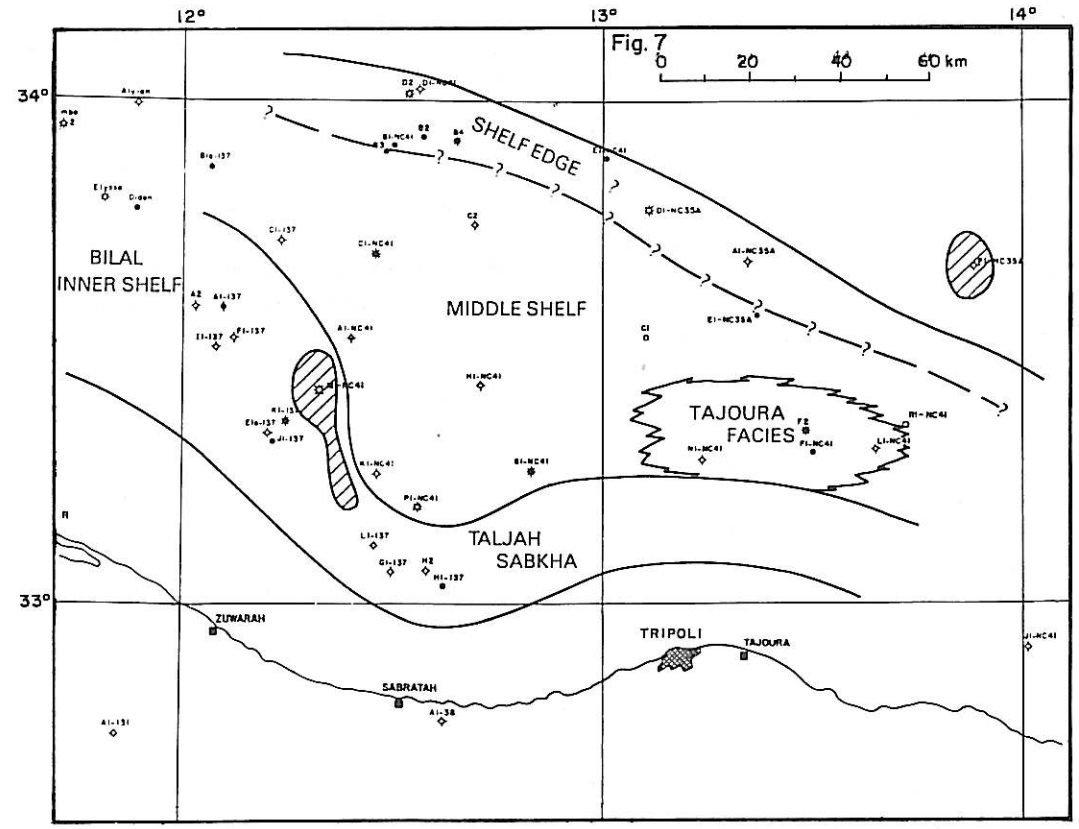


FIG. 7. Farwah Group. facies and environment of Lower Jdeir.

north and northeast it changes to the deep water lithofacies of Hallab and Ghalil Formations.

Normally, these lithofacies represent the Lower Jdeir Member but there are a few wells where the Upper Jdeir Members are missing. Therefore the Jdeir Formation consists mainly of lithofacies of Lower Jdeir Member only in G1, P1, K1 and R1-NC41 wells.

Environment

The lithofacies and fauna of the Lower Jdeir Member suggest a deposition in broad shallow water carbonate shelf which is dominated by middle shelf lagoon. In the slightly restricted middle shelf lagoon, the pelecepods are the major skeletal components. In the middle shelf lagoon, the dominant lithofacies is large foraminifers wackestone-packstone, where Alveolina, Orbitolites, Discocyclina with skeletal debris of echinoids, pelecepods and algae are very common.

These shelf lagoon lithofacies of the middle shelf probably represent back-bank setting during lower Jdeir deposition, with foraminifers/pelecepods bank, probably developed along the shelf edge extending from D1 and B1-NC41 wells to E1-NC41 wells to E1-NC41 and A1-NC35A. This bank and back-bank perhaps represent the substratum for the later nummulite bank system to be developed during Upper Jdeir deposition. If the foraminifers/pelecepods bank did exist this will result in some restriction behind the bank thus explaining the presence of some restricted lagoon and sabkha type lithofacies in the wells located at the southern edge of the shelf. The other explanation is the restriction in the southern edge of the shelf is as a result of a damping effect of the vast expanse of shallow waters of this board carbonate shelf that prevailed during the deposition of the Lower Jdeir Member (Fig. 7).

However, the Lower Jdeir lithofacies continued to be deposited in the southern edge of the shelf while the nummulitic bank lithofacies of the Upper Jdeir begin to develop along the north margin of this shelf which makes the Lower Jdeir lithofacies in the south equivalent to the Upper Jdeir lithofacies in the north.

The Lower Jdeir lithofacies are laid down in shelf lagoon of water depth that range from 10 to 50 m, as recent work on large foraminifers indicated that they generally live in water of such a depth in tropical to sub-tropical shelf water and they are especially abundant in the reef environment as the case of the Great Barrier Reef Hottinger (1977). For example, Orbitolites lives in warm calm seas among seaweeds and down to 50 m depth, and Alveolinids seldom are a major part of most foraminifers faunas in shallower waters of 50 to 15 m deep and they are most common in water depth from 25 m to about 80 m, and they prefer quiet condition and fine-grained soft sediments.

Upper Jdeir lithofacies (Fig. 8)

The Upper Jdeir lithofacies are found to contain mainly nummulitic lithofacies that range from packstone to grainstone locally wackestone with mudstone interbeds. It is beige to cream, light tan in colour, porous, vuggy sometimes chalky. The main constituents of these lithofacies are nummulite large and small and they are *Nummulite rollandi*, *N. irregularis* and *N. gizaensis*. Locally at B2 and E1-NC41 Assilina and Operculina are present. However, nummulites tend to be less significant in the lower beds. Fragments of gastropods pelecepods, echinoids and algae also occur in different proportions. Locally at A1-NC35A broken fragments of nummulite and echinoids and pelecepods dominate these lithofacies. A1-NC41 it appears that pelecepods and gastropods debris become rather important but nummulitis still very abundant and prolific and cores from this well show that many nummulite are oriented towards the horizontal plane.

The nummulitic packstone-grainstone facies of the Upper Jdeir Member are widespread in the study area and they are the main lithofacies of the member in most of the well drilled in the offshore. In concession 137 these lithofacies are found in B1a, A2 and C1 wells and in concession NC41 they dominate B1, B2, E1, D1 wells and E1, C1, D1 and A1 in concession NC35A. These high energy lithofacies grades to wackestone/packstone and wackstone at C1, A1 and H1-NC41 and A1-137 locally at F1-137 changes into wackestone/mudstone facies. The thickness of Upper Jdeir lithofacies vary greatly from one well to another for example, they are 60 feet at B1-NC41 and 230 feet at B2-NC41 and they are only 6 km apart. Similarly, they are 88 feet at E1-NC41,257 feet at D1-NC35A well and 157 feet at A1-NC41, and only 62 feet thick at C1-NC35A. The nummulitic lithofacies of the Upper Jdeir member is locally poorly developed and tend to be very thin and represented in some wells by reworked conglomerate nummulitic lithofacies as the case in I1, K1 and L1-137 and H1-NC41. These poorly developed and thin lithofacies probably indicate the southern and western limit of the nummulite bank.

Further, southward the bank lithofacies grades into the back-bank lithofacies of Alveolina-Orbitolite wackestone/packstone of lower Jdeir with local development of high energy and reefoidal facies of Tajoura Formation which becomes more restricted southward with Sabkha and supratidal lithofacies of Taljah and Bilal sequences (Fig. 8).

Environment

The lateral and vertical analysis of the Upper Jdeir lithofacies suggest the existence of a wide broad Nummulitic Bank during the Upper Jdeir time that dominated most of the central part of the offshore basin

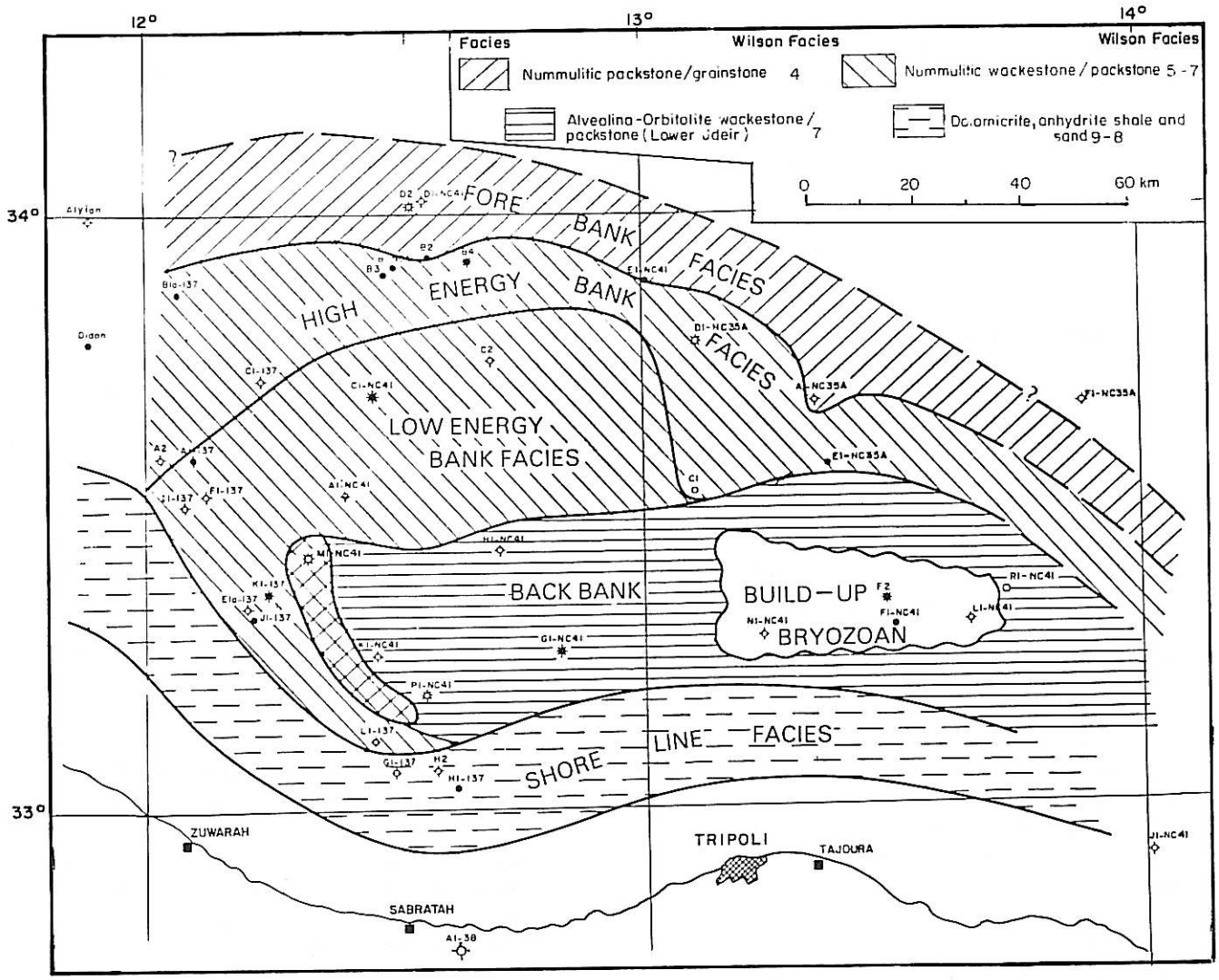


FIG. 8. Farwah Group. Upper Jdeir nummulitic bank facies.

and cover a belt extending from E1-NC35A in the east of Bla and A2-137 in the west. This bank is widest in the centre just offshore Sabratah where it is 70 km wide from H1-NC41 to D2-NC41. This bank becomes narrower in the eastern section between R1-NC41 and F1-NC35A where it is estimated to be only 25 km wide and extending perhaps due south-east. In the western section offshore Zuwarah the south-western limit of this bank is A2-137 and the northern edge of this bank is probably north of Bla-137 well (Fig. 8).

A back-bank setting is located landward behind the bank covering the area between H1-NC41 in the centre and H2-137 in the south, R1-NC41 to the east and K1-NC41 to the west, in turn the back-bank condition changes southward to an inner shelf restricted supratidal to sabkha condition that prevailed along a narrow belt that extends parallel to the present shoreline.

Two main lithofacies make up the bank sequence: nummulite packstone/grainstone and nummulite wackestone/packstone. The higher energy lithofacies are commonly found along the northern edge of the bank extending from E1-NC35A to Bla 137, whereas the relatively lower energy lithofacies are located just in the centre of the bank. Such a distribution would perhaps indicate that the high energy nummulitic lithofacies in fact represent a shoal setting as the case in the Ypresian nummulite sequence in the onshore Tunisia as reported by Fournie (1975) or a for-bank environment similar to the Eocene of Turkey (Henson 1950). This point is discussed further in the following pages.

Discussion

The problem is whether the high energy nummulitic facies of grainstone and packstone are deposited along the bank margin or the fore-bank is not helped by the different reporting of nummulite lithofacies depositional environment.

The Eocene nummulites in the north-east Iraq is reported to be of a reef, back-reef and fore-reef where large nummulite with abundant echinoid remain dominant the fore-reef shoals, similarly nummulitic grainstones are interpreted to form fore-reef shoals in the Eocene of Turkey (Henson 1950) and in the case of Ypresian sequence from the onshore Tunisia (Fournie 1975), the nummulitic lithofacies are interpreted to deposit in the outer platform as a shoal, resembling in many aspects the oolitic shoals. Whereas (Arni 1965) in his study on the Eocene nummulite rocks of Sirt Basin, suggested the nummulite lithofacies to be deposited in banks, back-bank and fore-bank environments, and different nummulite tend to occupy different setting within the bank complex. There are also reports of nummulitic rocks associated with coarse cross-bedded classic rock that are deposited in the littoral zone (Roniewcz 1969). However, in recent study of the nummulitic beds in the Eocene of Egypt (Aigner 1982) pointed out that most nummulitic accumulation is in situ build-up that tends to be reworked, winnowed and redeposited very close to its original site of accumulation, normally at a lower depression within the bank complex. Aigner also suggested that such removal and reworking can happen at depth of up to 100 m. water depth where storm induced wave currents are strong enough to move the nummulite tests and he added that nummulite accumulation does not necessarily reflect an actual habitate condition and their local presence is not direct reflection of in situ accumulation. If this holds true in the case of the Upper Jdeir nummulite lithofacies then one should not only look for the best condition of nummulite accumulation but also to the likely place where it may be removed to and redeposited. This of course will be within the bank complex.

Studies of recent large foraminifers in the Red Sea of the type resembling nummulite are found to live in water depth that range from 50 m to over 100 m (Hottinger 1977) and they prefer quite muddy water, this range of water depth of the deposition of the nummulitic lithofacies is reported by many workers on their studies of Eocene nummulite accumulations.

In conclusion, the presence of larger foraminifera in the Upper Jdeir such as Assilina and Operculina at E1 and B1-NC41 and the abundant broken fragments of nummulites and echinoids at A1-NC35A, perhaps make it safe to suggest the occurrence of fore-bank lithofacies belt that extends from B1 to E1-NC41 to A1-NC35A. The line separating the bank from the fore-bank is very arbitrary and the width of this fore-bank is very difficult to outline at this stage fore-bank setting is followed by wide broad bank that dominated most of the shelf which is characterized by nummulitic packstone, grainstones and wackestones. In turn back-bank lithofacies condition prevailed behind the bank where foraminifers/skeletal wackestone is dominating the rest of the area. This is flanked by Inner shelf deposits of dolomicrite, mudstone, shale with anhydrite and levels of sandy beds and sandstone that indicate close by shorelines.

Lithofacies and Environment of Tajoura Formation

This formation comprises bryozoan packstone/grainstone and oolitic packstone/grainstone with dolomitic wackestone and nummulitic pelecypod wackestone at F1-NC41 (Fig. 9). It grades eastward at L1-NC41 into argillaceous skeletal grainstones and packstones; dolomite and dolomitic wackestones, locally with anhydrite nodules and fossiliferous wackestone/mudstone. Further east, towards R1-NC41, Tajoura Formation changes into Lower Jdeir lithofacies of Farwah Group which consists mainly of Alveolina/Orbitolite packestone with perhaps deep shelf influence. These high energy lithofacies extends eastward and grades into algal grainstone lithofacies near N1-NC41 and towards and northwest where oolitic and interclastic lithofacies are interbedded with the nummulitic lithofacies of the Jdeir Formation at C1-NC35A.

This suggests, as shown in Figure 9 the presence of bryozan organic buid-up at or near F1-NC41 which grades north and northwest into a probable shelf lagoon lithofacies at F2-NC41 and nummulitic bank lithofacies at C1 and E1-NC35A. South of the E1 at the winnowed edge, oolitic grainstone lithofacies developed which extended towards L1-NC41 where argillaceous skeletal grainstone predominate which is less restricted. At N1-NC41 the high energy lithofacies is mainly algal grainstone, suggesting perhaps some algal development within the bryozan build-up which supply of algal debris for the grainstone at N1-NC41. Behind the organic build-up and winnowed edge, a shelf lagoonal belt was developed protected by the organic build-up and the oolitic barrier, but however some water circulation must have been possible. The shelf lagoon lithofcies which is dominated by quite water facies, rich in fauna are characterized by pelecypod, nummulite, alveolina and orbitolite wackestone and packestone lithofacies. These lithofacies are present south, east and west. At R1-NC41 the Alveolina/Orbitolite packstone/wackstone lithofacies exhibit shelf influence as they are not protected and perhaps directly grades into the nummulitic bank lithofacies and open sea lithofacies. Between the shortline and the shelf lagoon a wide belt of restricted lagoon and supratidal/Sabkha lithofacies possibly existed as the vertical section at L1-, F1 and N1-NC41 suggest.

The development of this shallow water carbonate lithofacies at F1-NC41 area could be a reflection of tectonic high or swell which persisted during Eocene which is perhaps related to Tripoli Nose, other explanation could suggest that the reason for such organic

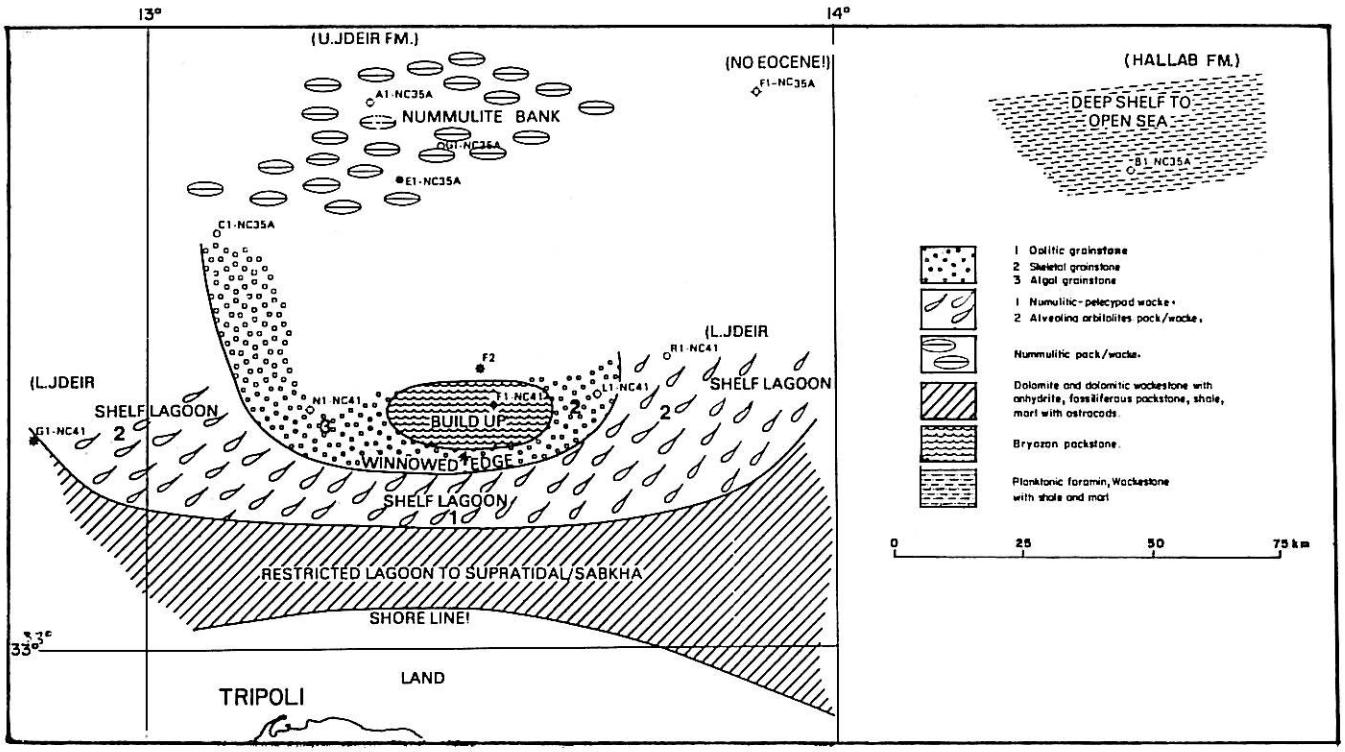


FIG. 9. Facies and environment of Early Eocene, Tajoura Formation.

build-up is the local development of carbonate Bank during the Paleocene time near the F1 area, which is probably the case, because a thick Paleocene carbonate sequence is locally developed at F1-NC41, or most likely is due to the combination of both tectonic and sedimentological factors.

It is important to note that Bryozoans are not known to be a significant build up contributor in the geological time, and only reported to be of some importance in the Middle Ordovician and locally during the Silurian and in the brackish late Miocene and Pliocene of Eastern Europe. (Heckel P.H., 1974).

Lithofacies and Environment of Hallab Formation

Hallab Formation is encountered only in one well that is B1-NC35A. It is composed of mainly alternating shales, calcareousl shales, marl and limestones that are rich in planktonic foraminiferas. The limestones are white, cream, chalky and consist of pelagic mudstone, wackestone to packestone lithofacies.

The lithofacies and faunal assemblage suggest a deposition in quite deeper water environment, where rate of sedimentation were low. This condition of deposition is found to prevail in the open sea shelf or basinal environment that dominated the northeast part of the basin.

ACKNOWLEDGEMENT

I would like to express my thanks to N.O.C. for the support and permission to publish this work.

The work was conducted during my stay as an academic visitor at Imperial College, London, 1982–1985.

REFERENCES

Aigner. T, 1982, Event-stratification in Nummulite, Accumulation and in Shell Beds from the Eocene of Egypt. In: *Cyclic and Event Stratification* (Ed) Ensele and Seilacher. Published by Springer Verlag.

Arni P., 1965, L, Evolution des Nummulites en tant Que Facteur de Modifications des Deposits Littoraux. In: *Memories du Bureau de Recherches Geologique at Mineres*, Paris, No. 32.

Bannerjee. S., 1980, Stratigraphic Lexicon of Libya, *Department of Geological Researches and Mining Bulletin* No. 13, Industrial Research Centre, Tripoli.

Bishop, W.F. 1975, Geology of Tunisia and adjacent part of Algeria and Libya *A.A.P.G. Bull.* Vol. 59, n. 3, p. 413–458.

Busson, G., 1967, Mesozoic of Southern Tunisia in Martin L. (Ed), Guide book to the geology and History of Tunisia, P.E.S.L., Tripoli.

Fatmi, A.N., Sbeta, A.M., and Eliagoubi, B.A., 1978, Guide to the Mesozoic Stratigraphy of Jabal Nefusa, Libyan Jamahiriya. *Arab. Dev. Inst.*, Tripoli, Pub. no. 7, 35p.

Fatmi, A.N., Eliagoubi, B.A., Hammuda, O.S., 1980, Stratigraphic Nomenclature of the pre-Upper Cretaceous Mesozoic Rocks of Jabal Nafusah, NW Libya. In: *The geology of Libya Volume I* (Eds.

Salem; M.J. and Busrewil) Academic Press, London, pp. 57–65.
Fournie, D., 1975, L'Analyse-sequentielle et la sedimtologie de L'Ypresian de Tunisie: Bull. Centre Rech. Pau., *SNPA* V9, p. 27–75.
Fournie, D., 1978, Nomenclature Lithostratigraphique Des Series Du Cretace Superieur Au Tertiaire De Tunisie: *Bull. Cent. Rech. Explor. Prod.* Elf Aquitaine.
Hammuda O.S., Sbeta A.M., Mouzughi A.J., and Eliagoubi B.A., 1985, The Stratigraphic Nomenclature of the Northwestern offshore Libya Published by ESSL, Tarabulus–Libya.
Heckel, P.H., 1972, Recognision of ancient shallow marine environments, In: Recognision of Ancient Sedimentary Environments, In: Rigby, J.L., Hamblin, W.K. Eds., Soc, Econ. *Paleonto logists mineralogists Spec. Publ.* 16, 226–286.
Henson, F.R.S., 1950, Cretaceous and Tertiary Reef formations and associated sediments in Middle East Bull. *Amer. Ass. Petrol. Geol.* v. 34, no. 2, pp. 215–236.
Hinnawy, M. and Chechitev, G., 1975, Geological Map of Libya, Sheet Tarabulus (N1-33-13) *Explanatory Booklet* Industrial Research centre, S.P.L.A.J., Tripoli.
Hottinger L., 1977, Distribution of larger peneruplidae, Borelis and Nummulitidae in the Gulf of Agaba Red Sea in Utrecht, Micropal. *Bull. 15*, p. 35–109.
Pitman, III, W.C., Cochran, J.R.; Ryan, W.B.F. and Ladd, J.W., 1981, Evolution of the Libyan Margin, Annex II–6 in (*Continental Shelf, Technical Annexes to the Reply* Vol. II SPLAJ).
Roniewicz, P. 1969, Sedimentation of the nummulite Eocene in the Tara Mnt. *Acta. Geol.* Polon, 19:503,601.
Sbeta, A.M. 1981, the stratigraphic nomenclature of the Lower Eocene. The offshore of the northwest Libya: *N.O.C. Internal Report.*
Sbeta, A.M., 1983, The main results of the Investigation on the Eocene of the Offshore northwest Libya: *N.O.C. Internal Report.*
Wilson, J.L., 1975, Carbonate Facies in Geologic History published by Springer-Verlag.

PRJ, Vol. 2 (January 1990); P. 57–62, 8 FIGS, 3 TABLES.

Short Note

HIGH TEMPERATURE CORROSION OF 316 AUSTENITIC STAINLESS STEEL IN H_2S/CO_2 CONTAINING ENVIRONMENT

S.Y. Gjam* and K. Abosowa**

التآكل الحراري للفولاذ الأستينيتي 316 في وسط حاوي لغاز يد٢ كب وك١

د. سليمان قجم وخليفة أبو صوه

لوحظ أن أطباق الفولاذ الأستينيتي من نوع 316 ، والتي تستعمل في مصنع الإستقطاف بحقل جالو النفطي ، ذات مقاومة ضعيفة للتآكل ، وذلك عند تعرضها لغازات هيدروكربونية تحتوي على كميات ضئيلة من غازي يد٢ كب وك١ في درجات حرارة تتراوح ما بين 400 – 600 درجة مئوية .

وخصصت هذه الدراسة لفهم عملية التآكل باستعمال نسب مختلفة من يد٢ كب وك١ لتعطي وسطا من الأكسدة والكبرته في درجات حرارة تتغير من 450 إلى 600 درجة مئوية .

تمت دراسة الرقائق القشرية الناتجة عن عمليات التآكل باستخدام الفحص المجهري والأشعة السينية ، ووجد أن معدل التآكل كان أكثر فعالية في الوسط المكبرت .

INTRODUCTION

The increasing demand of alloys for use at high temperatures in sulphur bearing atmosphere has stimulated a number of investigations [1–4] on sulphidisation of metallic materials by sulphur vapours or H_2-H_2S gas mixture.

Low sulphur vapour pressures, 10^{-4}–10^{-10} atmospheres are generally encountered in actual practice such as in the petroleum industry and thermal power plants. Process gas streams generated by many petrochemical and gasification processes contain sulphur as H_2S. The sulphidisation behaviour of a variety of commercial alloys ranging from stainless steel to nickel-and cobalt-base alloys has been reported recently in a reducing sulphidising environment, mostly at temperatures exceeding 700°C [5]. Sulphidising behaviour at temperatures, less than 600°C, has not received much attention. In some petrochemical processes temperature encountered are in lower regions. The present paper reports preliminary results of a long term research on sulphidisating behaviour of 316 austenitic stainless steel in the temperature range, 450–600°C in a wide range of gas mixtures. Study being reported here was carried out in the H_2S-CO_2-N_2 gas mixture.

EXPERIMENTAL PROCEDURE

Standard AISI 316 austenitic stainless steel was used and its chemical composition is given in Table 1, specimens of the size 8 × 5 × 1 mm were cut from the sheet. They were polished on different grades of emery paper finishing with 600 grit paper, washed with water, rinsed with alcohol and weighed. Sulphidisation was performed in a gas mixture consisting of H_2S, CO_2 and N_2 at 450°, 500° and 600°C up to a period of three hours.

Fig. 1 shows a schematic diagram of the experimental set-up for carrying out sulphidisation. Flow rate of each gas was measured by capillary flowmeters. N_2, H_2S and CO_2 gases at predetermined flow rates were mixed in a gas mixer of 60 cm length and 1.2 cm diameter having four perforated glass discs fused at

Table 1. Chemical composition of 316 Austenitic Stainless Steel
(Wt %)

C	Cr	Ni	Mn	Si	P	S	Mo
0.08	16	10	2.0	1.0	0.045	0.04	2.5

*Materials Science and Metallurgical Engineering Dept., Al-Raya Al-Khadra University, Tripoli, Libya (G.S.P.L.A.J.).
**Petroleum Research Centre, Tripoli, Libya (G.S.P.L.A.J.).

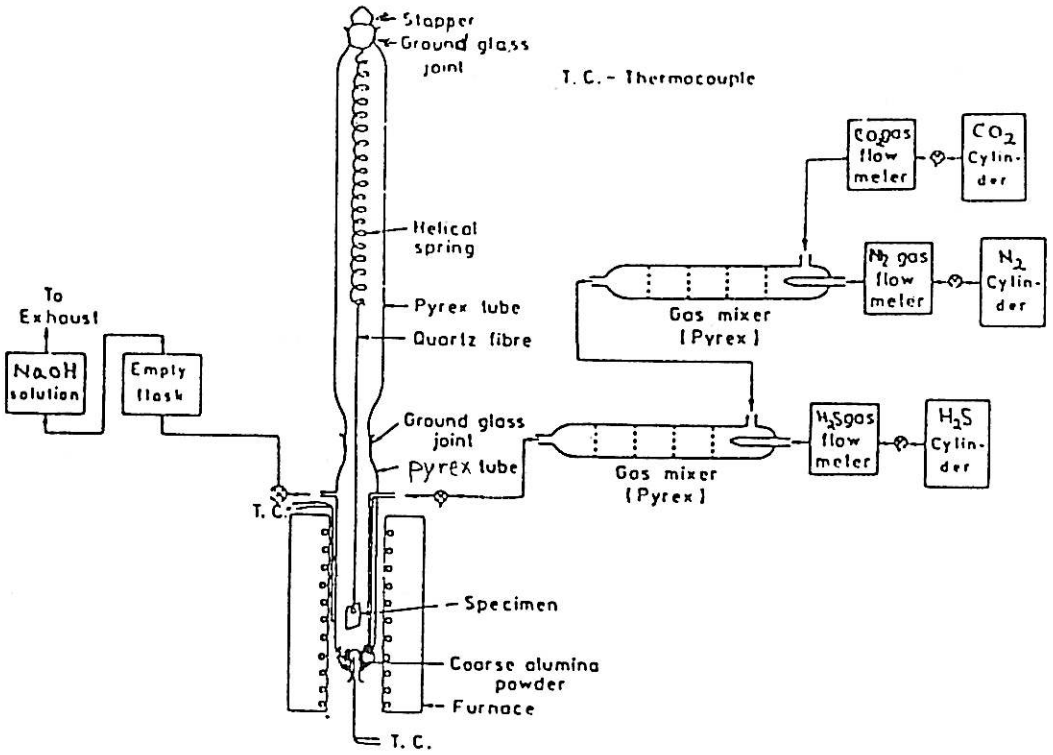


FIG. 1. Schematic diagram of experimental set-up for sulphidisation in H_2S-CO_2-N_2 environment.

equidistance. The gas mixture was introduced into pyrex glass reaction tube. The thermogravimetric set-up consisted of a borosilicate glass helical spring of sensitivity 100 μ gm. The specimen was attached with a glass fibre to the spring. Weight gain data was recorded by measuring extension of the spring with a cathetometer.

The gas mixture was first passed through the reaction tube for 30 minutes at room temperature and then, tubular furnace heated to desired temperature was raised to surround the reaction tube. After completion of the experiment, the furnace was lowered and specimen was cooled in the gas stream.

The sulphidisation samples were analysed by x-ray diffractometry and conventional metallography. Cuk_α radiation with Ni filter and a scanning speed of 2°/min. was used.

RESULTS

Kinetics of Sulphidisation

Effect of temperature on suphidisation of 316 stainless steel in higher H_2S concentration gas mixture, 30% H_2S, 30% CO_2 and 40% N_2 by volume is shown in Fig. 2. Weight gain versus time plot gave a straight line relationship revealing that sulphidisation follows the parabolic rate law. Table 2 gives parabolic rate constant as a function of temperature. Parabolic rate constant was found to depend on temperature. It increased from 0.83×10^{-9} at 450°C to 4.07×10^{-9} gm cm^{-4} s^{-1} at 600°C.

Based on this data, activation energy using Arhenius plot shown in Fig. 3 was determined to be 54 KJ/mole. KJ/mole.

In order to examine the role of CO_2 in sulphidisation of 316 stainless steel, a run was made in the gas mixture, 30% H_2S and 70% N_2 free from CO_2 at 600°C. Results are plotted in Fig. 4 which shows that presence of CO_2 decreases sulphidisation rate. Parabolic rate constant was found to be 8.61×10^{-9} gm^2 cm^{-4} s^{-1} without CO_2 compared with 4.07×10^{-9} gm cm^{-4} s^{-1} in the presence of CO_2 in the gas mixture. A test was also run at 600°C in the gas mixture, 30% CO_2 and 70% N_2 free from H_2S. Weight gain was too small and was within the sensitivity of helical spring balance.

Table 2. Parabolic rate constants of 316 Austenitic Stainless Steel in 30% H_2S, 30% CO_2 40% N_2 at different temps

Temperature (C°)	Kp (gm^2 cm^{-4} sec^{-1})
600	4.07×10^{-9}
500	2.12×10^{-9}
450	0.83×10^{-9}

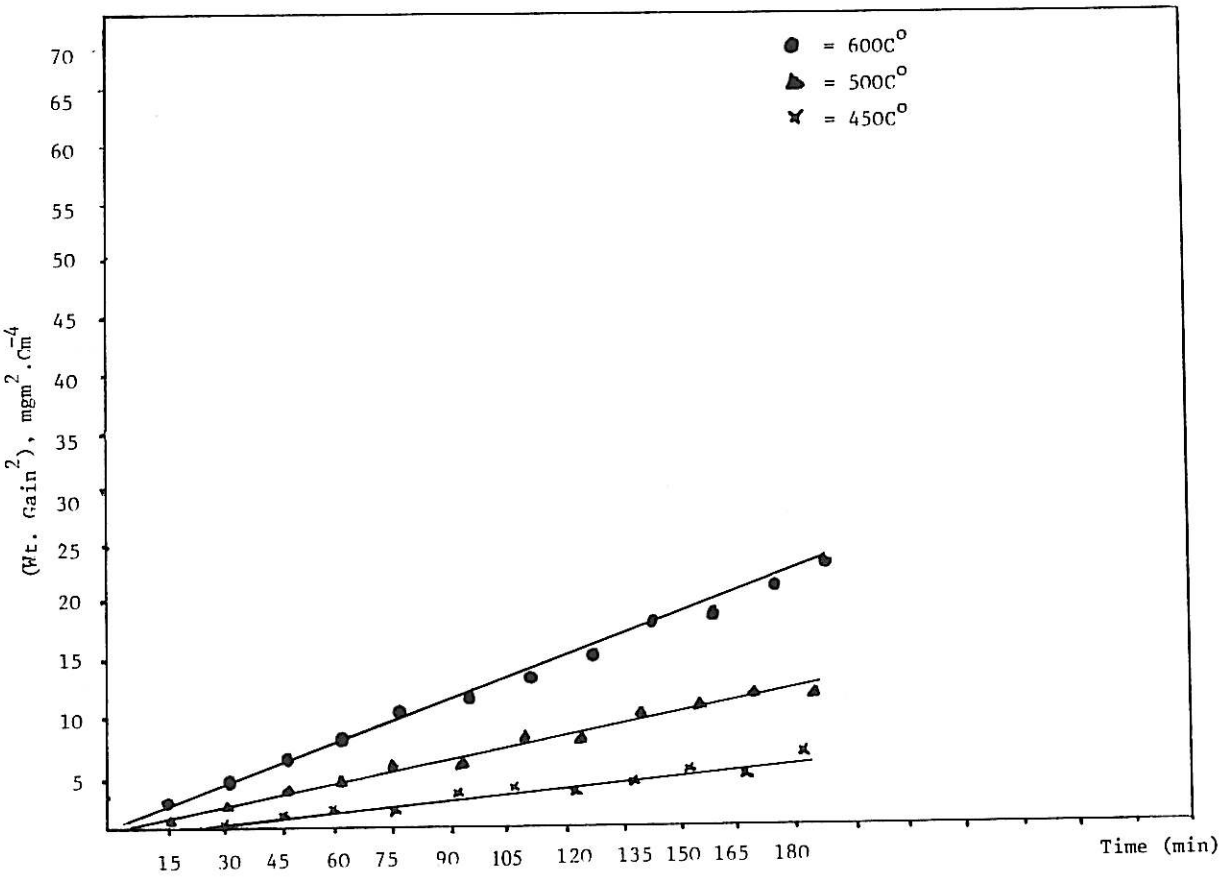


FIG. 2. Effect of temperature on sulphidisation of 316 Stainless Steel in 30%, H-30% CO_2-40% N_2.

Table 3. Parabolic rate constants at different H_2S gas composition and 600°C

Composition %	($gm^2\ cm^{-4}\ sec^{-1}$)
30	4.07×10^{-9}
10	3.15×10^{-9}
5	2.69×10^{-9}

Since H_2S concentration in the gas mixture investigated was rather too high, the effect of lower concentrations of H_2S, 5% and 10% respectively on sulphidisation at 600°C was studied. Results are plotted in Fig. 5 showing parabolic rate law at lower concentrations of H_2S. Reducing H_2S concentrations from 30% to 5% decrease parabolic rate constant from 4.07×10^{-9} to 2.69×10^{-9} gm $cm^{-4}\ s^{-1}$ (Table 3).

Scale Morphology-Fig. 6 shows macroscopic appearance of sulphidised sample. The scale formed was highly fragile particularly at 500° and 600°C as in Figs. 6b and 6c. It came off easily from the specimen surface. Visual observations revealed that the outermost scale was bright grey in colour and scale layer underneath outer layer was black in colour. Fig. 7 shows outer scale having poor adherence and inner

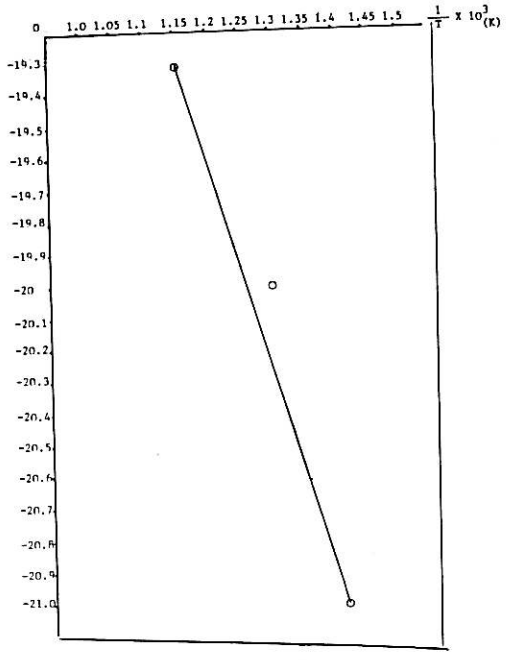


FIG. 3. Temperature dependence of the sulphidisation rate of 316 Stainless Steel in 30% H_2S-30% CO_2-40%, N_2 in the Arrhenies plot.

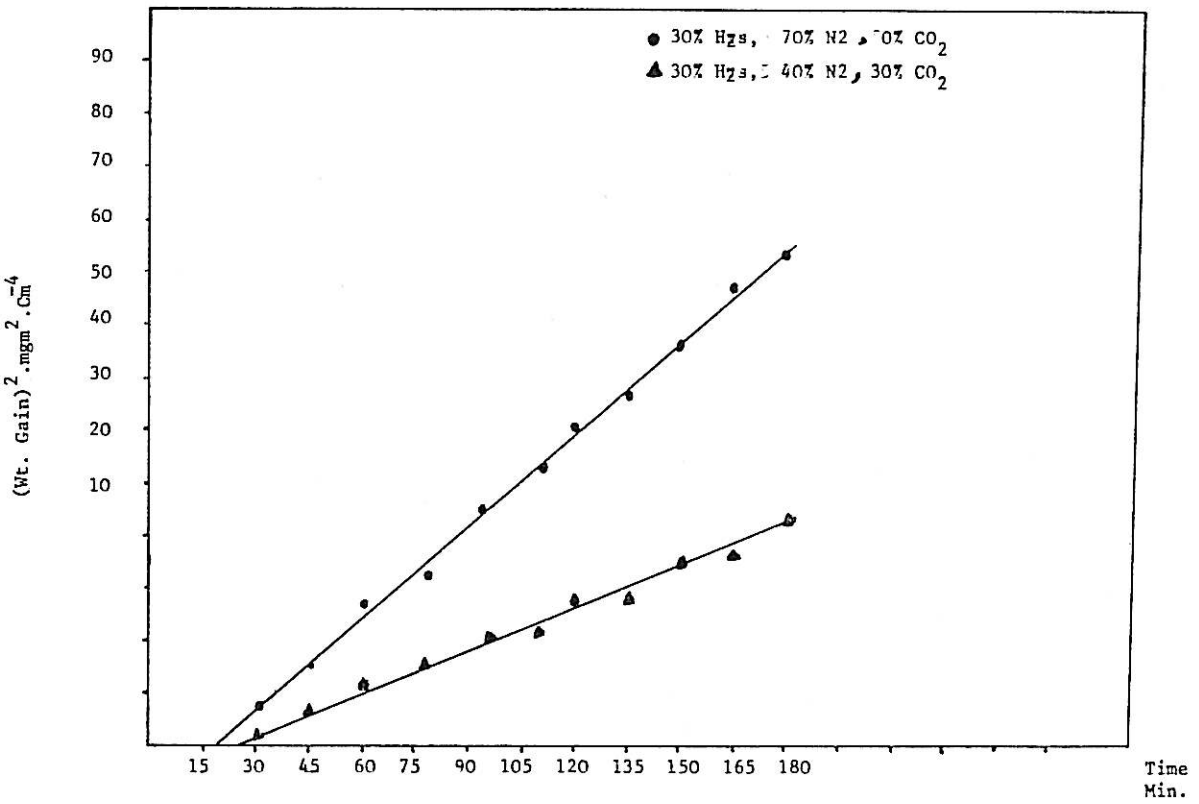


FIG. 4. Effect of CO_2 on sulphidisation of 316 Stainless Steel.

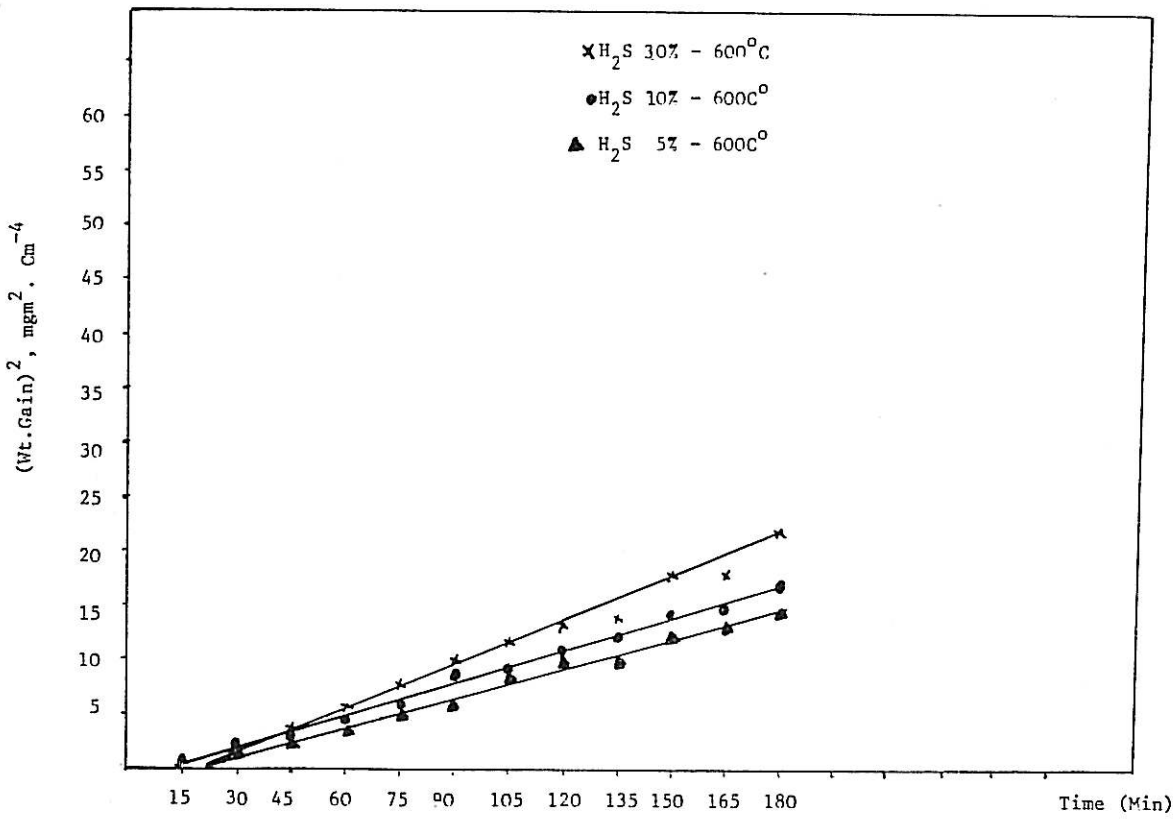


FIG. 5. Effect of H_2S concentration in the gas mixture, H_2S-CO_2-N_2 on sulphidisation of 316 Stainless Steel at 600°C.

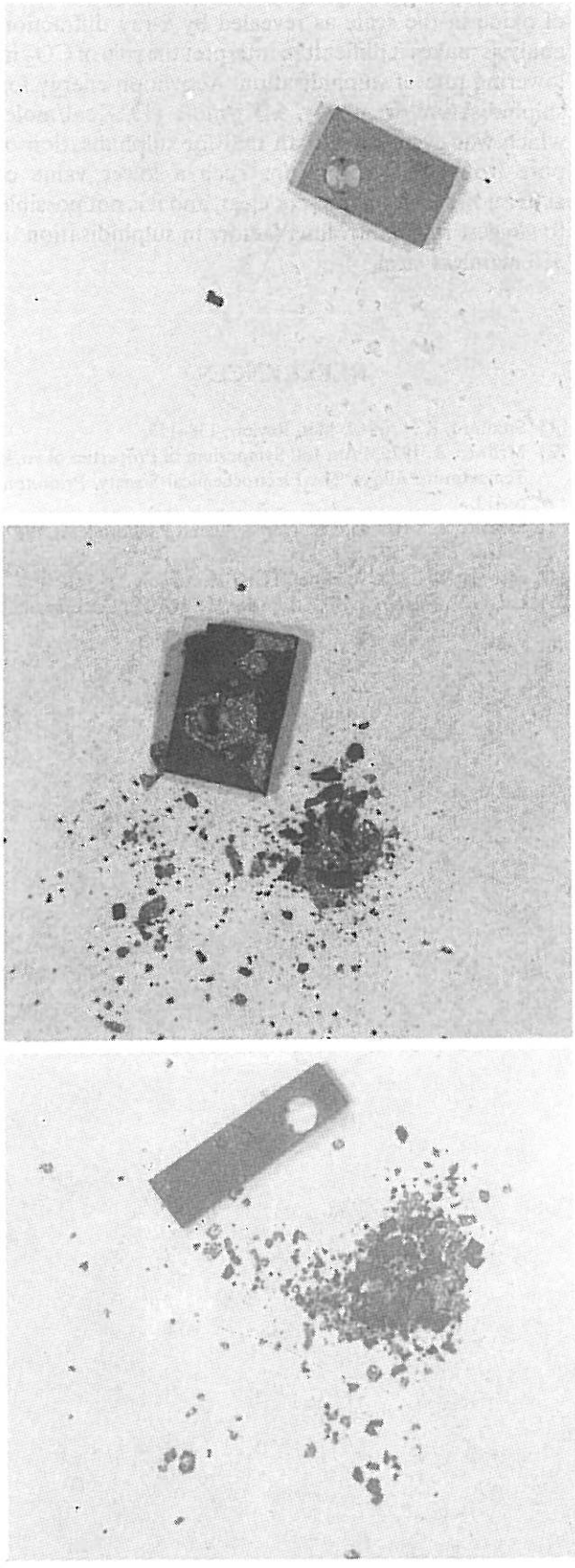


FIG. 6. Macroscopic appearance of scale formed on specimens sulphidised in 30% H_2S-30% CO_2-40% N_2 (a) 450C (b) 500°C (c) 600°C.

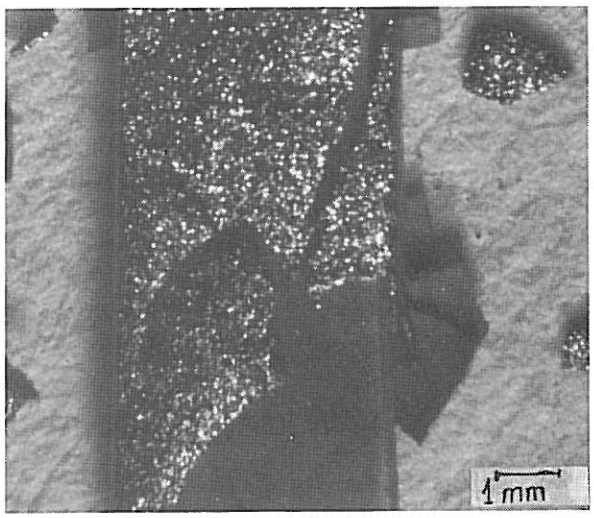


FIG. 7. Outer and inner scale formed on specimen sulphidised at 600°C in 30%, H_2S-30% CO_2-40% N_2.

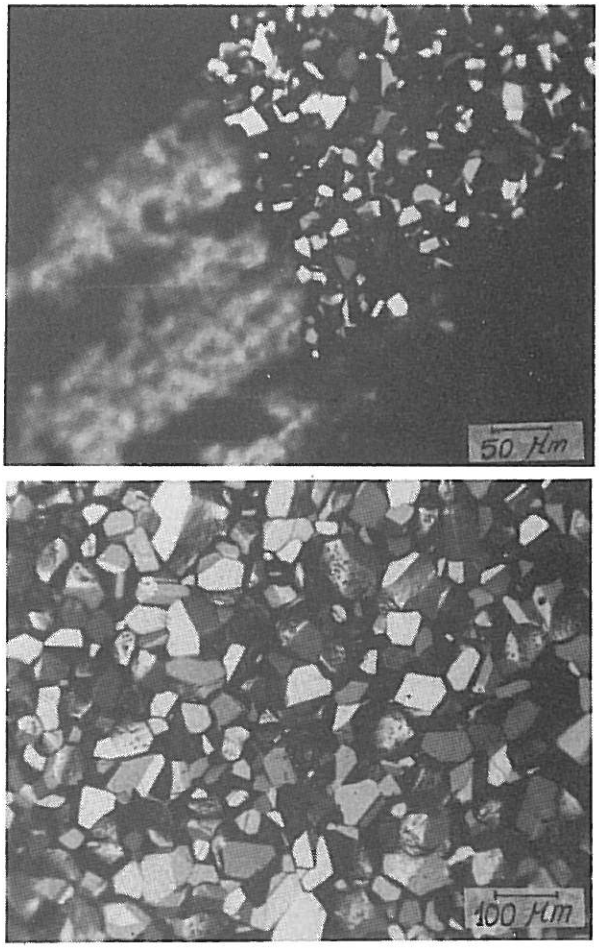


FIG. 8. (a) and (b) Microstructure of outer scale showing polyhedral crystals formed on specimen sulphidised at 500°C in 30% H_2S-30% CO_2-40% N_2.

scale, relatively smooth. Higher magnification revealed outer scale structure consisting of polyhedral crystals as seen in Figs 8a and 8b.

X-ray Diffraction Analysis: This was carried out on specimens sulphidised at 500°C for three hours in the gas mixture consisting of 30% H_2S, 30% CO_2 and 40% N_2. Spalled material consisted of $Fe_{1-x}S$ and Cr_2S_3. Scale scratched from the specimen surface was identified to have presence of $Fe_{1-x}S$, $FeCr_2S_4$ and FeS. Black scale still remaining on specimen surface showed some results as the scale scratched from the specimen surface.

CONCLUDING DISCUSSION

Results reveal that 316 stainless steel has poor resistance to sulphidisation even at lower temperatures, 450–600°C. Sulphide scale formed is highly fragile and outer scale comes off easily. Duplex sulphide scale is formed, outer scale consisting of FeS and Cr_2S_3, while inner has presence of FeS, $FeCr_2S_4$ and FeS. Absence of oxide in the scale as revealed by x-ray diffraction analysis makes it difficult to interpret the role of CO_2 in lowering rate of sulphidisation. Activation energy for sulphidisation was only 54Kj/mole (13 Kcal/mole) which was even lower than that for sulphidisation of pure iron [4]. Reasons for such a lower value of activation are not at present clear, and it is not possible to suggest rate controlling factors in sulphidisation of 316 stainless steel.

REFERENCES

[1] Strafford, K.N., 1969, Met. Review, 138–153.
[2] Mrowec, S., 1976, Proc. Int. Symposium of Properties of High Temperature Alloys, The Electrochemical Society, Princeton, p. 413.
[3] Mrowec, S., Tochowicz, S., Werber, T. and Podhorodecki, 1967, Corros. Sci, 7–697.
[4] Mrowec, S., 1980, Werkstoffe Und Korrosion, 31–371.
[5] Lai, G.Y., Paper No. 73, Corrosion/84, NACE, Louisiana.

PRJ, Vol. 2, (January 1990); P. 63–66, 5 FIGS, 1 TABLE.

Short Note

H_2S INDUCED LOCALIZED CORROSION OF AUSTENITIC STAINLESS STEEL BELLOW: A CASE STUDY

M.L. Mehta* and A.T. Hassan*

دراسة ظاهرة تآكل صمامات التهوية الفولاذية تحت تأثير غاز يد$_2$ كب

د . م . ل . مهتا وعبدالفتاح حسن

أجريت الإختبارات الميكانيكية والميتالوغرافية اللازمة لإيجاد أسباب تآكل صمامات التهوية لخزانات النفط بحقل الحمادة ، ومن خلال فحص هذه الإختبارات وتحليل نواتج التآكل المتواجدة على سطح الصمام بواسطة الأشعة السينية ، إتضح بأن غازكبريتيد الهيدروجين المبلل هو السبب الرئيسي في تآكل هذه الصمامات المصنوعة من الحديد الفولاذي نوع 321.

INTRODUCTION

Bellow is the component of pilot operated relief valve on surge crude oil tanks. Material of the bellow as per specification is austenitic stainless steel, type 321. Environment inside the bellow is that of the tank gases entering the bellow through pilot valve.

Since flange of the relief valve is connected to the flare line, external surface of bellow is exposed to the gases of the flare line. Operational pressure within the bellow is maintained in the range from 0.02 to 0.06 kg/cm^2 above atm pressure and temperature about 38°C. Bellow was observed to suffer from localized corrosion, causing perforations (Fig. 1) resulting in gas leaks making it difficult to maintain desired pressure within the bellow for operation of the valve.



FIG. 1. Localized corrosion causing perforation.

METALLOGRAPHIC STUDIES

Macroscopic Examination

Extensive pitting were observed both on internal and external surfaces of the bellow. Some of the pits have propagated through wall thickness (0.3 mm) of the bellow. Fig. 2 shows pitting on the external surface of the bellow in their different stages of developments. Some pits had initiated revealing that pitting can start from outer surface and environment surrounding the external surface of the bellow is also corrosive enough to cause pit initiation and their propagation. Deposit

*Petroleum Research Centre, Tripoli, G.S.P.L.A.J.

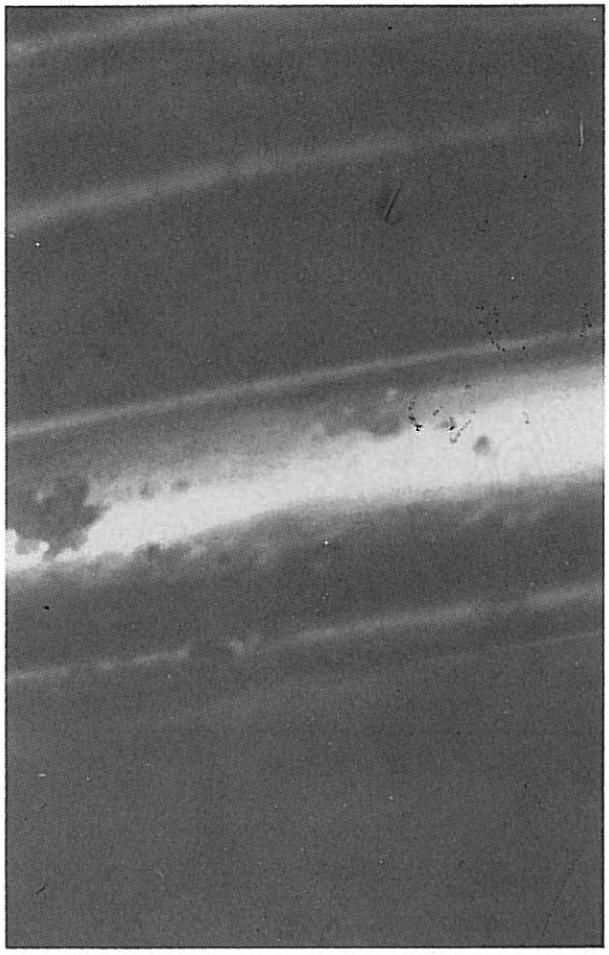


FIG. 2. Pitting on external surface of the bellow showing different stages of their growth X6.

of particles on surfaces of bellow was also observed. Sites of pit formation had presence of thin black film.

Microscopic examination

Samples having different degrees of pitting were cut from bellow. Morphology of localized corrosion in the form of intercrystalline cracking, intercrystalline corrosion as well as pitting corrosion were detected as seen in Fig. 3. Figs. (4a, 4b) show early stages of localized attack which started from grain boundaries and progressed into grains to form pits.

X-RAY DIFFRACTION ANALYSIS

Material deposited on the surface of bellow was scrapped. Corrosion product film on pit sites was thin and adherent. Material coming from those sites was only a very small fraction of material collected.

Table 1 gives results of X-ray diffraction analysis. The main component of the material are kaolinite and

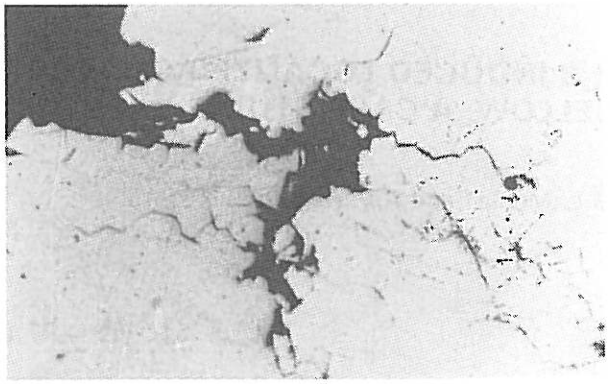


FIG. 3. Intercrystalline cracking and pitting (unetched) X500.

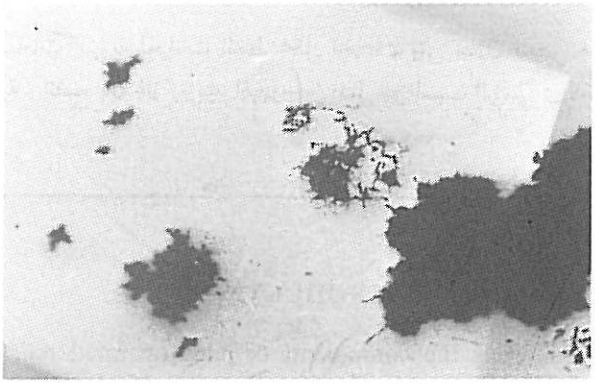


FIG. 4(a). Showing pits in their different stages X125.

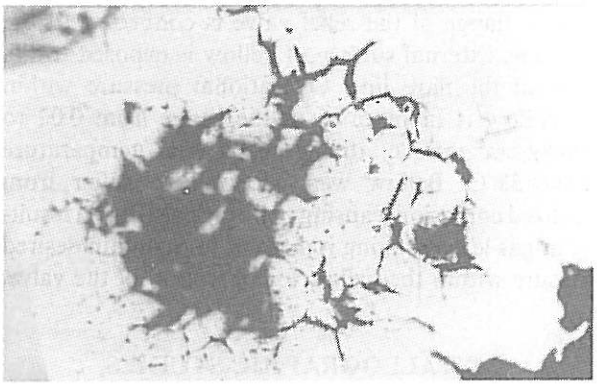


FIG. 4(b). Encircled area in Fig. 4a showing intergranular attack leading to formation of pits X500.

quartz. The rest of the components (Iron sulphide and siderite) are present in very small quantities as revealed by very weak intensity of reflections due to these substances.

Analysis of environment

Gas stream from the tank entering pilot valve had

Table 1. Results of X-Ray Diffraction Analysis of materials from the surfaces of the bellow

Compound	Relative peak Intensity	Remarks
Kaolinite, $Al_2Si_2O_5(OH)_4$	Very strong	Major component
Quartz, SiO_2	Strong	Major component
Siderite, $FeCo_2$	Weak	Minor component
Marcasite, FeS_2	Very weak	Very small amount
Greigite, Fe_3S_4	Very weak	Very small amount

pungent odour indicating the presence of H_2S and carried with it water vapour. Gas sample was taken from the side tube connecting tank and pilot valve and the condensate was found to contain 8.11 ppm of H_2S.

LABORATORY INVESTIGATIONS

In order to ascertain that wet H_2S gas can cause pitting corrosion of bellow material, small samples from bellow after cleaning were exposed to wet H_2S gas as described here. Distilled water, (75 ml), was taken in 250 ml Duran glass bottle with a tight cap. It was first purged with high purity Nitrogen gas for 10 minutes and then H_2S gas for 15 minutes. One sample was fully immersed in the solution and the other one was exposed above the solution level. The bottle was sealed to prevent entry of air and to generate wet H_2S gas environment above solution level. Temperature was maintained at 38°C. After two days small black spots appeared on the sample above solution level which grew with time. Solution was observed to turn milky. Samples were removed from the bottle after seven days and solution was analysed to contain 0.8 ppm H_2S. Fully immersed sample did not show any corrosion. Fig. 5 shows localized corrosion on the sample exposed to wet H_2S gas above water level. Solution had turned milky indicating that there was presence of residual oxygen in the solution reacting with H_2S to form sulphur.



FIG. 5. Pitting caused by exposure to wet H_2S above solution level X6.

DISCUSSION

The observation that bellow has also suffered from intercrystalline cracking is difficult to explain as they could be caused by either corrosion fatigue or stress corrosion cracking. Since bellow is subject to pressure variation due to its nature of operation, corrosion fatigue appears to be more probable. It is also observed that initially intergranular attack occurs as illustrated in Fig. 4 and this spreads leading to formation of pits.

Pitting of austenitic stainless steel, of which the bellow is made, is the cause of its failure. Results of present studies attribute pitting corrosion to the presence of wet H_2S gas in the environment to which the bellow is exposed during its service. In the available literature there are only few references to pitting corrosion of stainless steel in chloride free solutions [1]. Ijzermans and Vander Krogt [2] observed pitting corrosion on 18 Cr-2 Mo Stainless steel in 0.5 M $H_2SO_4 + H_2S$ gas solution and reported that the presence of H_2S gas is essential because H_2SO_4 does not cause pitting corrosion. Recent investigations [3–4] show that austenitic stainless steels like other iron base alloys are susceptible to microbial corrosion in the presence of sulfate reducing bacteria (SRB). The resultant corrosion manifests in the form of pitting. It is attributed to H_2S produced by SRB which leads to break down of passive film on the stainless steel followed by pitting corrosion. However, mechanism of localized corrosion of austenitic stainless steel in the presence of H_2S in the environment is far from clear.

In the present case, the environment entering bellow is essentially gaseous containing water vapours and solid particles. For corrosion to start and continue, there has to be a water film on bellow surface i.e. surface has to remain wet which would result from condensation of water vapour. This film would readily absorb H_2S from the environment and would also contain various species such as clay, deposited from the environment and those originating from the corroding metal. Presence of such species helps to keep metal surface wet by lowering critical humidity required to form moisture film on the metal surface [5] and also makes it corrosive.

CONCLUSION

1 Pitting corrosion starts both from internal and external surfaces of the bellow and is caused by the presence of wet H_2S gas in the environment.

2 Propagation of pits to form perforations in the bellow wall is responsible for failure of the bellow.

ACKNOWLEDGEMENT

The authors would like to thank Dr. S.O. Tumi for his helpful discussion and the staff members of Hamada oil field for their assistance.

REFERENCES

[1] Smialowska, Z.S. 1986, *Pitting Corrosion of Metals*: NACE, Houston, p. 212.
[2] Ijzermans, A.B., Van der Krogt, A.J. 1968, *Corrosion Science*, v, 8, p. 679.
[3] Ringas, C. Robinson, F.p.A. 1988, *Corrosion* v. 44, p. 386.
[4] Ringas, C. Robinson, F.p.A. 1988, *Corrosion*, v. 44, p. 671.
[5] Mattson, E. 1982, *Materials Performance*, v. 22, p. 9.

PRJ, Vol. 2 (January 1990); P. 67–70, 5 FIGS, 1 TABLE.

Short Note

EVALUATION OF OIL FIELD CORROSION INHIBITORS BY NACE STATIC TEST METHOD AND THE WHEEL TEST METHOD

M.A. Sherif*, A. Hassan* and A. Abusnena*

تقييم موانع التآكل بالحقول النفطية باستعمال طريقتي الإختبار الساكن والعجلة الدوارة

محمود الشريف ، عبدالفتاح حسن وعبدالواحد أبوسنينه

تم إختيار وتقييم أربعة من موانع التآكل المتعددة والشائعة الإستعمال في الحقول النفطية الليبية ، وذلك باستعمال طريقتي الإختبار الساكن والعجلة الدوارة ووجد أن نتائج العجلة الدوارة أكثر واقعية من نتائج الإختبار الساكن نظراً لتقارب طبيعة التجربة الأولى من الظروف البيئية الموجودة بالحقل ، وتشير النتائج بأن مانع التآكل الذي يشار إليه في هذه التجربة برقم III يوفر أعلى قدر من الحماية من التآكل.

INTRODUCTION

There are many types of inhibitors which were developed by empirical testing [1]. Many of the known inhibitors are proprietary of the producing companies so that their composition is not released by the formulators [2]. Inhibitors act on the environment in different ways, such as adsorbing to the metal surface to form an invisible thin film or visible coat which protects the metal from the aggressive environment [3]. The type and concentration of inhibitor that can be used in specific corrosive environment is established by testing [4].

Oil and Gas production facilities are known to experience corrosion problems due to the aggressive nature of the produced fluids and gases [5]. Carbon steel is the most common construction material used in the fabrication of the oil production and gas processing equipment. By nature carbon steel is susceptible to corrosion attack in presence of brine and associated carbon dioxide and hydrogen sulphide. It is also well established that the corrosion inhibitors affect the anodic or cathodic reactions or both. The adsorbtion of the corrosion inhibitor is accepted to be dominating the entire surface rather than specific anodic or cathodic sites, resulting in the stifling of both reactions [6]. Inhibitors attach to metal surface by their polar groups such as organic N, amines, S and OH groups. The size, orientation, shape, and electric charge of molecule determine the effectiveness of the inhibitor [6].

The effectiveness of inhibitors in protecting oil and gas production facilities is dependent on the inhibitor composition and the aggressiveness of oil field produced fluids and gases. Inhibitors must be tested under simulated or nearly simulated oil field conditions in order to prove their performance and ability to reduce the corrosion attack of the produced fluids and the associated corrosive gases.

The objective of the paper is to evaluate performance of different inhibitors manufactured by different suppliers.

EXPERIMENTAL

To achieve test conditions as close as possible to the actual conditions of the corrosive environment in the oil field, test medium must contain the corrosive species known to exist in the oil field fluids. NACE static test method [7] and NACE wheel test method [8] are both designed so that the corrosive test medium be used under atmospheric pressure. Only saturation concentrations of the corrosive gases can be achieved under atmospheric pressure at room temperature.

For the purpose of saturating the synthetic brine with the corrosive gases an apparatus was developed as shown schematically in Fig. 1.

The wheel test method is a dynamic test performed by placing fluids (oil, brine and inhibitor) in 250 ml bottle with low carbon steel coupon; and capping the bottle. The bottle is then agitated for a period of 72 hrs by securing it to the circumference of a "wheel" and rotating it. At the end of this time the metal coupon is

*Petroleum Research Centre, Tripoli, Libya, G.S.P.L.A.J.

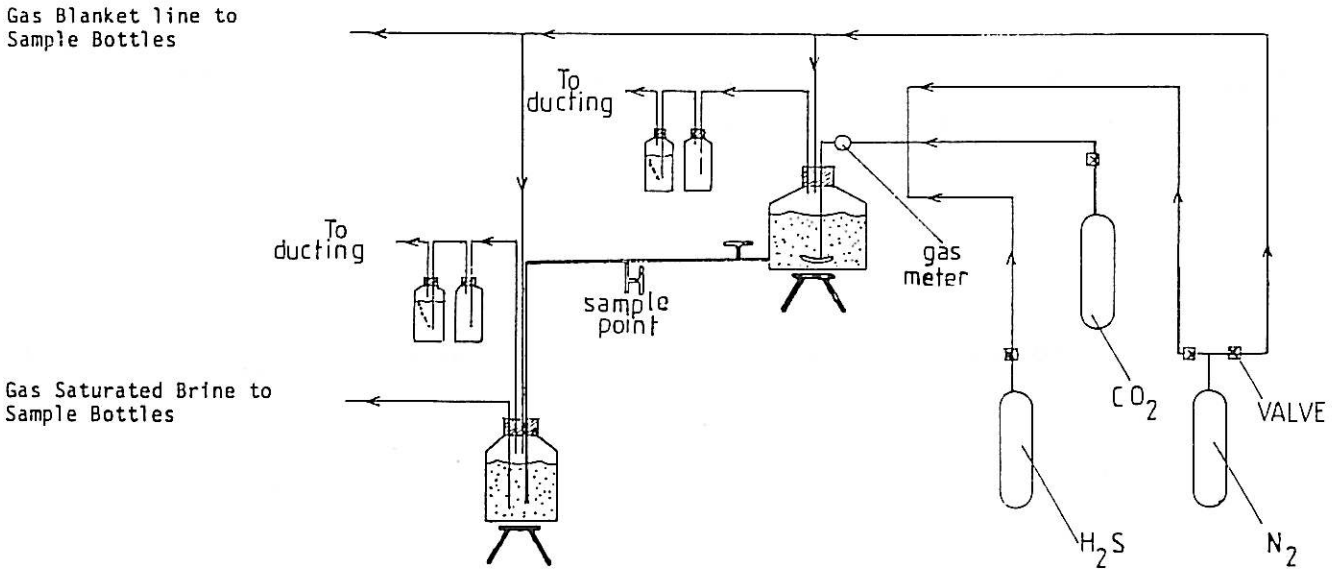


FIG. 1. Schematic diagram of the gas purging system and gas blanket system.

removed and cleaned and the weight loss is measured.

The static test method is a test which does not involve stirring or shaking. Similar quantities of four corrosion inhibitors were added into six hundred ml bottle as per NACE Standard. Brine and crude oil (450, 50 ml) respectively were added one after the other. At the end of the test duration coupons were removed and cleaned and the weight losses were measured.

RESULTS AND DISCUSSION

Four types of corrosion inhibitors namely (Inhibitor I, Inhibitor II, Inhibitor III, Inhibitor IV) were evaluated by using wheel test method [8] and static test method [7]. The tests were performed at five different concentration (0, 10, 25, 50, 100 ppm) of each inhibitor under the same experimental conditions as shown in Table 1.

The most important parameters are temperature and velocity. Test temperature for both tests were 50°C. Velocity for wheel test was chosen to be 6 rpm. The effect of temperature is generally conceded that the effectiveness of inhibitors usually is adversely influenced by increases in temperature and the effect of the velocity is important in inhibition performance of inhibitors as inhibition usually is affected by high velocity. On the other hand, performance of certain inhibitors in some environment is affected by too low velocity. The comparative inhibition efficiency of different types of corrosion inhibitors are shown in Fig. 2 for the Wheel Test Method.

Fig. 3 shows the percent of inhibitions of inhibitor I, inhibitor II, inhibitor III, and inhibitor IV at different concentrations tested under static test conditions. The effect of the different inhibitor concentrations on the corrosion rate is shown in Fig. 4 and Fig. 5. Fig. 2 shows that inhibitor III is the best corrosion inhibitor at concentration lower than 75 ppm, by comparison below this concentration inhibitor I shows the lowest percent of inhibition efficiency at all concentrations.

It is clear from Fig. 3 that inhibitors III and IV are better. Inhibitor II performs the least and has the lowest efficiency.

This is also supported by the results of the calculated

Table 1. Test conditions for all experiments

Test method	Temperature (°C)	Time (hrs)	CO_2 solubility at room temp.	H_2S solubility at room temp.	O_2 solubility at room temp.	Crude Oil (ml)	Brine (ml)
Wheel test method	50	72	1.5 g/l	3.5 g/l	0.001 g/l	85*	85*
Static test method	50	168	1.5 g/l	3.5 g/l	0.001 g/l	50*	450*

*As per NACE standard.

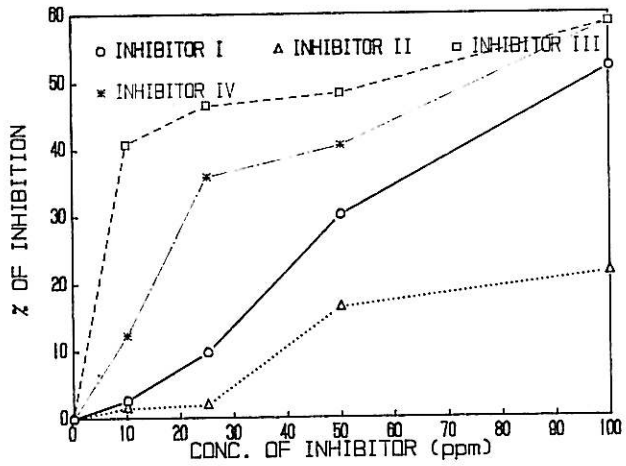


FIG. 2. Corrosion testing for different types of crude oil corrosion inhibitors by using wheel test method.

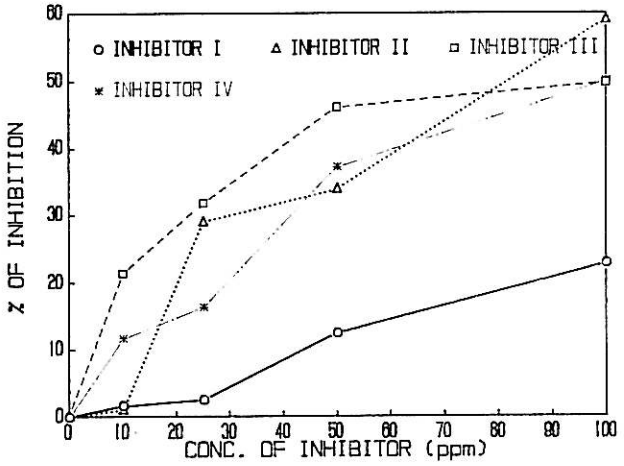


FIG. 3. Corrosion testing for different types of crude oil corrosion inhibitors by using static test method.

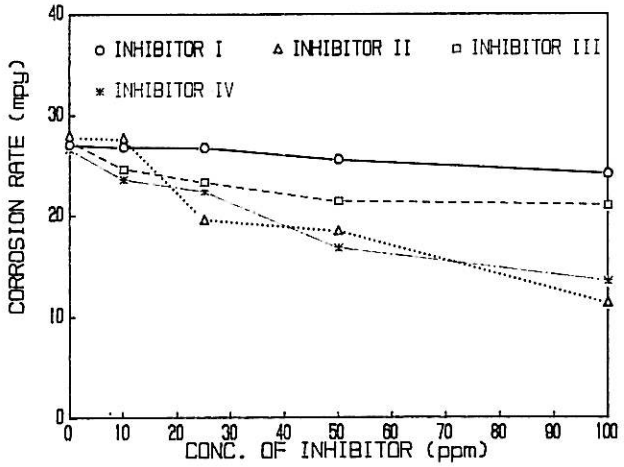


FIG. 4. Corrosion testing for different types of crude oil corrosion inhibitors by using wheel test method.

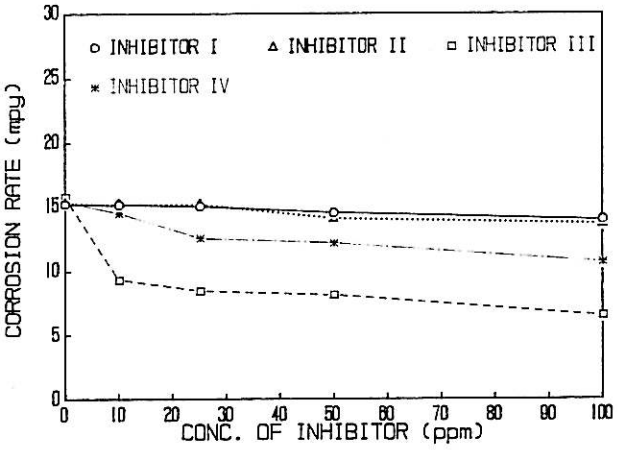


FIG. 5. Corrosion testing for different types of crude oil corrosion inhibitors by using static test method.

corrosion rate as illustrated in Fig. 4 for the wheel test and Fig. 5 for the static test. By comparing the wheel test method and the static test method the first one is more reliable than the second, since conditions in the wheel test method are closer to field conditions. The wheel test method involves rotation which attempts to simulate the time and frequency of specimen immersion in both phases (brine and Crude oil).

Structure of inhibitors was not disclosed by manufacturers. Therefore it is rather difficult to discuss how they differ from each other in their performance. IR Spectroscopy of inhibitors was carried out. The analysis revealed that the inhibitors are amine types.

CONCLUSION

1 The maximum possible percentage of inhibition which could be achieved was only 60%. This is offered by inhibitor III in the static test method and by inhibitor II in the wheel test method.
2 The optimum percent of inhibition in both the wheel test method and static test method was shown by inhibitor III.
3 The optimum level was 47% inhibition which required 30 ppm and 50 ppm of the inhibitor III in static and wheel test methods respectively.

REFERENCES

[1] Corrosion Inhibitor Manufacture and Technology, 1976, Noyes Data Corporation, London, *Chemical Technology Reviews.*
[2] Fontana, M.G. & Greene N.D., 1967, *Corrosion Engineering*: McGraw Hill, p. 198.
[3] Evans, U.R., 1982, An Introduction to Metallic Corrosion: Edward Arnold, *ASM Publication*, p. 200.
[4] Nathan C.C., 1977, Corrosion Inhibitors, NACE Houston, Texas.

[5] Ailor, W.H., Handbook on Corrosion Testing and Evaluation: John Wiley & Sons Inc., p. 873.
[6] Gosta Warngle'm, 1985, An Introduction to Corrosion & Protection of Metals: Chapman & Hall Publication, p. 170.
[7] Nace, T-1K, 1960, Proposed Standardized Static Laboratory screening test for materials used inhibitors in sour oil and gas wells, *Corrosion* 16, 63 t.
[8] NACE PUBLICATION 1D182, 1982, Wheel Test Method for Evaluation of Film Persistant Inhibitors for Oil field Applications: *Material Performance*, p. 45.
[9] Jayaraman, A., Oberoi, H.C. and Himmet Singh, 1980, Quantification of a Standard Test of Corrosion Inhibitor Evaluation: *Material Performance*, p. 48.

PRJ, Vol. 2 (January 1990); P. 71–77, 3 FIGS, 1 TABLE.

Short Note

A PRELIMINARY PHOTOGEOLOGIC INVESTIGATION AND STRUCTURES OF THE BASEMENT ROCKS, SOUTHERN PART OF JABAL EIGHEE AREA, LIBYA

M. Ben Isa*

إستخدام الصور الجوية في دراسة أولية لجيولوجية الصخور القاعية المتكشفة بالمنطقة الجنوبية لجبل إيقي — ليبيا

محمود بن عيسى

تمت دراسة الجيولوجيا التركيبية للصخور القاعية المتكشفة لمنطقة جبل ايقي ، بشمال شرق تيبستي وذلك باستخدام الصور الجوية بمقياس رسم 1:60.000 ، ومن خلال تفسير هذه الصور الجوية وصور القمر الصناعي الفرنسي (سبوت) تم التعرف على تسع وحدات صخرية بمنطقة الدراسة . . قسمت هذه الوحدات الصخرية المتكشفة إلى : صخور متحولة من أصل رسوبي صخور الشيست ، دخلات الصهير البركاني ، الصخور الجرانيتية ، الحجر الرملي الكمبرو — أوردوفيشي ، ترسبات السيلوري البحرية ، الحجر الرملي الديفوني ، البيروكلاستيك البركانية والرسوبيات الحديثة . . ووجد بأن منطقة الدراسة كانت قد تعرضت إلى حركات رجية ذات إتجاهات مختلفة تشابه نظام التصدع المتعارف عليه بمنطقة حوض سرت .

INTRODUCTION

In this investigation, a mirror stereoscope with magnifying binoculars and a stereo zoom transfer scope with variable magnification ranging from 2.3X to 16.1X were used. This instrument is adapted for viewing of prints or transparencies of two sizes (13 by 13 cm or 23 by 23 cm).

During the investigation 130 black and white aerial photographs (scale 1:60,000) taken in 1962 were analysed. SPOT images were used as a base map with a scale of 1:400,000 to correlate the results obtained from the aerial photographs and to add more information about the structure of the area.

Preliminary photo-interpretation and construction of a mosaic of the study area resulted in a photogeologic map, (Figs 1 and 2).

The aim of this study is to serve as a first step towards documenting the tectonic/structural evolution of Libya by mapping and analysing the structural features of the exposed basement in southern Libya.

The area under study represents the southern part of Jabal Eighee. It lies between Al Kufrah basin in the east and Sarir Tibisti to the west on the extreme northern end of the Tibisti massif (Fig. 1).

STRUCTURE OF THE AREA

The structures presented herein are tentative as they are based on photo-interpretation and compilation of identified structures on rose diagram plots (Fig. 3) without substantiation of field checking.

Two major linear systems (NW–SE and NE–SW) are evident from the data presented in the photogeological map and the generalized geological interpretation map (Fig. 1 and 2).

The NW–SE and NE–SW fault systems represent the major trends of possible faults and true faults. These fault systems are thought to have been active at various times with faults being abadoned, rejuvenated or extended. These identified structural trends are also present and equally salient in the basement rocks on a very broad regional scale; occuring in the Tibisti area (Conant and Goudarzi, 1977).

The majority of the linears are the surface reflection of zones of weakness (fractures) associated with the basement, and are recognizable in the overlying rock cover. Although they may represent a one time movement within the Precambrian, many of the fractures seem to have been rejuvenated later during geologic time as reflected in the overlying sediments of Palaeo-

*Petroleum Research Centre, Tripoli, Libya (G.S.P.L.A.J.)

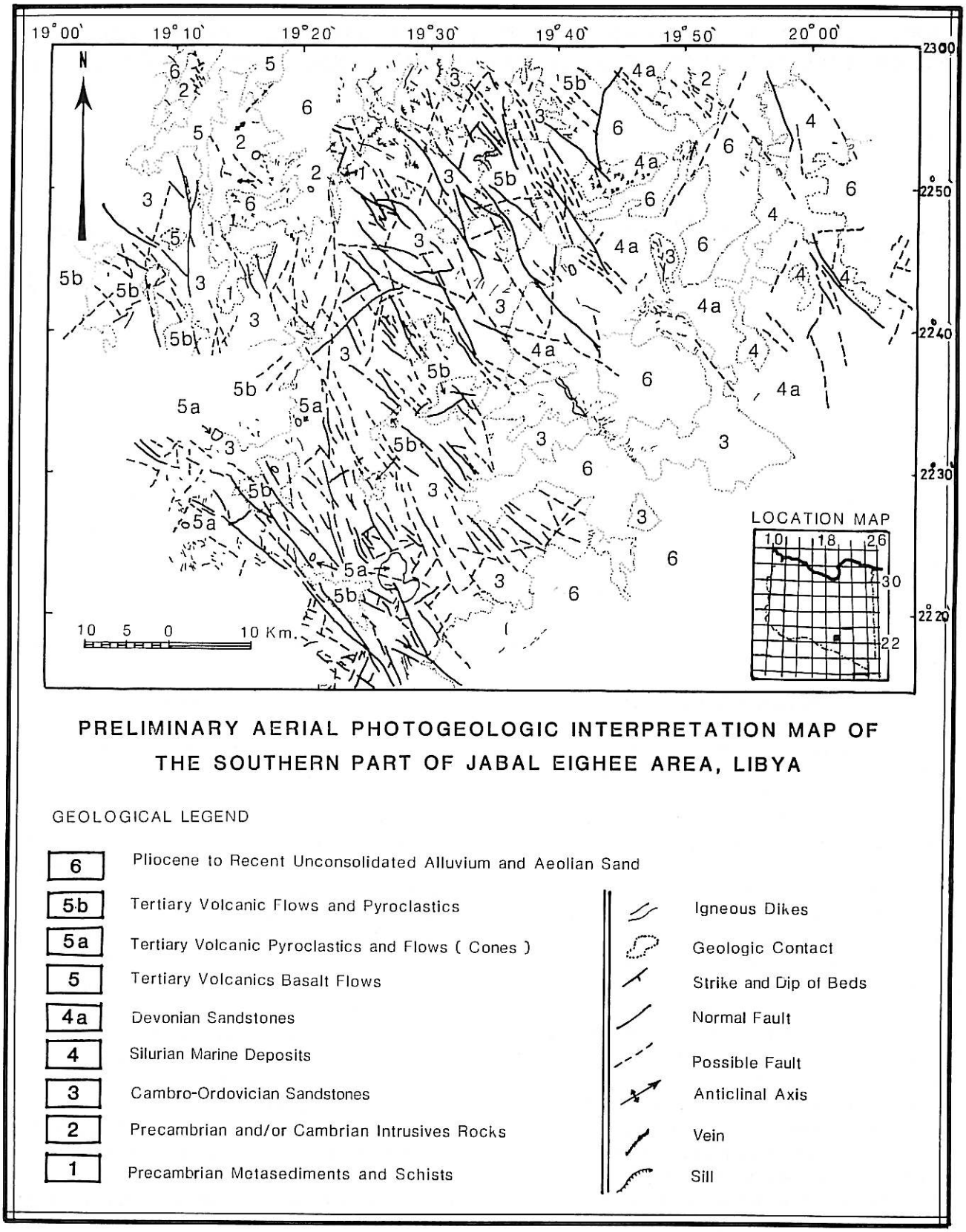


FIG. 1 Photogeologic map of the area of study.

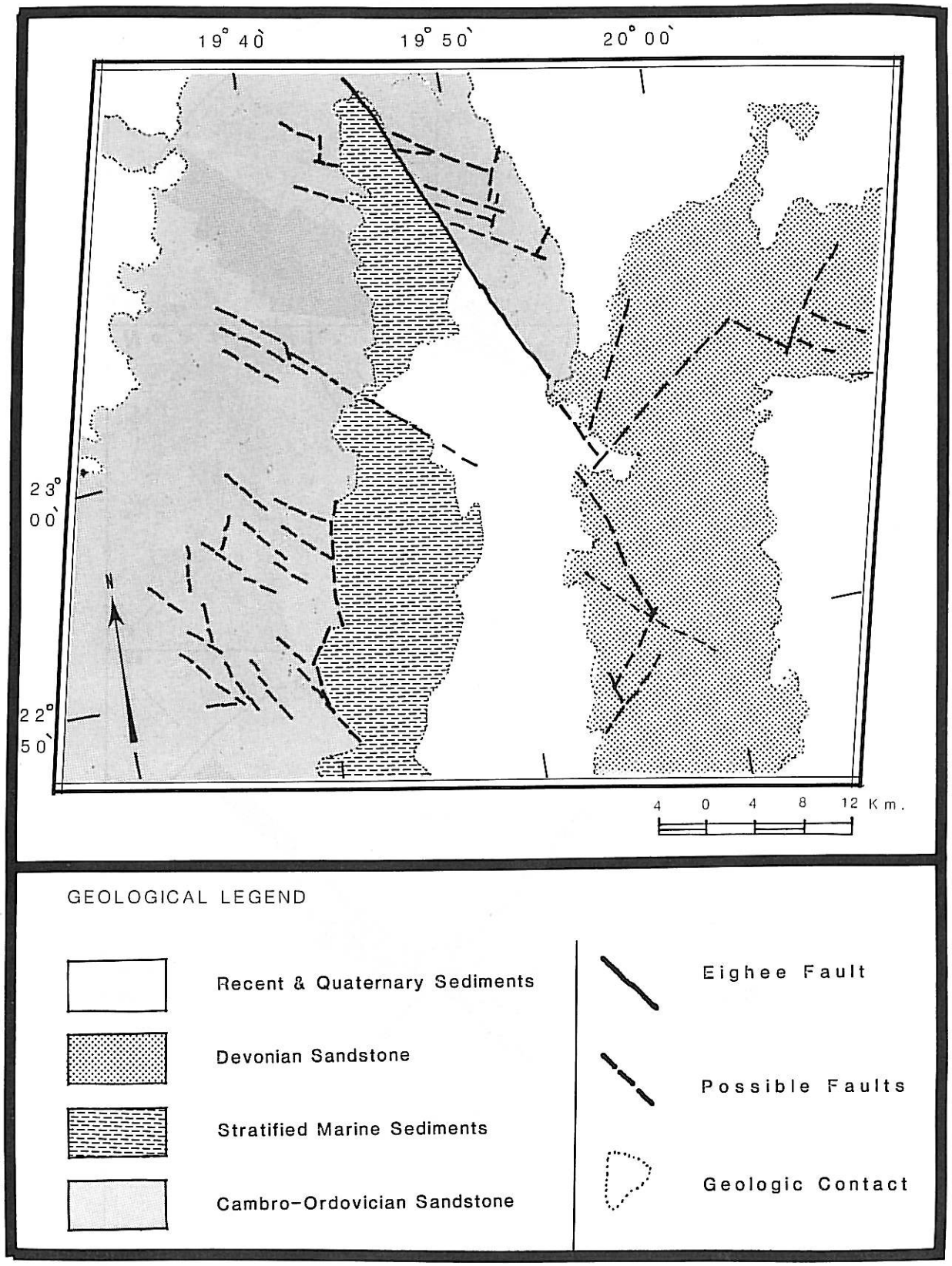


FIG. 2. Generalized Geological interpretation map based on SPOT Images.

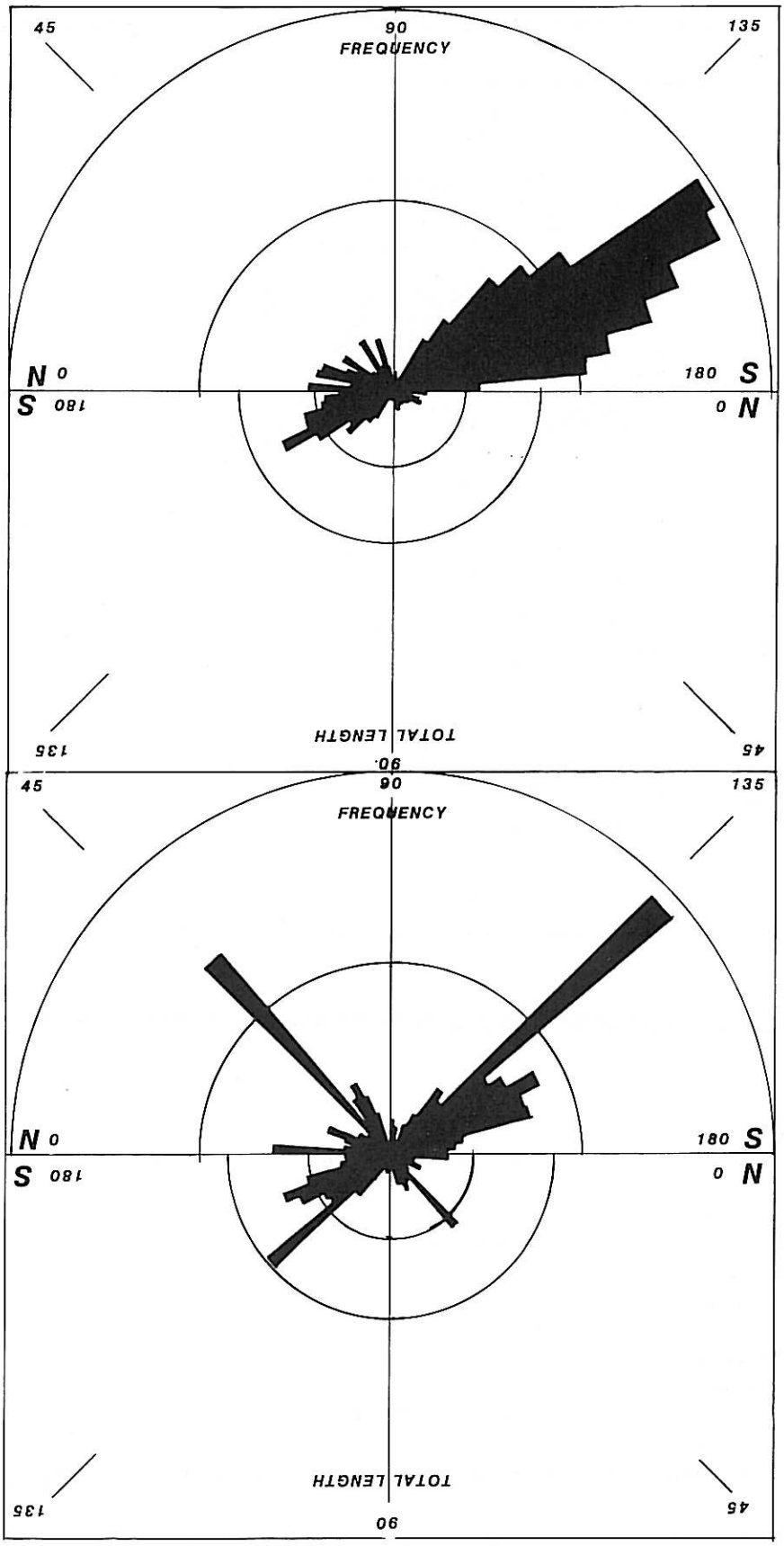


FIG. 3. Rose diagram (frequency and total length) of mapped faults and dikes, southern part of Jabal Eighee area, Libya.

zoic age. Some linears, however, may represent fractures of the sedimentary rocks caused by differential compaction on ancient topographic ridges.

This investigation indicates that long linears are most common in the Cambro-Ordovician sandstone and the surrounding areas. It was found that the orientations of dikes, faults, and possible faults exhibit great variations. These variations may be explained by differences in strike of local and regional structures (Table 1). The major tectonic activities include the Caledonian and Hercynian orogenies and disturbances during Cretaceous, Middle Tertiary (Oligocene-Miocene) and Holocene time (Klitzsch, 1966, 1971). These events caused uplifts, subsidences, tilting, faulting and intrusions. However, the effects of these tectonic events were generally broad.

Caledonian Trends and Movements

The main Caledonian phase was dated as Middle Silurian and Devonian. This has been suggested in several localities; south of the Ghadamis basin, Murzuq basin and also in Al-Kufrah basin. The fault trends associated with the Caledonian orogeny are toward NW–SE direction (Bellini and Massa, 1980).

TABLE 1 STRIKE OF THE LINEARS

Frequency (ϕ) From North to South (0°-180°)

LINEARS	FAULTS	DIKES	POSSIBLE FAULTS	TOTAL
00-04	9	43	18	70
05-09	3	17	11	31
10-14	4	14	5	23
15-19	7	17	2	26
20-24	8	24	8	40
25-29	5	12	9	26
30-34	5	13	6	24
35-39	4	8	7	19
40-44	1	9	13	23
45-49	4	06	14	114
50-54	1	12	10	23
55-59	4	24	8	36
60-64	0	29	7	36
65-69	4	23	5	32
70-74	5	16	3	24
75-79	2	7	1	10
80-84	0	7	5	12
85-89	1	9	2	12
90-94	2	13	0	15
95-99	1	2	3	6
100-104	1	10	1	12
105-109	1	6	1	8
110-114	1	6	2	9
115-119	2	12	4	18
120-124	8	17	5	30
125-129	10	30	10	50
130-134	10	26	7	43
135-139	16	134	24	174
140-144	14	44	18	76
145-149	23	49	26	98
150-154	32	60	36	128
155-159	24	52	25	101
160-164	24	53	25	101
165-169	19	27	23	69
170-174	18	24	22	64
175-179	9	21	10	40

Data in Libya supporting Caledonian movement have been described for the east Murzuq basin (western Sirt basin) by Klitzsch, (1963). He mapped NW trending faults in Cambrian strata, which do not cut younger strata, and an angular unconformity of up to 40 degrees between Cambrian and Ordovician rocks all of which could point to early Caledonian movements.

Hercynian Trends and Movements

This corresponds to the second major tectonic phase which has affected the Palaeozoic rocks. Its initial phases were dated as Middle to Late Carboniferous and were thought to be persisting throughout the Permian time, (Bellini and Massa, 1980). The Hercynian Orogeny has caused foldings, faulting and strong subsidences in many parts of Libya, generally oriented in NE–SW direction.

These North-West and North-East-trending faults intersect near the central part of the country, the site of the largest outpourings of lava in Jabal al Haruj, Libya (Goudarzi, 1980).

The individual linears vary in length, and the major linear features in the study area are parallel to Eighee fault as well as the main fault trends of the Sirt basin units (Fig. 1).

LITHOLOGIC INTERPRETATION

Nine rock units have been identified and mapped. Each of these units have been identified using standard aerial photograph interpretation techniques, i.e., analysis of textural, tonal, geomorphological and erosional characteristics.

Their classification by age is based upon the rock units, spatial relationships, and the geological map of Libya (Conant and Goudarzi; 1977). Wherever possible, the contacts of the units beneath the overburden have been mapped by identifiable slight topographic and tonal variations as well as isolated exposures of the units (Fig. 1).

The Precambrian Meta-sediments and Schists (Unit 1)

This unit appears as a series of narrow ridges having associated tonal-banding of grey tone on the exposed tops of ridges while the topographic lows are of lighter tone depending upon the degree of exposure. This unit is probably equivalent to the Upper Tibistian Metasediments described by Schurmann (1974).

The Precambrian and/or Cambrian Intrusives (Unit 2)

When exposed, this unit appears on the aerial photographs with a dark grey tone and a very coarse texture. Jointing in this unit is very well developed with

the major trend in a NW direction throughout the entire study area.

Cambro-Ordovician Sandstones (Unit 3)

This unit appears on the aerial photographs as beds of rocks with a medium to moderately dark grey tone and an extremely coarse texture due to the very dense, well developed multiple jointing. The major distinguishing features of this unit is the strong drainage controlled by the joints as compared to the lack of joint drainage control in the area of intrusive bodies.

Silurian Marine Deposits (Unit 4)

This unit is not well exposed as it is mainly covered by alluvium and aeolian sand. When exposed, the bedding is apparent at about 30 degrees, toward the NE. The major trend of faults in this unit is NW (Fig. 2).

Devonian Sandstones (Unit 4a)

The distinguishing features of this unit is the presence of a dendritic drainage pattern and a darker tone compared to the Cambro-Ordovician. This unit is less resistant than the Cambro-Ordovician sandstone observed in this investigation.

Tertiary Volcanic Basalt Flows (Unit 5)

The constructional surfaces of lava flows, make conspicuous topographic features readily observed on aerial photographs. The surface of such flows can be identified by the presence of general lobate form extending from the extrusive source, which may often consist of fissures, volcanic cones and to a lesser extent volcanic vents. Lava flowing down a wadi has an elongate form and during its filling of the wadi, it changed the paleodrainage system.

Tertiary Pyroclastic Cones and Flows (Unit 5a)

A variety of different pyroclastic cones and flows are present within the study area. The youngest of these are small.

These cones are not older than Tertiary and not younger than Pleistocene age. There are also low sloping vents of medium to dark tone within the Tertiary basaltic flows (unit 5).

Tertiary Volcanic Flows and Pyroclastics (Unit 5b)

The pyroclastics appear as a very dark toned rock, and usually, is capping the Cambro-Ordovician sandstone. In many areas the drainage within this unit is controlled by the underlying rock unit.

Pliocene to Recent Unconsolidated Alluvium and Aeolian Sand (Unit 6)

This unit is abundant in the topographically low areas where aeolian sand, which occurs as extensive sand sheets of varying thickness, overlies older alluvial sand. In this preliminary investigation, a large alluvium fan is thought to have been deposited from high area (Cambro-Ordovician) to cover the bedding of Silurian marine deposits (Fig. 2).

Dikes

Extensive dike swarms have been observed throughout the area. The trends and abundance of these dikes are thought here to be indicative of local tectonic events prior to and during emplacement (Fig. 1).

CONCLUSIONS

The deposition and/or erosion of Phanerozoic sediments appear to have been largely controlled by epeirogenic fluctuations along earlier, mostly Precambrian structures resulting in Cambro-Ordovician sandstone and younger exposed rocks. The major linear features in the study area are parallel to the Eighee fault as well as to the main fault trends of the Sirt basin. These identified structural trends are also present and equally salient on a very broad regional scale, in the basement rocks in the Tibisti area (Conant and Goudarzi, 1977).

The chronostratigraphic arrangement of the rock units is based on the observed spatial relation of the rock units (from oldest to youngest), the Precambrian meta-sediments are interpreted as being the oldest rock units within the study area.

ACKNOWLEDGEMENTS

I would like to express my thanks to all members of the staff, in the Exploration and Oil Exploitation Department in Petroleum Research Centre for their support. Thanks are also extended to Dr. M.J. Salem and Dr. M.T. Busrewil for their critical review of the text and for their valuable suggestions throughout this project.

REFERENCES

Bellini, E. and Massa, D., 1980, A stratigraphic contribution to the Palaeozoic of the southern basins of Libya. In: *The Geology of Libya* (eds: M.J. Salem and M.T. Busrewil) London, Academic Press, Vol. 1, 3–57.

Conant, L.C. and Goudarz, G.H., 1977, *Geologic map of Libya*, 1:2,000,000. 2nd edition, Ind. Res. Cent. (Tripoli).

Goudarzi, G.H., 1980, Structure Libya. In: *The Geology of Libya* (eds: M.J. Salem and M.T. Busrewil). Academic press, London, 879–892.

Klitzsch, E., 1963, Geology of the north-east flank of the Mursuk basin. In: *First Saharah Symposium*, (ed.:) Petroleum Exploration Society of Libya, 97–113.

Klitzsch, E., 1966, Geology of the north-east flank of the Marzuk basin. In: *south-central Libya and northern Chad* (ed.: J.J. Williams) Petrol Explor. Soc. Libya, 8th annu. Field Conf. 19–32.

Klitzsch, E., 1971, A structural developments of parts of North Africa since Cambrian time. In: *Symposium on the Geology of Libya* (ed.: C. Gray), Fac. Sci., Univ. Libya, Tripoli, 253–262.

Schurmann, H.M.E., 1974, The Precambrian in North Africa, E.J. Brill, Leiden, LTD 404 p.

Vail, J.R., 1968, The southern extention of the East Africa Rift System. geol. Rdsch., 57, 601–614.

Vail, J.R., 1970, Dike swarms and volcanic activity in North-Eastern Africa. In: *Symposium on the Geology of Libya*, (ed.: C. Gray) Fac. Sci. Univ., Tripoli, Libya, 341–343.